Temporally resolved single-nucleus RNA-sequencing profiling of the cortex reveals mechanisms of neuronal vulnerability in Huntington's disease

Dissertation zur Erlangung des naturwissenschaftlichen Doktorgrades „Doctor rerum naturalium“ (Dr. rer. nat.) an der Fakultät für Biologie der Ludwig-Maximilians-Universität München

Dennis Feigenbutz

2024

Diese Dissertation wurde angefertigt unter der Leitung von Prof. Dr. Rüdiger Klein in der Abteilung Moleküle – Signale – Entwicklung und Prof. Dr. Irina Dudanova in der Forschungsgruppe Molekulare Neurodegeneration am Max-Planck-Institut für biologische Intelligenz in Martinsried, Deutschland.

Erstgutachter:	Prof. Dr. Rüdiger Klein
Zweitgutachter:	Prof. Dr. David Keays
Tag der Abgabe:	07.08.2024
Tag der mündlichen Prüfung:	04.02.2025

Eidesstattliche Erklärung

Ich versichere hiermit an Eides statt, dass die vorgelegte Dissertation von mir selbständig und ohne unerlaubte Hilfe angefertigt ist.

München, 17.02.2025	Dennis Feigenbutz
Ort, Datum	Unterschrift

Eidesstattliche Erklärung

Hiermit erkläre ich, dass die Dissertation nicht ganz oder in wesentlichen Teilen einer anderen Prüfungskommission vorgelegt worden ist und ich mich anderweitig einer Doktorprüfung ohne Erfolg nicht unterzogen habe.

München, 17.02.2025	Dennis Feigenbutz
Ort, Datum	Unterschrift

Abstract

Huntington's disease (HD) is a fatal neurodegenerative disease characterized by severe motor impairments. HD is caused by the expansion of CAG repeats in the Huntingtin (*HTT*) gene, resulting in the mutated HTT protein (mHTT) to form aggregates predominantly in the striatum and cortex of patients. Within these brain regions, neuronal populations exhibit varying degrees of cell loss, with cortical projection neurons (CPNs) in the motor cortex (MC) being particularly vulnerable, while locally projecting GABAergic interneurons are mostly spared. Despite extensive research, the underlying disease pathogenesis and molecular factors rendering certain populations more vulnerable remain elusive, with no effective treatments available.

In this study, we utilized the transgenic R6/2 mouse model of HD to conduct a longitudinal single-nucleus RNA (snRNA-seq) study, investigating transcriptomic changes in the MC across three distinct time points from presymptomatic to disease onset to advanced disease stage. Our analysis uncovers several key mechanisms at play in R6/2 mice. We show that the vulnerable glutamatergic CPNs undergo a pronounced transcriptomic shift, while locally projecting GABAergic interneurons remain largely unaffected. Additionally, a subset of genes exhibits a bidirectional temporal expression pattern, characterized by early downregulation followed by late-stage upregulation, potentially contributing to disease onset. Furthermore, we demonstrate a decrease in marker gene expression across a multitude of cell populations in the MC of R6/2 mice.

Moreover, our findings highlight two potentially disease-modifying molecular mechanisms. Firstly, we provide evidence for the occurrence of chronic endoplasmic reticulum (ER) stress and the subsequent upregulation of the unfolded protein response (UPR) in R6/2 mice. Interestingly, several receptors for autophagy of the ER (ER-phagy) are upregulated, suggesting a compensatory mechanism to alleviate ER stress. We demonstrate that ER-phagy is increased in cellular models of HD. Potentially, modification of ER-phagy might be utilized to prevent chronic ER stress in HD.

Lastly, we identified a set of neuronal essential gene with increased expression in GABAergic interneurons, which might contribute to the enhanced resilience of interneurons to HD. Among these genes, the chaperone proSAAS emerged as an upregulated hub gene in R6/2 mice. Here, we demonstrate that proSAAS translocates to the nucleus in the presence of nuclear mHTT aggregates, suggesting an interplay between proSAAS and mHTT.

Taken together, our temporally resolved analysis of single-nucleus transcriptomic changes in HD mouse cortex provides novel insights into the mechanisms of neuronal vulnerability, and points to new disease-relevant pathways that could be targeted for future therapeutic interventions.

Contents

List of abbreviations

Abbreviation	Term
α-Syn	alpha-Synuclein
Aβ	beta-Amyloid
AD	Alzheimer's disease
ALS	amyotrophic lateral sclerosis
Atp6v0c	ATPase H+ transporting V0 subunit c
BICCN	Brain Initiative Cell Census Network
BiP	binding immunoglobulin protein
Bdnf	brain-derived neurotophic factor
BSA	albumine Fraction V
Cacna1a	calcium voltage-gated channel subunit alpha1 A
Cacna2d1	calcium voltage-gated channel subunit alpha2delta 1
CAG	cytosin-adenin-guanin
Camk2a	calcium/calmodulin dependent protein kinase II alpha
Canx	calnexin
Calr	calreticulin
Caly	calcyon neuron specific vesicular protein
Cbp	CREB-binding protein
Ccpg1	cell cycle progression 1
Cox8a	cytochrome c oxidase subunit 8A
CPN	cortical projection neurons
CT	cortico-thalamic
Ctsd	cathepsin D
Ctsf	cathepsin F
DA	differential abundance
Dad1	defender against cell death 1
DEG	differentially expressed gene
DIV	Days in vitro

DMEM	Dulbecco's Modified Eagle Medium
Dnajb9	DnaJ heat shock protein family (Hsp40) member B9
EBSS	Earle's Balanced Salt Solution
Endo	endothelial cells
ER	endoplasmatic reticulum
ERAD	ER-associated degradation
ER-phagy	autophagy of the ER
ET	extratelencephalic
Fan1	FANCD2/FANCI-Associated Nuclease 1
Fan2	FANCD2/FANCI-Associated Nuclease 2
FBS	fetal bovine serum
FC	fold change
FDR	false discovery rate
Fezf2	FEZ family zinc finger 2
Fkbp2	FKBP prolyl isomerase 2
Fosb	FosB proto-oncogene
Fus	FUS RNA Binding Protein
GABA	gamma-aminobutyric acid
Gabra2	GABA A receptor subunit alpha2
Gabrg2	GABA A receptor subunit gamma2
Gad1	glutamate decarboxylase 1
Gad2	glutamate decarboxylase 2
Grik3	glutamate ionotropic receptor kainate type subunit 3
Grin2a	glutamate ionotropic receptor NMDA type subunit 2A
Grin2b	glutamate ionotropic receptor NMDA type subunit 2B
GWAS	genome-wide association study
HBSS	Hanks' Balanced Salt Solution
HD	Huntington's disease
HEK cells	HEK-293T cells
Herpud1	homocysteine inducible ER Protein with ubiquitin like domain 1
Hivep2	human immunodeficiency virus type I enhancer binding protein 2
Homer1	homer scaffold protein 1
Hsp90aa1	heat shock protein 90 alpha family class A member 1
Hsp90ab1	heat shock protein 90 alpha class B member 1
Hsp90b1	heat shock protein 90 beta family member 1

Hspa5	heat shock protein family A (Hsp70) member 5
Hspa8	heat shock protein 8
HTT	huntingtin
ICC	immunocytochemistry
Id2	inhibitor of DNA binding 2
IRE1	inositol-requiring enzyme 1
iPSCs	induced pluripotent stem cells
IT	intratelencephalic
Itm2b	integral membrane protein 2b
Junb	JunB proto-oncogene, AP-1 transcription factor subunit
Kcnip4	potassium voltage-gated channel interacting protein 4
KD	knockdown
KEGG	Kyoto Encyclopedia of Genes and Genomes
KO	knockout
Lamp1	lysosomal associated membrane protein family member 1
Lamp5	lysosomal associated membrane protein family member 5
Laptm4a	lysosomal protein transmembrane 4 alpha
Lhx2	LIM Homeobox 2
Lhx6	LIM Homeobox 6
LV	lentivirus
MAM	mitochondria-associated membrane
MC	motor cortex
mHTT	mutant Huntingtin
mRNA	messenger RNA
mtRNA	mitochondrial RNA
Msh2	mutS homolog 2
Msh3	mutS homolog 3
MSN	medium spiny projection neuron
mTOR	mammalian target of rapamycin
ND	neurodegenerative disease
Ndufa3	NADH:ubiquinone oxidoreductase subunit A3
NE	nuclear envelope

NEAA	MEM non-essential amino acids
Nell1	neural EGFL like 1
Neurod1	neurogenic differentiation 1
NF-κb	nuclear factor 'kappa-light-chain-enhancer' of activated B-cells
Nfix2	nuclear factor I X
Nrgn	Neurogranin
OPC	Oligodendrocyte precursor cells
Os9	OS9 ER Lectin
OXPHOS	oxidative phosphorylation
p53	tumor protein P53
PBS	Dulbecco´s Phosphate Buffered Saline
PCA	principal component analysis
PCR	polymerase chain reaction
Pcsk1n	proprotein convertase subtilisin/kexin type 1 inhibitor
PD	Parkinson's disease
Pdia3	protein disulfide isomerase A3
PDL	Poly-D-Lysin-hydrobromid
Peri	pericytes
PFA	Paraformaldehyde
Pgc-1a	peroxisome proliferator-activated receptor-g coactivator-1a
polyQ	poly-glutamine
Pgrmc1	progesterone receptor membrane component 1
proSAAS	proprotein convertase subtilisin/kexin type 1 inhibitor
Pv	parvalbumin
Rbfox1	RNA binding fox-1 homolog 1
REST	RE1 silencing transcription factor
Retreg1	reticulophagy regulator 1
Rpl41	ribosomal protein L41
Rrm2	Bribonucleotide reductase regulatory TP53 inducible subunit M2B
Rtn3	Reticulon 3
Ryr2	ryanodine receptor 2
Scg5	Secretogranin V

scRNA-seq	single-cell RNA-sequencing
Serpine2	serpin family E member 2
Serpini1	serpin family I member 1
siRNA	small interfering RNA
Slc17a7	solute carrier family 17 member 7
Slc24a2	solute carrier family 24 member 2
Slc30a3	solute carrier family 30 member 3
Sncg	synuclein gamma
snRNA-seq	single-nucleus RNA-sequencing
ss	signal sequence
Sst	somatostatin
Taf4	TATAbox binding protein associated gactor 4
Tafa1	TAFA chemokine like family member 1
Tex264	Testis expressed gene 264
TF	transcription factor
TDP-43	TAR DNA-binding protein 43
Tomm20	translocase of outer mitochondrial membrane 20
TRKB	tyrosine receptor kinase B
Tshz2	teashirt zinc finger homeobox 2
Ubb	Ubiquitin B
UMAP	Uniform manifold approximation and projection
UMI	unique molecular identifier
UPR	unfolded protein response
Vip	vasopressin
VLMC	vascular leptomeningeal cells
WGCNA	weighted gene co-expression network analysis
WT	wild type
XBP1	X-box binding protein 1
XBP1s	XBP1 spliced
Zeb2	zinc finger E-box-binding homeobox 2

List of Figures

1 Introduction

1.1 Neurodegenerative diseases

Neurodegenerative diseases (NDs) constitute a diverse group of neurological disorders characterized by the progressive loss of neurons in the nervous system of patients. Some of the most common NDs are Alzheimer's disease (AD), Parkinson's diseases (PD) and amyotrophic lateral sclerosis (ALS). The symptoms patients suffer from are distinct for each ND and encompass a wide variety of symptoms. In AD, which is the most prevalent ND, typical symptoms include the progressive loss of memory and other cognitive functions (McGirr, Venegas, & Swaminathan, 2020). PD primarily affects the movement of patients and characteristic symptoms encompass resting tremor, bradykinesia and impaired coordination (Beitz et al., 2014). ALS is manifested by a progressive degeneration of the voluntary motor system, resulting in the loss of motor control in patients (Mead, Shan, Reiser, Marshall, & Shaw, 2023).

Despite their differences in symptomatology, NDs share certain features. For instance, NDs typically start at an advanced age. Moreover, neuronal loss occurs in specific brain regions unique to each ND, resulting in the characteristic sets of symptoms (Fu, Hardy, & Duff, 2018). In all NDs, disease-specific hallmark proteins aggregate in the brain regions affected by neurodegeneration (Fig. 1.1) (Soto & Pritzkow, 2018). For example, tau and beta-Amyloid (Aβ) are the hallmark proteins of AD, and aggregate in the hippocampus and the entorhinal cortex, which are involved in memory and cognitive functions (Fig. 1.1) (Masters et al., 1985; Goedert, Spillantini, Jakes, Rutherford, & Crowther, 1989; Z.-T. Wang et al., 2020). In PD, aggregates of the disease-characteristic alpha-Synuclein (α-Syn) can be detected in the patients as early as 20 year before the diagnosis (Braak, Rüb, Gai, & Del Tredici, 2003). α-Syn aggregates are most prevalent in the substantia nigra, a structure of the basal ganglia involved in the voluntary control of movements (Fig.

1.1) (Spillantini et al., 1997; Surmeier, Obeso, & Halliday, 2017). In ALS, a wider range of characteristic protein aggregates can be found, including aggregates of FUS RNA Binding Protein (FUS) and TAR DNA-binding protein 43 (TDP-43), which aggregate primarily in upper motor neurons of the brain and lower motor neurons of the spinal cord (Fig. 1.1) (Blokhuis, Groen, Koppers, van den Berg, & Pasterkamp, 2013).

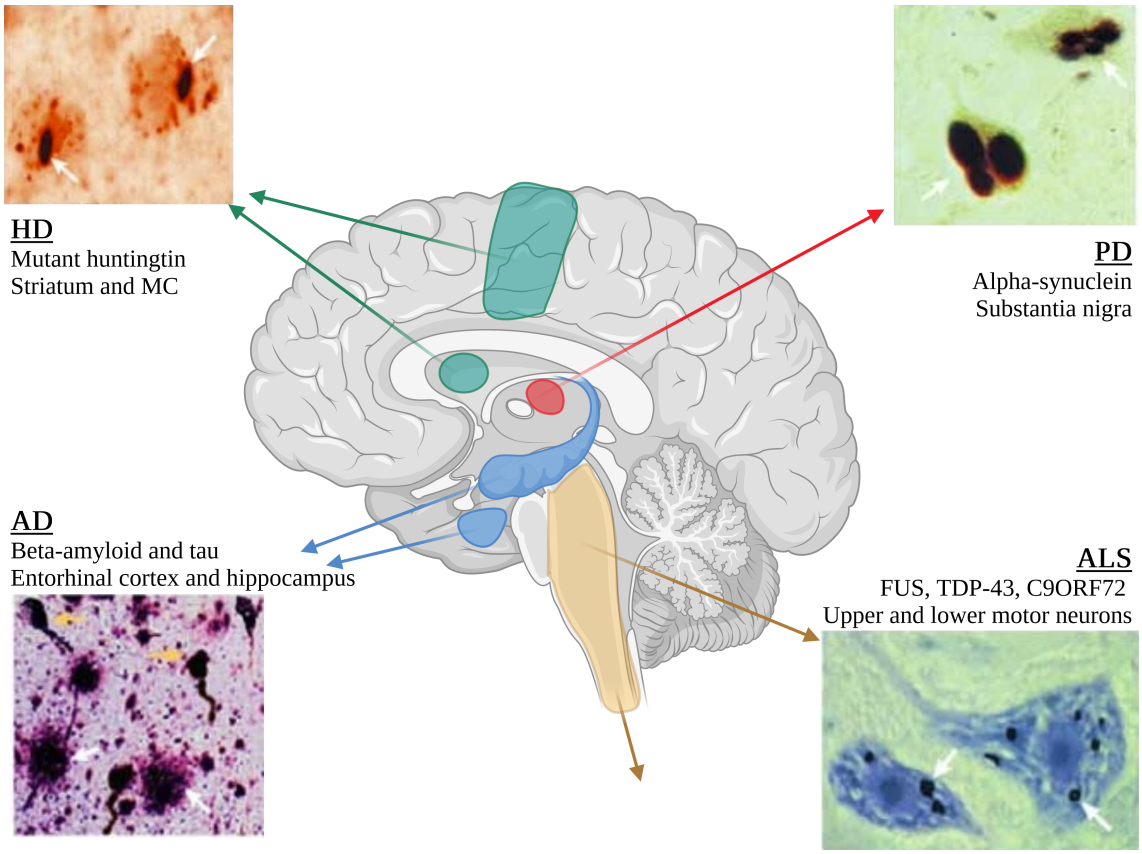

Fig. 1.1: Protein aggregation in various NDs
In each ND, neurodegeneration affects specific brain areas, which are characteristic for the individual NDs. The loss of neurons is preceded by the occurrence of protein aggregates composed of disease-specific proteins. This figure is based on Fu et al. (2018) and images of aggregates are taken from Soto (2003). All figures of the introduction chapter, except figure 1.8, were created using BioRender.

A family of genetically caused diseases within the family of NDs are the polyglutamine (polyQ) disorders. These diseases are caused by the expansion of the glutamine-encoding triplet, cytosin-adenin-guanin (CAG), in a disease-specific gene, which renders the mutated protein prone to form aggregates (Chen, Berthelier, Yang, & Wetzel, 2001). To these

diseases belong spinal muscular atrophy, bulbar muscular atrophy, and the spinocerebellar ataxias 1, 2, 3, 6, 7 and 17 (Fan et al., 2014).

Among the polyQ diseases, Huntington's disease (HD) is the most prevalent disease (Landles & Bates, 2004). HD is caused by the expansion of CAG repeats in the exon-1 of the *Huntingtin* (*HTT*) gene above a threshold of 35 CAG repeats (Gusella et al., 1983). As a result, the mutated Huntingtin protein (mHTT) forms aggregates in neurons primarily of the striatum and cortex (Fig. 1.1) (Gutekunst et al., 1999). Following mHTT agreggation, these brain regions are affected by neurodegeneration and symptom onset occurs approximately 15 years after the first signs of striatal atrophy (Ross et al., 2014). Since the striatum and motor cortex (MC) play a crucial role in the control of movement, symptoms of HD include a variety of severe motor disturbances (Saudou & Humbert, 2016). The monogentic nature of HD allows for accurate modeling of the disease in cellular systems and animal models, with many findings also applicable to other sporadic neurodegenerative diseases.

To date, none of the NDs can be cured. A successful search for a cure is hindered by the lack of a comprehensive understanding of the underlying disease mechanisms of the individual NDs. Additionally, it remains unknown why NDs affect specific brain regions and specific cell populations, while others remain spared. Therefore, research aiming at unraveling the disease mechanisms and comprehending why the disease mechanism affects certain cells, is urgently needed in order develop new therapeutic strategies, and ultimately help patients suffering from NDs.

1.2 Huntington's disease

1.2.1 Epidemiology of HD

Today, world-wide, on average approximately 4.88 out of 100,000 people are affected by HD (Medina, Mahjoub, Shaver, & Pringsheim, 2022). However, this rate varies strongly by ethnicity. For example, in East Asian countries, the prevalence was estimated at 0.41 cases per 100,000 people, while individuals with Caucasian ethnicity have a higher prevalence of

6.37 per 100,000 (Medina et al., 2022). This disparity in prevalence can be attributed to a higher length of the CAG repeats in the *HTT* gene within these populations. Individuals of Asian ethnicity have an average CAG repeat length of around 16 to 17, whereas Caucasians typically have around 18 to 19 CAG repeats (McColgan & Tabrizi, 2018). The higher repeat number of CAG repeats in the *HTT* allele presumably increases the likelihood of the CAG repeats surpassing the critical threshold in people of Caucasian descent.

1.2.2 Symptoms of HD

The symptoms of HD manifest in a triad of motor, cognitive, and psychiatric symptoms (Kirkwood, Su, Conneally, & Foroud, 2001; Victorson et al., 2014). Typically, the onset of the disease is between the age of 35 and 45, but rare cases of juvenile onset occur (Foroud, Gray, Ivashina, & Conneally, 1999; Bakels, Roos, van Roon-Mom, & de Bot, 2022). The motor symptoms can be categorized into early-stage symptoms with choreiform movements, and late-stage symptoms with bradykinesia and rigidity (Kirkwood et al., 2001; Saudou & Humbert, 2016). In the initial phase of the disease, the involuntary movements lead to gait disturbances and uncontrolled movements of arms, legs and head (Danoudis & Iansek, 2014; Reilmann, Bohlen, Kirsten, Ringelstein, & Lange, 2011). Due to the uncontrollable movements reminding doctors of dance movements, the disease was also named "Chorea Huntington" ("Chorea" is the Latin word for "dance"). Approximately a decade after the onset, the secondary phase ensues, marked by a deceleration of movements and the emergence of bradykinesia (Thompson et al., 1988; Folstein, 1989). Psychologically, HD is associated with impaired impulse control, apathy, and depression. Cognitive symptoms are among the earliest and can occur up to 10 years before the diagnosis (Jason et al., 1988; Epping & Paulsen, 2011; Morris, O'Callaghan, & Le Heron, 2022). Cognitive symptoms include cognitive slowing, a decrease in attention span and a lack of mental flexibility (Carlozzi et al., 2011; Montoya, Price, Menear, & Lepage, 2006; Saudou & Humbert, 2016). Additionally, patients may experience other symptoms that significantly impact their daily lives, such as fatigue, insomnia, loss of smell, and weight loss (Bates et al., 2015).

Through all these symptoms, the quality of life of patients, but also relatives and

caregivers, massively suffers. 10 years after onset, patients usually need to be taken care of 24 hours a day (McColgan & Tabrizi, 2018). The progressive nature of HD, coupled with psychological distress and absence of a cure, leads to an increased tendency of suicidal behaviour among HD patients (J. L. Cummings, 1995; Wetzel et al., 2011). HD always ends fatally with patient death occurring 15 to 20 years after disease onset. Pneumonia is the most common cause of death in individuals with HD, followed by cardiac diseases (Solberg, Filkuková, Frich, & Feragen, 2018).

1.2.3 CAG expansion of *HTT* causes HD

HD is an autosomal dominant disorder that occurs when the CAG repeat number of *HTT* exceeds 35 CAG repeats (MacDonald et al., 1993). *mHTT* carriers with more than 39 CAG repeats always develop the disease, whilst penetrance with a CAG repeat length of 36 to 39 is reduced (Caron et al., 2020). The age of disease onset is inversely correlated with the length of CAG repeats of the inherited *mHTT* gene. Hence, the longer the CAG repeats of the *mHTT*, the younger the patients are at disease onset. Typically, disease onset occurs between the 35th to 45th year of life with a CAG repeat length of 37 to 50 (Farrer, Cupples, Kiely, Conneally, & Myers, 1992). In rare cases where CAG repeats exceed 60 repeats, juvenile cases can occur with symptoms resembling Parkinsonian rigidity (J.-M. Lee et al., 2015; Squitieri, Cannella, & Simonelli, 2002; Gonzalez-Alegre & Afifi, 2006).

The CAG repeat length of *HTT* is unstable and spontaneous mutation can lead to an increase in CAG length in the germ line (Leeflang et al., 1999). Especially *mHTT* alleles are particularly unstable and a change in length occurs for 70–80% when passed on to the next generation (Wheeler et al., 2007). But also non-mutant *HTT* can undergo expansion or contraction of the CAG repeat length. This germ line instability can result in sporadic cases, where neither parent is a disease carrier, but their offspring can be affected by inheriting a *mHTT* allele that mutated in the germ line of a parent (Myers et al., 1993; Semaka, Creighton, Warby, & Hayden, 2006). The underlying cause for the instability of the CAG repeats in the *HTT* gene remains not fully understood. However, expansion of CAG repeat length in the germ line occurs more often when the allele is passed down

through the paternal germ line (Warby et al., 2009). Hence, the cellular environment likely influences the stability of the CAG repeat length of *HTT*.

The length of the inherited CAG repeats in *mHTT* explains approximately 60-70% of the variability in age at disease onset (Djousse et al., 2003; Li et al., 2003). In conclusion, 30-40% are explained by other factors. One of these factors could be instability of CAG repeats of *HTT* in somatic cells. Besides germ line instability, the CAG tract is unstable in somatic cells (Mouro Pinto et al., 2020; Arning & Nguyen, 2022). This instability can lead to further expansion in somatic tissue and especially in long-lived cells like neurons, in which expansions can accumulate over a longer lifespan (Mouro Pinto et al., 2020; J.-M. Lee, Pinto, Gillis, St. Claire, & Wheeler, 2011). This somatic expansion causes the CAG repeat length to differ between somatic cells of the same tissue and leads to mosaicism of CAG repeat length in the tissue (Telenius et al., 1994; Mouro Pinto et al., 2020; Arning & Nguyen, 2022).

A recent genome-wide association study (GWAS) of HD genetic modifiers identified the DNA repair factors FANCD2/FANCI-Associated Nuclease 1 (FAN1), FAN2, mutS homolog 2 (MSH2), MSH3 and ribonucleotide reductase regulatory TP53 inducible subunit M2B (RRM2B) as its top hits (J.-M. Lee et al., 2019, 2022). This suggests that DNA-repair mechanisms play a crucial role in keeping the somatic instability of the CAG repeats in check. Patients that carry the *mHTT* gene and have a harming mutation in one of these DNA repair genes could therefore face faster progression of CAG expansion in somatic cells (Goold et al., 2021; Benn, Gibson, & Reynolds, 2021). The increased CAG repeats in those cells are thought to drive increased neurodegeneration and thereby a faster disease progression. Furthermore, it has been observed in brain, liver, and heart tissues that somatic expansion occurs at different rates within cells of the same tissue, resulting in mosaic patterns of *mHTT* CAG lengths (J.-M. Lee et al., 2011; Mouro Pinto et al., 2020). Possibly, this causes cells with an increased CAG length to be more susceptible to disruption of cellular processes and cell death (Donaldson, Powell, Rickards, Holmans, & Jones, 2021).

1.2.4 Molecular pathogenesis of HD

Two hypotheses have been proposed to explain the toxicity of the *mHTT* mutation: the loss-of-function and the gain-of-function hypothesis. HD patients express one *mHTT* allele and one functional wild type (WT) *HTT* allele. This leads to WT HTT being expressed at roughly half of its normal physiological level (Saudou & Humbert, 2016). The loss-of-function hypothesis suggests that this decrease in level of functional HTT causes a diminished capability of HTT to perform its native cellular functions. In the following, this lack of functional HTT then leads to neurodegeneration. On the other hand, the gain-of-function hypothesis suggests that mHTT oligomers and mHTT aggregates gain toxic properties, which impair cellular processes and lead to neurodegeneration in the consequence.

HTT is a large 350 kDA protein, which is conserved among vertebrates. It is expressed during most developmental stages. In adulthood, HTT is expressed throughout the human body, but has its highest expression in the central nervous system. To date, the cellular function of HTT is still not fully understood and it was shown to be active in several cellular compartments. The intracellular localization of HTT is influenced by a variety of post-translational modifications and HTT can be subject to proteolytic activity, which produces HTT fragments with different cellular localization (Maiuri, Woloshansky, Xia, & Truant, 2013; Luo, Vacher, Davies, & Rubinsztein, 2005; Colin et al., 2008). HTT is primarily located in the cytoplasm, but exon-1 HTT fragments were shown to have a higher likelihood of localizing to the nucleus (Mende-Mueller, Toneff, Hwang, Chesselet, & Hook, 2001; Gofflot et al., 2007). Moreover, these modifications were shown to modify the interaction partners of HTT of which HTT was shown to have 200-300 (Saudou & Humbert, 2016; Kaltenbach et al., 2007). Hence, the cellular function of HTT is flexible and is influenced by developmental stage, post-translational modifications and cellular context.

Several pathways are possibly negatively affected by decreased levels of functional HTT. For example, HTT is involved in the autophagic pathway by binding autophagosome and regulating their trafficking to lysosomes. Especially, retrograde transport of autophago-

somes along the axon is regulated by HTT (Wong & Holzbaur, 2014). Additionally, HTT induces selective autophagy by recognizing cargo and bringing cargo into spatial proximity with autophagy initiation components (Rui et al., 2015; Ochaba et al., 2014).

Furthermore, when HTT in translocated to the nucleus, it can suppress or promote transcription through its interaction with transcription factors and transcription activators. HTT interacts with a wide range of TFs, including CREB-binding protein (CBP), tumour protein P53 (P53), nuclear factor 'kappa-light-chain-enhancer' of activated B-cells (NF-κb), neurogenic differentiation 1 (NEUROD1), and transcription activators like TATA-box binding protein associated factor 4 (TAF4) and RE1 silencing transcription factor (REST) (Cong et al., 2005; Steffan et al., 2000; Takano & Gusella, 2002; Marcora, Gowan, & Lee, 2003; Dunah et al., 2002; Zuccato et al., 2003). Through controlling transcription, HTT might be involved in keeping transcriptomic homeostasis.

The functions of HTT go beyond the aforementioned functions as HTT has about 200-300 interaction partners that mediate very different pathways. Other pathways HTT has been shown to be involved in are cell cycle control, chromatin remodelling, tissue maintenance, cell survival, vesicle transport, organelle trafficking, metabolism and synaptic homeostasis (Schulte & Littleton, 2011).

For the loss-of-function theory it can be argued that conditional knockout (KO) in brains of adult mice causes progressive neurodegeneration (Dragatsis, Levine, & Zeitlin, 2000). Furthermore, heterozygous KO of the *HTT* gene in WT and *mHTT* carrier mice lead to increased cognitive decline and motor deficits (Nasir et al., 1995; Van Raamsdonk et al., 2005). Homozygous KO of *HTT* in mice is lethal at embryonic stages (Nasir et al., 1995; Duyao et al., 1995).

In contrast to the loss-of-function hypothesis, the gain-of-function hypothesis proposes that toxic properties of mHTT, rather than the decreased level of functional HTT, are the primary driver of neurodegeneration in HD (Saudou & Humbert, 2016). The expanded CAG repeats of *mHTT* result in an expanded polyQ tract, rendering mHTT more susceptible to binding polyQ tracts of other mHTT proteins (Fig. 1.2). This interaction of multiple mHTT molecules leads to the formation of oligomers and insoluble aggregates, also called inclusions bodies (Sieradzan et al., 1999). Furthermore, mHTT is subject to increased

proteolytic cleavage, resulting in smaller N-terminal fragments containing the polyQ-tract. These mHTT fragments increasingly translocate to the nucleus, where they aggregate and form inclusion bodies (J. P. Miller et al., 2010).

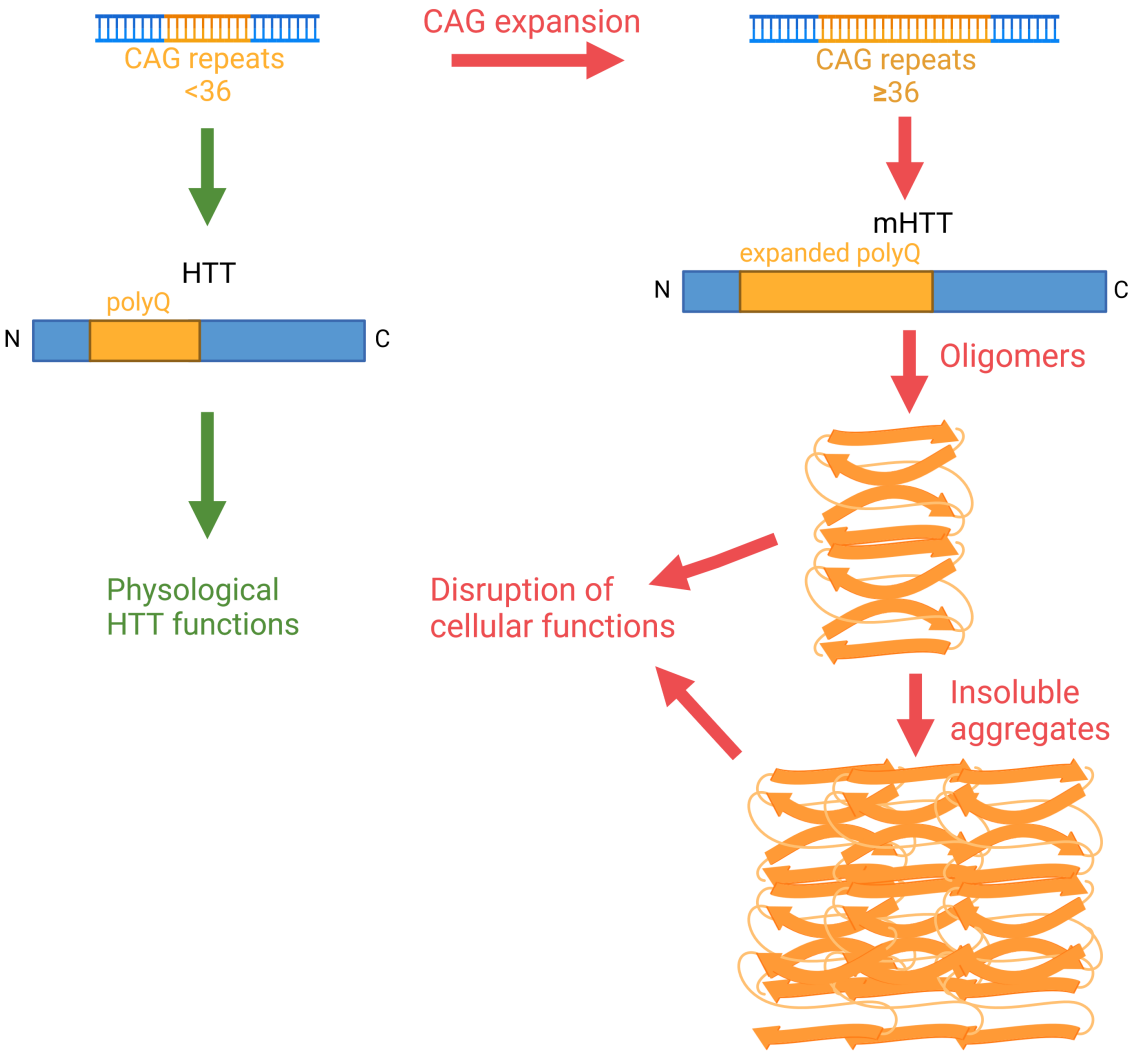

Fig. 1.2: CAG expansion causes mHTT to form aggregates

HTT with less than 36 repeats gives rise to functional HTT. If the CAG repeats exceed 36 repeats, the expanded polyQ tract renders mHTT prone to form oligomers and aggregates. Both, oligomers and aggregates, were shown to disrupt cellular functions (Hoffner & Djian, 2015; Irfan et al., 2022). The figure design was inspired by Jarosińska and Rüdiger (2021).

The gain-of-function hypothesis argues that mHTT oligomers and mHTT aggregates mediate cytotoxicity, driving the neurodegenerative process. Whether mHTT oligomers or

mHTT aggregates are the primary cause of the neurotoxic effect, remains a discussion in the research field of HD (Hoffner & Djian, 2015). So far, multiple cellular processes have been shown to be disrupted by mHTT oligomers and aggregates (Fig. 1.3).

Firstly, other proteins have been shown to co-aggregate with mHTT aggregates. Thereby, co-aggregating proteins are depleted and hindered from fulfilling their physiological function. As mHTT is increasingly translocated to the nucleus, proteins with a nuclear localization are particularly susceptible to co-aggregate (Fig. 1.3). Notably, mHTT aggregates were shown to co-aggregate with TFs like CBP, p53, NF-κb, NeuroD1, and transcription activators like TAF4 and REST (Cong et al., 2005; Steffan et al., 2000; Takano & Gusella, 2002; Marcora et al., 2003; Dunah et al., 2002; Zuccato et al., 2003). Through the depletion of these TFs, mHTT might dysregulate the transcriptome and the down-stream pathways of these TFs. This might affect a wide range of functions, as TFs like CBP and p53 act, on cell cycle, apoptosis, DNA repair and a multitude of other pathways (Illarioshkin, Klyushnikov, Vigont, Seliverstov, & Kaznacheyeva, 2018).

Similar to other NDs, like AD and PD, mitochondrial dysfunction has been associated with HD. Besides regular food intake, HD patients suffer from progressive weight lose, which has in parts been attributed to dysfunction of mitochondria (Jurcau & Jurcau, 2022). Nuclear magnetic resonance spectroscopy measured elevated levels of lactate and decreased activities of oxidative phosphorylation (OXPHOS) complexes II and III in HD patients brain (Browne et al., 1997). Moreover, the transcriptional master regulator for mitochondrial activity, peroxisome proliferator-activated receptor (PPAR)-γ coactivator-1α (PGC-1α) was shown to be impaired in HD (Johri, Chandra, & Beal, 2013). Recent studies showed that mitochondrial membranes are leaky and release mitochondrial RNA (mtRNA) in mHTT overexpressing mouse models (Fig. 1.3) (Wertz et al., 2020). In addition, interaction sites of mitochondria with the endoplasmic reticulum (ER) are disrupted, causing drawbacks in Ca^{2+} efflux and increased reactive oxygen species (ROS) production in mHTT overexpressing mouse models (Cherubini, Lopez-Molina, & Gines, 2020).

Furthermore, mHTT aggregates were shown to sequester mammalian target of rapamycin (mTOR), an inhibitor of autophagy. The sequestration of mTOR was shown to activate the autophagy pathway in a variety of HD models (Ravikumar et al., 2004).

In support of this, further studies reported an increased number of lysosomes in cellular and mouse models of HD (Martinez-Vicente et al., 2010; Erie, Sacino, Houle, Lu, & Wei, 2015). Interestingly, at the same time, cargo recognition and cargo loading into autophagosomes is defective leading to lysosomes with decreased cargo (Fig. 1.3) (Wong & Holzbaur, 2014). Thereby, the capability of cells to degrade proteins and organelles is decreased in mHTT expressing HD models (Martin et al., 2014).

Another structure commonly shown to be involved in HD pathogenesis is the ER, which will be discussed in chapter in 1.4 in more detail.

The gain-of-function hypothesis receives strong experimental support. A range of neurotoxic effects observed in HD patients are replicable in model organisms through the expression of a *mHTT* construct, even in the presence of two functioning *HTT* alleles (Menalled et al., 2009). Moreover, mouse models overexpressing *mHTT* exhibit more pronounced symptoms compared to mouse models with decreased *Htt* expression (Menalled et al., 2009). In addition, the overexpression of mHTT causes cell death in a range of *in vitro* models (C. Song, Perides, & Liu, 2002; Takahashi et al., 2008; J. Miller et al., 2010). Additionally, introduction of expanded CAG repeats into a gene, which is otherwise unrelated to neurodegeneration, results in the aggregation of the expressed protein in model mice, followed by neurodegeneration resembling that observed in polyQ disorders (Ordway et al., 1997).

Which or what combination of the above-mentioned causes leads to the neuronal death remains highly discussed in the field. It can be speculated, that several of the above-mentioned mechanisms and both, the loss-of-function and gain-of-function, contribute to the pathogenesis of HD (Saudou & Humbert, 2016; Illarioshkin et al., 2018). However, due to its strong experimental support and replicability across various models, the toxic gain-of-function of *mHTT* is thought to be the more crucial driver of neurodegeneration.

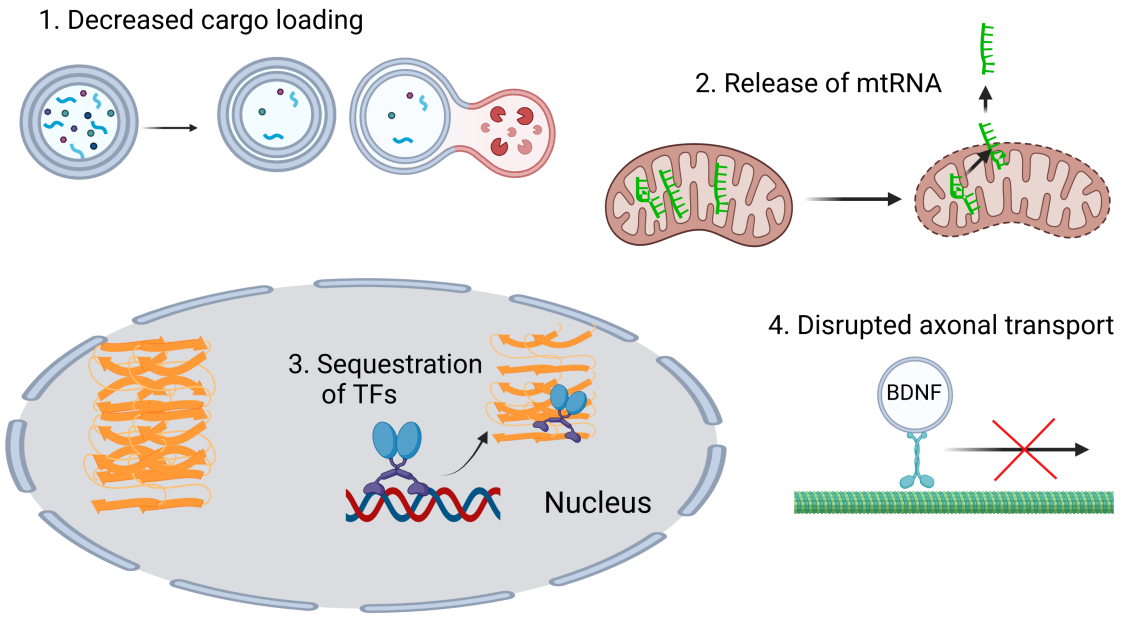

Fig. 1.3: Cellular processes disrupted in the presence of mHTT

The gain-of-function hyptothesis proposes, that mHTT disrupts cellular processes and thereby drives cell death. MHTT aggregation was shown to coincide with (1.) deficient cargo loading into autophagosomes, (2.) leaky mitochondrial membranes and the release of mtRNA, (3.) dysregulation of the transcriptome through the sequestration of TFs, and (4.) inefficient BDNF transport along axons (Wong & Holzbaur, 2014; Wertz et al., 2020; Illarioshkin et al., 2018; Zuccato et al., 2001).

1.2.5 Selective vulnerability in HD

A characteristic feature shared by NDs is the phenomenon of "selective vulnerability", which describes that certain brain regions and specific neuronal populations within these regions display varying susceptibilities to the pathological processes of NDs (Fu et al., 2018). The pattern of neuronal loss is specific for the individual NDs, and likely gives rise to the disease-specific set of symptoms. For instance, in early stages of AD, large pyramidal cells in the entorhinal cortex and in the hippocampus undergo neurodegeneration, likely contributing to the characteristic memory loss experienced by AD patients (Fu et al., 2018; Z.-T. Wang et al., 2020).

While *HTT* is expressed ubiquitously throughout the central nervous system, neurodegeneration most strongly affects the striatum and the cortex in HD (Strong et al., 1993;

Goto, Hirano, & Rojas-Corona, 1989; Morton, Nicholson, & Faull, 1993; Nana et al., 2014). The striatum, a nucleus of the basal ganglia, which is crucial for motor control, is thought to be the most susceptible region to HD (Blumenstock & Dudanova, 2020; Goto et al., 1989). In the striatum, the gamma-aminobutyric acid (GABA) producing medium spiny neurons (MSNs) undergo progressive degeneration. Loss of MSNs can be detected as early as 15 years before disease onset, and the progressive degeneration leads to up to 95% loss of MSNs being detected in post-mortem human tissue (Vonsattel & DiFiglia, 1998; Tabrizi et al., 2009). In contrast, locally projecting interneurons of the striatum are mostly spared, with the exception of parvalbumin (PV) expressing interneurons, which suffer from cell loss to a lesser extent (Reiner et al., 2013).

The cortex, particularly the MC, represents the second most affected brain region in HD. The MC consist of about 80% glutamatergic cortical projection neurons (CPNs) and around 20% locally projecting GABAergic interneurons (Huang, 2014; Blumenstock & Dudanova, 2020). The CPNs can be separated into several populations by their projection target and the cortical layer they are located in (Yao, Liu, et al., 2021; Yao et al., 2023). The most populous of the CPNs are intratelencephalic (IT) neurons, which primarily project to the striatum (Reiner, Hart, Lei, & Deng, 2010; Yao, Liu, et al., 2021). CPNs projecting outside the telencephalon are called extratelencephalic (ET) neurons, and they mostly project down the pyramidal tract to the spinal cord, where they are responsible for the induction of movement (Reiner et al., 2010; Moberg & Takahashi, 2022). Cortico-thalamic (CT) neurons project to the thalamus (Briggs & Usrey, 2008) (Fig. 1.4). Near-projection (NP) neurons project to the contralateral cortex hemisphere (E. J. Kim, Juavinett, Kyubwa, Jacobs, & Callaway, 2015; Yao, van Velthoven, et al., 2021). Together, these CPN populations make up the output circuit of the MC, whose most prominent function is the preparation and execution of movement (Park et al., 2022).

Interneurons of the MC project locally and are involved in the local network adjustment. Interneurons are subdivided by their expression of marker genes and can be separated into somatostatin (*Sst*), *Pv*, vasopressin (*Vip*), synuclein gamma (*Sncg*), and lysosomal associated membrane protein family member 5 (*Lamp5*) populations (Fig. 1.4) (Reiner et al., 2010; Yao, Liu, et al., 2021).

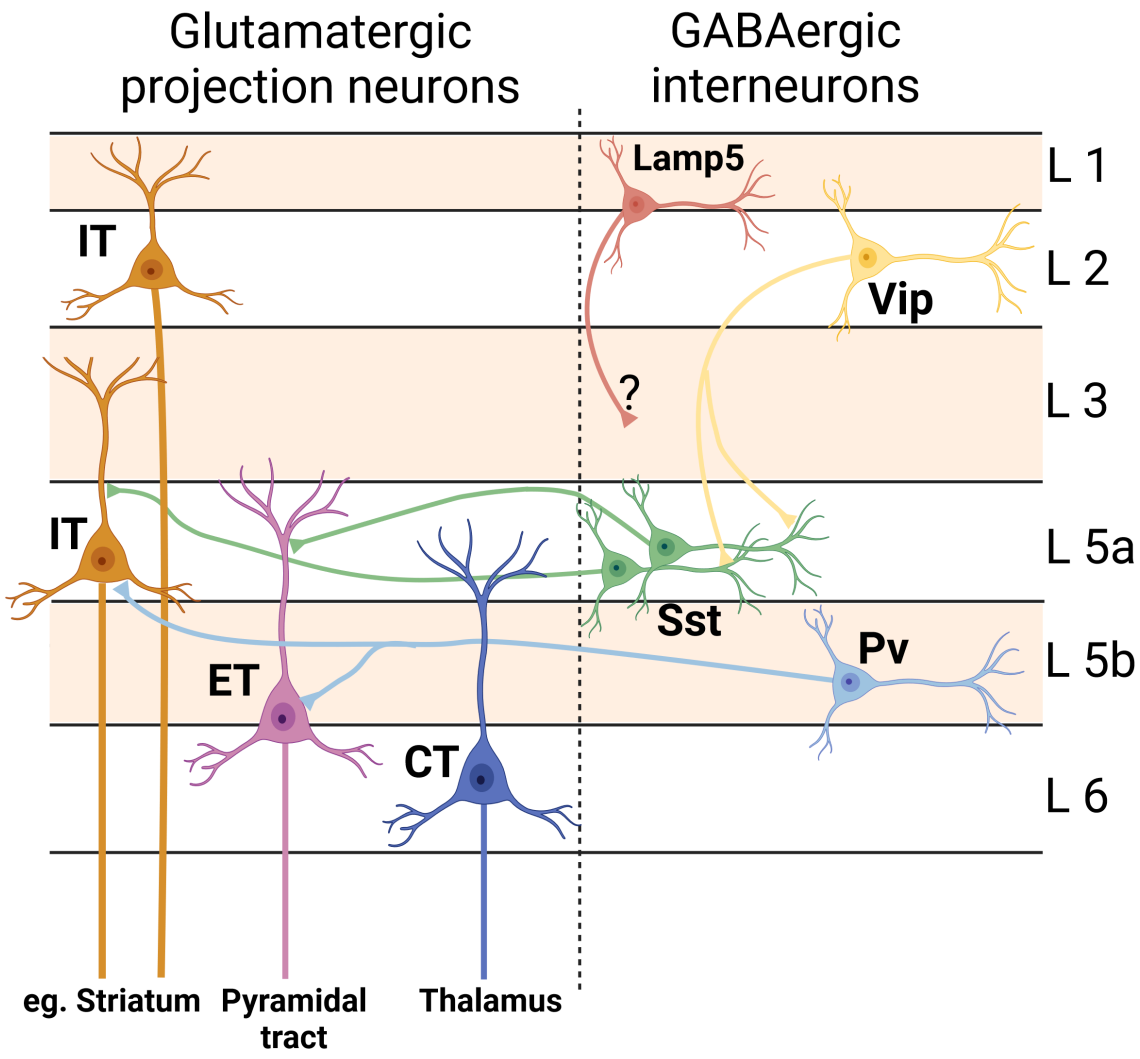

Fig. 1.4: Neuronal populations of the motor cortex

Scheme showing a subset of the neuronal populations, connectivities within the MC and outputs of the MC. Based on figures from McColgan, Joubert, Tabrizi, and Rees (2020) and Blumenstock and Dudanova (2020).

In HD, the MC undergoes cortical thinning and neurodegeneration (Rosas et al., 2002). Especially CPNs are lost in HD and depending on the study, an average loss of 27% and 42% of CPNs in post-mortem tissue was measured (Thu et al., 2010; Macdonald & Halliday, 2002). Among the CPNs, IT neurons are thought to be particularly susceptible (Bunner & Rebec, 2016; Rebec, 2018; Pressl et al., 2024). Similar to the striatum, locally projecting interneurons of the MC are less susceptible to neurodegeneration (Han, You, Kordower, Brady, & Morfini, 2010). Notably, the amount of neurodegeneration of the MC

correlates with the CAG repeat length (Halliday et al., 1998). Moreover, the intensity of motor symptoms of HD patients correlates with the amount of cell loss in the primary MC highlighting the role of the MC in HD pathogenesis (Thu et al., 2010).

Why selective vulnerability affects MSNs and CPNs has been a long-standing, yet unanswered question in the field of HD. Various hypotheses have been proposed for the emergence of the pattern of selective vulnerability. Potential causes include cell intrinsic properties, biochemical factors the neurons are exposed to and the connectivity network each of these neuronal populations is embedded in.

One potential cause for the increased vulnerability to HD pathogenesis could be that both, MSNs and CPNs, demand a high level of energy (Fu et al., 2018; Moya et al., 2022). Mitochondrial dysfunction, as mentioned earlier, might result in an energy deficit for these metabolically active neurons, rendering them more susceptible than the less energy intensive interneurons (Carmo, Naia, Lopes, & Rego, 2018; H. Lee et al., 2020). The energy deficit might affect energy intensive pathways like autophagy and in consequence insufficient clearing of misfolded proteins and impaired proteostasis.

Moreover, brain-derived neurotrophic factor (BDNF) has been shown to be crucial for survival of MSNs. However, BDNF is not synthesized in the striatum but in the cortex by projection neurons. In HD, a dysfunction of transport of BDNF along the axons of projection neurons to the striatum was shown, which consequently could lead to a fatal lack of BDNF in the striatum (Fig. 1.3) (Zuccato et al., 2001; Zuccato & Cattaneo, 2007; Gauthier et al., 2004).

Regarding the selective vulnerability of projection neurons in the cortex, the "dying back" theory has been proposed. It speculates that the initial demise of MSNs in the striatum leads to a loss of target neurons for CPNs. Without sufficient target neurons and synaptic connections, cortical projection neurons undergo degeneration (Han et al., 2010).

While a multitude of potential explanations have been discussed within the research field of NDs, the questions of how selective vulnerability arises still lacks an answer. Gaining insights into the factors responsible for selective vulnerability could contribute to explaining the progression of HD, unravel the mechanisms leading to the cell death of specific neuronal populations and ultimately developing a cell population-targeted,

disease-modifying therapeutic.

1.2.6 The R6/2 mouse model of HD

Most NDs, including AD, PD, and ALS are multicausal diseases where various factors influence the occurrence of the disease. In contrast, HD stands out from these NDs as a monogenetic disorder. Therefore, generation of HD mouse models most often relies on a single genetic factor in form of the *HTT* gene, and such models are most often generated by introduction of a *mHTT* gene into the mouse genome. Several mouse models have been generated through the introduction of a full-length *mHtt*, *mHTT* fragments or the knocking-in of CAG repeats into the endogenous mouse *Htt* allele (Gray et al., 2008; Sathasivam et al., 1999; Peng et al., 2016). The earliest generated HD mouse models were the R6 lines, for which the exon-1 of human *mHTT* was introduced into the mouse genome as a transgene (Sathasivam et al., 1999). The most popular of these mouse models is the R6/2 mouse, which expresses the human exon-1 *mHTT* with originally around 144 CAG repeats under the human *HTT* promotor (Mangiarini et al., 1996). Over the years, the CAG tract expanded and the R6/2 lines commonly available tend to have longer CAG repeats of around 160 to 170 repeats (D. M. Cummings et al., 2012).

Limitations of the R6/2 mice include the unusually long CAG repeat length, which normally does not occur as an inherited CAG repeat length in HD patients. This is a common limitation across all HD mouse models, as a CAG repeat length below 80 in *Htt* does not result in any phenotype in mice (Schilling et al., 2004; Morton, Skillings, Wood, & Zheng, 2019). Moreover, the R6/2 model only models the toxicity caused by the gain-of-function of *mHTT*, as the mouse still possesses two WT *Htt* alleles.

The R6/2 mouse model is a rather fast progressing mouse model of HD, with intranuclear mHTT aggregates appearing in the striatum and cortex before 5 weeks of age (Sathasivam et al., 1999; Stack et al., 2005; Voelkl, Schulz-Trieglaff, Klein, & Dudanova, 2022). At around 9 weeks, both the striatum and cortex undergo atrophy in R6/2 mice (Fig. 1.5). Notably, it is thought that little to no cell death occurs and the atrophy is thought to be caused by degeneration and demyelination of axons rather than cell loss (Stack et al., 2005; Dodds, Chen, Berggren, & Fox, 2014). R6/2 mice exhibit HD-like motor symptoms

including tremor, motor imbalance and coordination deficits. Typically, R6/2 mice die after 12 to 20 weeks of age, depending on the CAG repeat length in the *mHTT* allele (Sathasivam et al., 1999; Stack et al., 2005).

One important advantage of the R6/2 mouse model is that atrophy occurs without cell death allowing researchers to study the effects of *mHTT* on vulnerable cells with electrophysiology, transcriptomics, proteomics and the effect of drugs. This makes the R6/2 mouse model one of the best characterized and most often used mouse models for HD (Menalled et al., 2009).

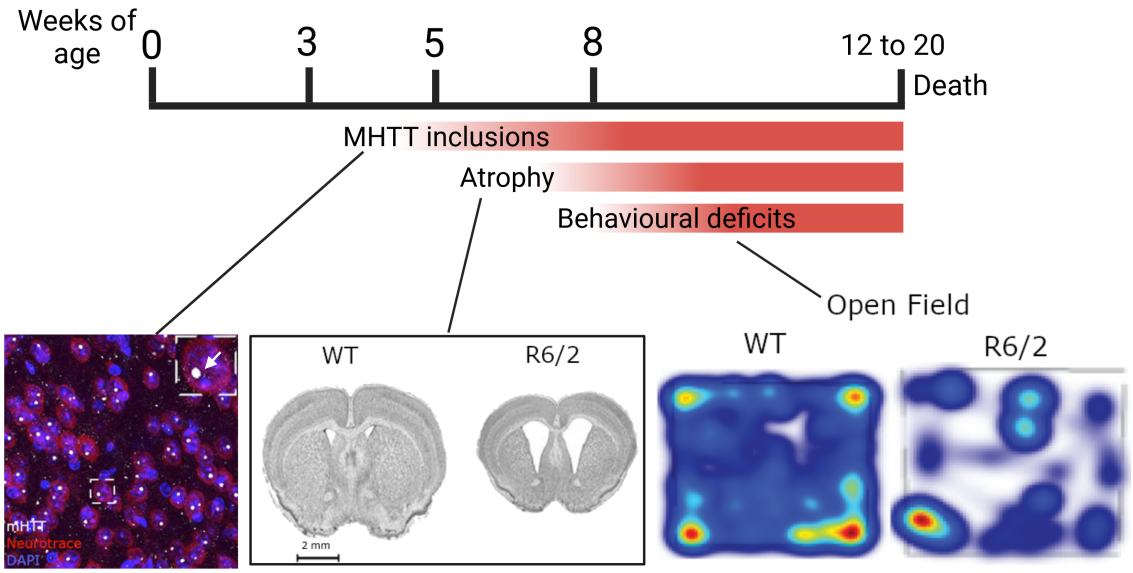

Fig. 1.5: Disease progression in the R6/2 mouse model

The R6/2 mouse is a fast progressing mouse model of HD. mHTT inclusion bodies can be detected by 5 weeks of age, followed by atrophy and behavioural deficits. R6/2 mice usually die between week 12 to 20 depending on the CAG repeat length in the *mHTT* allele (Menalled et al., 2009). The confocal image of mHTT aggregates in the MC was taken by Kerstin Voelkl. Images of brain sections from WT and R6/2 mice are taken from Stack et al. (2005). Heat maps of open field experiments comparing WT and R6/2 mice were done by Sara Gutiérrez-Ángel.

1.3 ER stress and ER-phagy in HD

1.3.1 ER structures and functions in HD

The ER is a vast, continuous, membranous organelle spanning the cytoplasm. The ER has a multitude of functions including protein synthesis, protein folding, protein maturation, lipid synthesis and acting as a Ca^{2+} storage, regulating intracellular Ca^{2+} levels. The ER comprises three major domains: the nuclear envelope (NE) surrounding the nucleus, responsible for selective molecular transport into the nucleus; ER sheets, mainly involved in protein synthesis and folding; and the tubular ER, located in the cell periphery and extending into axons and dendrites of neurons, serving as a crucial Ca^{2+} reservoir for neuronal signalling (Schwarz & Blower, 2016).

As the ER is essential for proteostasis, the ER continually monitors the level of unfolded and misfolded proteins within its lumen. Upon accumulation of misfolded or unfolded proteins, also called ER stress, the ER triggers an adaptive mechanism to restore proteostasis, called unfolded protein response (UPR) (Read & Schröder, 2021). There are three known pathways of the UPR. All of them are triggered by the central ER chaperone heat shock protein family A (Hsp70) member 5 (HSPA5), also known as binding immunoglobulin protein (BiP) (Kaufman et al., 2002; Bertolotti, Zhang, Hendershot, Harding, & Ron, 2000). Under non-stress conditions, HSPA5 binds to transmembrane ER stress sensors (Fig. 1.6). When unfolded or misfolded proteins accumulate in the ER lumen, HSPA5 binds to the misfolded or unfolded proteins and dissociates from the transmembrane ER stress sensors. These ER stress sensors then trigger a pathway, which induces the expression of UPR target genes. For instance, the ER stress sensor inositol-requiring enzyme 1 (IRE1) dimerizes, when it is not bound by HSPA5 under ER stress conditions. IRE1 dimers then catalyse the splicing of the TF X-box binding protein 1 (*XBP1*) (Fig. 1.6) (Joshi et al., 2015). The spliced form of *XBP1* (*XBP1s*) translocates to the nucleus, where *XBP1s* promotes the transcription of various UPR target genes including ER and Golgi structural component, several chaperones like DnaJ heat shock protein family (Hsp40) member B9 (*DNAJB9*) and *HSPA5* itself (A.-H. Lee, Iwakoshi,

& Glimcher, 2003; Acosta-Alvear et al., 2007; Uemura, Oku, Mori, & Yoshida, 2009). *XBP1s* also promotes the transcription of genes of the ER-related degradation (ERAD) pathway (Frakes & Dillin, 2017). ERAD is a degradatory process for misfolded proteins, in which misfolded proteins get transported from the ER lumen to the cytosol. There, the misfolded proteins get polyubiquitinated and degraded by the proteasome.

Due to the role of the ER and the UPR in protein homeostasis, the ER has often been linked with NDs. Cellular models of HD showed an upregulation of the UPR upon the formation of mHTT oligomers, preceding the occurrence of large aggregates (Leitman, Ulrich Hartl, & Lederkremer, 2013). This was caused by the mHTT oligomers inhibiting ERAD, which, in consequence, led to the accumulation of misfolded proteins in ER lumen. This accumulation of misfolded proteins subsequently triggered the UPR (Leitman et al., 2013; Duennwald & Lindquist, 2008). In HD mouse models, ER showed swelling, which is one of the hallmarks of ER stress (Trettel et al., 2000). ER stress is an early event in HD and ER stress precedes symptom onset in HD model mice (Carnemolla et al., 2009). Furthermore, ER stress marker mRNAs of *HSPA5* and homocysteine inducible ER Protein with ubiquitin like domain 1 (*HERPUD1*) were upregulated in post-mortem cortex tissue of HD patients (Carnemolla et al., 2009). While initial activation of the UPR can be beneficial for restoring proteostasis, chronic activation of the UPR triggers apoptotic pathways and can lead to cell death (Sano & Reed, 2013; Kalathur et al., 2015).

In summary, mHTT oligomers cause the inhibition of the ERAD and thereby decrease the capability of protein folding and degradation in the ER. This causes a disruption of ER proteostasis and triggers the UPR (Leitman et al., 2013). Increasing the capability of the ER to restore proteostasis or dampening ER stress might be beneficial for preventing neurodegeneration in HD (X. Wu & Rapoport, 2018).

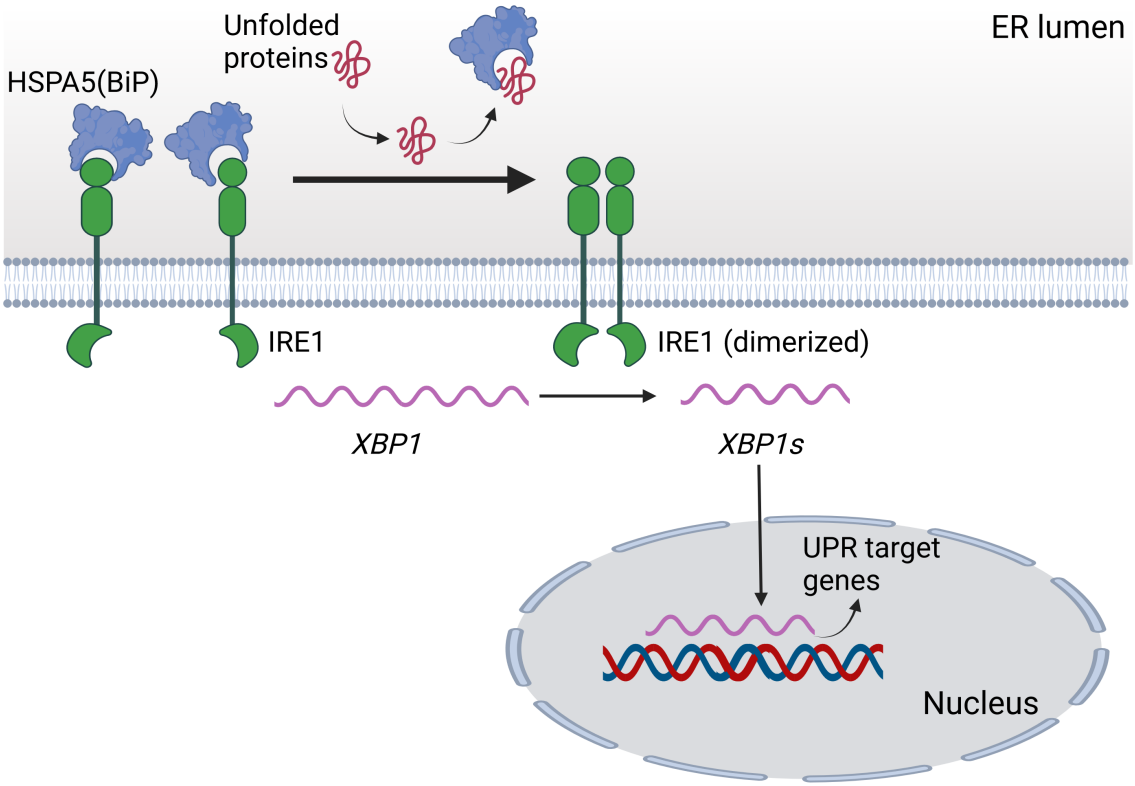

Fig. 1.6: ER stress causes the activation of the UPR via the IRE1 pathway
ER-stress triggers the UPR by HSPA5 dissolving from IRE1 to bind unfolded proteins. IRE1 dimerizes and splices *XBP1*. *XBP1s* then increases the transcription of UPR target genes.

1.3.2 ER-phagy

Under ER stress conditions, the ER tries to restore proteostasis by triggering UPR and ERAD (Read & Schröder, 2021; X. Wu & Rapoport, 2018). Another mechanism gaining increasing attention in recent years for its role in ER proteostasis and ER reshaping is ER autophagy, also known as ER-phagy (Yang et al., 2021). In ER-phagy, segments of the ER which are damaged, are being reshaped or degraded during starvation through engulfment by autophagosomes. These autophagosomes then fuse with lysosomes, leading to the degradation of the ER cargo (Chino & Mizushima, 2020; Yang et al., 2021).

ER-phagy is directed to specific ER compartments by ER-phagy receptors located on the ER membrane. These ER-phagy receptors recruit the autophagosome machinery to the designated region of the ER. So far, six mammalian membrane-anchored ER-phagy

receptors have been identified, each characterized by their functional domain on the ER and the conditions under which they get activated (He, Qian, & Cui, 2021). For example, SEC62 homolog, preprotein translocation factor (SEC62) is located on the NE and is responsible for nucleophagy, a subtype of ER-phagy. Testis expressed gene 264 (TEX264) mediates ER-phagy of ER-sheets and Reticulon 3 (RTN3) mediates ER-phagy of the tubular ER (Fig. 1.7).

A recent study showed that ER-phagy is able to degrade α-Syn, which forms the characteristic aggregates in PD, from the ER and restore ER functionality (D. Y. Kim et al., 2023). Despite increasing attention in the ER research field, so far, ER-phagy has not yet been linked with HD to our knowledge. However, as our understanding of ER-phagy continues to evolve, future research may uncover its potential implications in various cellular processes and disease contexts, including HD.

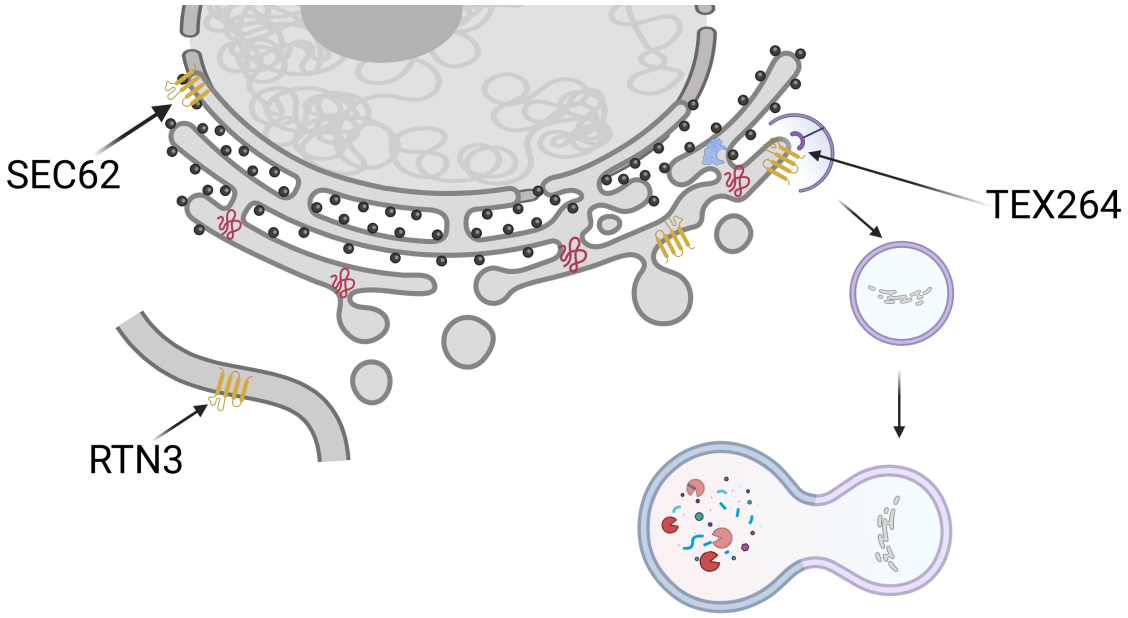

Fig. 1.7: ER-phagy receptors mediate autophagy of the ER
ER-phagy is mediated by ER-phagy receptors. Specific ER-phagy receptors recruit the autophagy machinery to specific ER compartments (Yang et al., 2021).

1.4 The role of the chaperone proSAAS in NDs

Chaperones play a crucial role in maintaining proteostasis by participating in protein quality control, translation, protein folding, protein processing, and protein degradation (Chaplot, Jarvela, & Lindberg, 2020). Given their importance in proteostasis, it is no surprise that chaperones are prominently implicated in NDs in which disruption of proteostasis is a central mechanism of pathogenesis.

The chaperone proprotein convertase subtilisin/kexin type 1 inhibitor (proSAAS, gene name: *PCSK1N*) was initially described as a secreted chaperone (Fricker et al., 2000). Secreted chaperones like proSAAS are released to the extracellular matrix, where they assist in protein folding or can be taken up by other cells through endocytosis (Chaplot et al., 2020). Other examples for secretory chaperones are Secretogranin V (SCG5), integral membrane protein 2b (ITM2B) and serpin family I member 1 (SERPINI1). For instance, SCG5 was shown to prevent the aggregation of several ND-related proteins, including Aβ_{1-42} and α-Syn (Helwig et al., 2013). ProSAAS is a 225-residue polypeptide, which is predominantly expressed in neural and endocrine tissues (Fricker et al., 2000; Lanoue & Day, 2001). Notably, proSAAS was demonstrated to colocalize with extracellular Aβ deposits in the brain of AD patients. Furthermore, proSAAS was able to prevent the fibrillation of Aβ_{1-42} *in vitro* (Hoshino et al., 2014).

Interestingly, proSAAS was also shown to act intracellularly in response to cell stress. In particular ER stress was shown to increase the expression of proSAAS and additionally, promotes its cellular retention (Shakya, Yildirim, & Lindberg, 2020). It was speculated that intracellular retention of proSAAS may serve a defence mechanism to mitigate cytototoxic damage and enhance cell viability during periods of increased cellular stress (Shakya et al., 2020). Furthermore, cytoplasmic proSAAS constructs have been observed to form intracellular spheres with liquid droplet-like properties, which encapsulated cytoplasmic TDP-43 aggregates and thereby, act as a cytoprotectants (Peinado et al., 2022). Additionally, an artificial proSAAS construct, with the substitution of four lysines for arginines, was shown to translocate to the nucleus, suggesting the potential for proSAAS to exert nuclear functions (Peinado et al., 2022).

Despite these intriguing findings in other NDs, research on the involvement of secreted chaperones and proSAAS in HD remains scarce. No studies investigating the role of proSAAS in HD have been conducted to our knowledge.

1.5 The emergence of single-cell RNAseq technologies

In recent years, the field of transcriptomics has witnessed a massive leap forward with the advent of single-cell RNA sequencing (scRNA-seq) technologies. Traditional RNA-seq methods relied on sequencing a bulk of cells or tissue, resulting in average expression values for the whole tissue. scRNA-seq technologies are able to capture each cell separately and thereby retrieve the transcriptome for each cell individually (Macosko et al., 2015; Haque, Engel, Teichmann, & Lönnberg, 2017). This enables the identification of cellular diversity within the tissue and the individual transcriptomic changes of cell types in different contexts, such as developmental stages, age, drug treatment or diseases.

One of the most widely used technologies for scRNA-seq is the 10X Chromium technology, which utilizes droplets to capture individual cells and subsequently add unique barcodes to the mRNA of captured cells. Afterwards, cells are lysed and the origin of each mRNA can be traced back to the cell of origin with the barcodes. This method gained popularity due to its high throughput, enabling the capture of up to 12,000 cells per experiment (Macosko et al., 2015). In recent years, single-nucleus RNA-seq (snRNA-seq) has become increasingly popular, as nuclei are more reliable to isolate from fragile cells, interconnected tissue and post-mortem frozen tissue (Mathys et al., 2019). Instead of using whole cells, for snRNA-seq nuclei are isolated and used for sequencing (Habib et al., 2017). snRNA-seq was shown to deliver similar results in terms of cell type capturing to scRNA-seq with whole cells (Bakken et al., 2018). In particular, in the field of neurodegeneration, snRNA-seq has proven superior over scRNA-seq , as neurons are very fragile and neurons of adult mouse tissue are highly interconnected (Bakken et al., 2018; Malaiya et al., 2021).

The widespread adoption of scRNA-seq was heavily supported by advances in the fields of microfluidics, barcode technology and sequencing technology. Another pivotal development is the development of scRNA-seq atlases. These atlases constitute publicly

available, curated datasets for a specific tissue or region with annotated cells types (Yao, van Velthoven, et al., 2021). Prior to the introduction of scRNA-seq atlases, researchers relied on clustering methods, which are based on individually chosen parameters, thereby resulting in subjective choices for cell type annotation. With the availability of scRNA-seq atlases, researchers can integrate their data sets into reference atlas and thereby identify the cell types in their own data set (Webb & Haniffa, 2023). Consequently, these atlases play a crucial role in achieving a much-needed unified annotation of cell types.

An outstanding role has the Brain Initiative Cell Census Network (BICCN) by the Allen Brain Institute, as the BICCN published the first single-cell teanscriptomics atlas for the mouse MC in 2019, and recently, a whole brain atlases for the whole mouse brain (Yao, Liu, et al., 2021; Yao et al., 2023). Their annotation approach encompasses three levels of neuronal cell annotation: cell class, marked by common neurotransmitter expression(e.g., GABAergic, glutamatergic); cell subclasses, categorized by their cortical layer and projection targets (e.g., L5 IT); and cell types, distinguished primarily by their transcriptomic profiles (Yao, van Velthoven, et al., 2021; Yao, Liu, et al., 2021) (Fig. 1.8). As the BICCN atlases represent by far the most comprehensive efforts for a unified cell annotation, the BICCN MC atlas will also be used as a reference atlas for the snRNA-seq data set of this thesis.

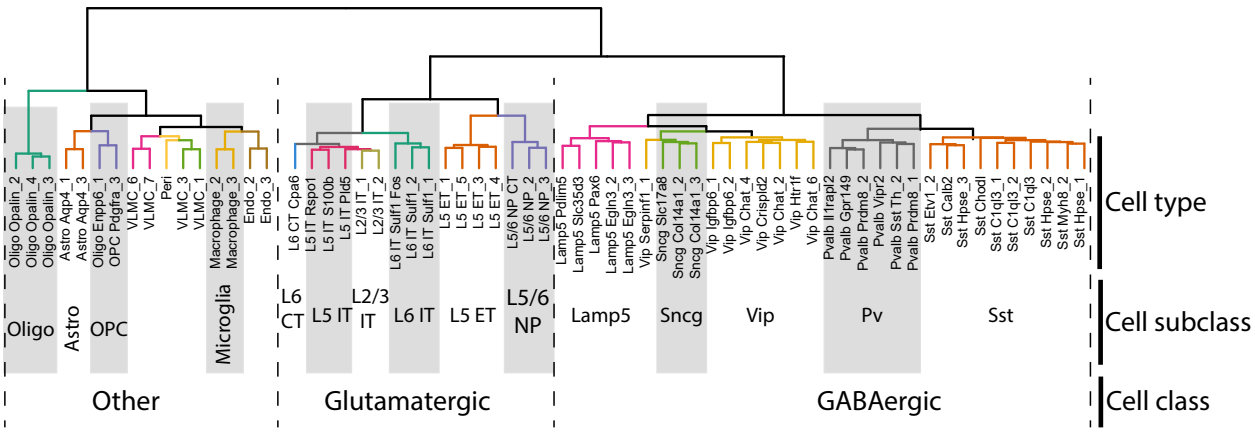

Fig. 1.8: Hierarchical annotation for cell types of the BICCN

The BICCN classifies cells on three levels: cell class, cell subclass and cell type. Here, the cell types identified in our data set are shown and their transcriptomic correlation is depicted as a dendrogram. Furthermore, the cell subclass and cell class each cell type is part of are indicated. The design of the figure is based on Yao, Liu, et al. (2021).

After the cellular diversity of the brain areas is being more and more uncovered, the research focus is now shifting towards investigating the involvement of specific cell populations in disease contexts. This promises a much more defined way of resolving the role of different cellular populations, surpassing the traditional bulk RNA-seq methods. Especially in the field of NDs, where selective vulnerability affects neuronal populations differentially, scRNA-seq promises to give rise to a more comprehensive understanding of the role of the distinct cell populations.

1.6 Ultimate goal and specific aims

New therapeutic approaches for HD rely heavily on understanding the molecular mechanism contributing to neurodegeneration and why certain cell populations show an increased vulnerability to these disease mechanisms. However, studies using post-mortem tissue from HD patients are limited to observing the disease at a single time point and can not capture the vulnerable cell populations, as they are already lost in post-mortem tissue. Therefore, the overall goal of this study is to identify novel pathways involved in the pathogenesis in vulnerable cell populations and which could be intervention points for a therapeutic treatment for HD.

In this study, this goal is achieved through leveraging the potential offered by the snRNA-seq technology to investigate the roles of the various cell populations within the MC in HD, utilizing the R6/2 mouse model (1). Moreover, we will conduct snRNA-seq across multiple time points allowing us to compare early and late stage transcriptomic changes, and uncover the transcriptomic dynamics with disease progression in R6/2 mice (2). Finally, we aim to uncover novel pathways that contribute to the molecular pathogenesis of HD and explore how these mechanisms could give rise to the pattern of selective vulnerability (3).

2 Materials and Methods

2.1 Materials

2.1.1 Sterile experiments

Tab. 2.1: Materials for sterile experiments

Product	Manufacturer	Catalogue Nr.
B-27 Supplement	Thermo Fisher Scientfic	17504044
Borax	Sigma-Aldrich	71997
Boric acid	Sigma-Aldrich	B0394
Dulbecco's Modified Eagle Medium (DMEM), high glucose	Thermo Fisher Scientific	41965062
DNAse I	Thermo Fisher Scientific	EN0521
Doxycycline Hyclate	Sigma-Aldrich	D9891
Dulbecco´s Phosphate Buffered Saline (PBS)	Sigma-Aldrich	D8537
Fetal bovine serum (FBS)	Sigma-Aldrich	F7524
Hanks' Balanced Salt Solution (HBSS)	Thermo Fisher Scientific	24020-117
HEPES	Biomol	05288-100
L-Glutamine	Thermo Fisher Scientific	25030123
Laminin	Gibco	23017015
Lenti-X Concentrator	Takara Bio	631232
Lipofectamine LTX Reagent	Thermo Fisher Scientific	A12621
MEM non-essential amino acids (NEAA)	gibco	1140-035
$MgSO_4$	Sigma-Aldrich	M2643
Microscope cover glasses	vwr	631-1578
Neurobasal medium	Thermo Fisher Scientific	21103049
Opti-MEM	gibco	31985-070
Paraformaldehyde (PFA), 4% in PBS	Thermo Fisher Scientific	J19943.K2
Penicillin/Streptomycin	Thermo Fisher Scientific	10378016
Poly-D-Lysin-hydrobromid (PDL)	Sigma-Aldrich	P7886
Puromycin	MP Biomedicals	11497610
TransIT-Lenti Transfection Reagent	mirus bio	MIR 6603
Triton X-100	Carl Roth	6683.1
Trypsin-EDTA solution	Sigma-Aldrich	T4299

2.1.2 Non-sterile experiments

Tab. 2.2: Materials for non- sterile experiments

Product	Manufacturer	Catalogue Nr.
2-mercaptoethanol	Sigma-Aldrich	M-7522
Albumine Fraction V (BSA)	Carl Roth	8076.4
$CaCl_2$	Sigma-Aldrich	C1016
Chromium Single Cell 3' reagent kit v3.1	10X Genomics	PN-1000121
Chromium Next GEM Chip G Single Cell Kit	10X Genomics	PN-1000120
Chromium Controller	10X Genomics	PN-120223
D-Glucose anhydrous	vwr	MOLE13002238
DAPI	Sigma-Aldrich	D9542
Dilution buffer from the Phire Tissue Direct PCR Master Mix Set	Thermo Fisher Scientific	F170S
DNARelease additive from the Phire Tissue Direct PCR Master Mix Set	Thermo Fisher Scientific	F170S
Dounce Tissue Grinder 2ml	DWK Life Sciences	D8938-1SET
Epredia SuperFrost Plus Slides	Thermo Fisher Scientific	10149870
KCl	Sigma-Aldrich	P9541
Ketamine 10%	MEDISTAR	
K_2SO_4	Sigma-Aldrich	60528
$Mg(CH_3COO)_2$*4 H_2O	Sigma-Aldrich	12664957
$MgCl_2$	Sigma-Aldrich	M8266
NaCl	Sigma-Aldrich	S3014
NaN_3	Sigma-Aldrich	S2002
Na_2SO_4	Sigma-Aldrich	71959
Normal donkey serum	abcam	ab7475
OptiPrep Density Gradient Medium	Sigma-Aldrich	D1556
Platinum II Hot-Start Green PCR Master Mix	Invitrogen	F170S
Pre-Separation Filters, 30 µm	Milenty Biotec	130-041-407
ProLong Glass Antifade Mountant	Thermo Fisher Scientific	14001013
Sartorius Minisart NML Syringe Filters 0.45 µM	Thermo Fisher Scientific	10109180
Single Index Kit T Set A	10X Genomics	PN-1000213
Sodium chloride (NaCl)	Sigma-Aldrich	S7653
Sorenson Dolphin microcentrifuge tubes	vwr	SORE27270
Sucrose	Sigma-Aldrich	S0389
SUPERaseIn RNase Inhibitor	Invitrogen	AM2694
Tergitol, type NP-40, 70% in H_2O	Sigma-Aldrich	NP40S
Trizima hydrochloride solution, pH 7.8	Thermo Fisher Scientific	T2569
UltraPure 0.5M EDTA, pH 8.0-4	Thermo Fisher Scientific	15575020
Xylazine 2%	MEDISTAR	

2.1.3 Antibodies

Tab. 2.3: Primary Antibodies

Antigen	Host	Dilution	Manufacturer	Catalogue Nr.
His-tag	Mouse	1:500	Diazol	Dia-900-100
Myc-tag	Chicken	1:500	Invitrogen	A21281
ProSAAS	Rabbit	1:200	Sigma-Aldrich	ABN2268

Tab. 2.4: Secondary Antibodies

Target species	Host	Fluorophore	Manufacturer	Catalogue Nr.
Chicken	Donkey	Alex fluor 647	Jackson	703-605-155
Mouse	Donkey	Alex fluor 647	Jackson	715-065-140
Rabbit	Donkey	Alex fluor 488	Jackson	711-545-152

All secondary antibodies (ABs) were diluted 1:250 for immunocytochemistry (ICC).

2.1.4 Plasmids

Tab. 2.5: Plasmids

Insert	Vector	Origin
HTTQ25-His	pcDNA3.1	Cloned by Kerstin Voelkl and Sophie Keeling[1]
HTTQ72-His	pcDNA3.1	Cloned by Kerstin Voelkl and Sophie Keeling[1]
HTTQ25-Myc	pPGK	Cloned by Kerstin Voelkl[1]
HTTQ72-Myc	pPGK	Cloned by Kerstin Voelkl[1]
VSV-G	pcDNA3.1	Kuhn et al. (2010)
	psPAX2	Addgene plasmid #12260; gift from Didier Trono[2]
ss-RFP-GFP-KDEL	pCW57-CMV	Addgene plasmid #128257; gift from Noboru Mizushima[3]

[1] Voelkl et al. (2023)

[2]Kindly provided by Dieter Edbauer, German Center for Neurodegenerative Diseases, Munich, Germany

[3] Chino and Mizushima (2020)

2.1.5 Genotyping primers

Tab. 2.6: Genotyping primers

Mouse line	Primer	Sequence (5' → 3')	Product size (bp)
R6/2	Forward	CCG CTC AGG TTC TGC TTT TA	170
	Reverse	TGG AAG GAC TTG AGG GAC TC	

2.2 Methods

2.2.1 Animals

Animal experiments were approved by the Government of Upper Bavaria, Germany (animal protocol ROB-55.2-2532.Vet_02-20-05, generation of primary cultures ROB-55.2-2532.Vet_02-23-213) and performed in accordance with the relevant guidelines and regulations. Mice were housed in SPF-free environment with ad libitum access to food and water. The transgenic R6/2 line (Sathasivam et al. (1999); JAX stock #002810) was maintained by breeding hemizygous R6/2 males with the female F1 progeny of a cross between CBA (Janvier Labs) and C57BL/6 (Janvier Labs) mice.

2.2.2 Genotyping and sizing of CAG repeats

For genotyping of R6/2 mice, hair follicles were collected from mice and stored at 4°C until genotyping. DNA was extracted by incubating hair follicles with 20 µl dilution buffer and 0.5 µl DNARelease Additive for 5 min at room temperature, and 2 min at 98°C. For polymerase chain reaction (PCR), 1 µl DNA extract, 5 µl Platinum II Hot-Start Green PCR Master Mix and 0.5 µM of each primer in a total volume of 10 µl were prepared. Primers are described in Table 2.6. PCR reaction consisted of heating up the PCR mix to 94°C for 2 min, followed by 30 cycles of 94°C for 15 sec, 60°C for 15 sec and 68°C for 15 sec. Finally, the sample was cooled down to 12°C. PCR products were analysed using agarose gel electrophoresis. Genotyping was conducted by Magdalena Böhm.

Length of the CAG repeat tract in the R6/2 mice used for snRNA-seq experiments was determined by Laragen, Inc., and averaged 204 ± 5.85 (SEQ CAG No., mean ± SD).

2.2.3 Tissue dissection

Tissue was harvested from 12 R6/2 and 14 WT mice: 4 R6/2 and 4 WT mice at 5 weeks; 4 R6/2 and 6 WT mice at 8 weeks; and 4 R6/2 and 4 WT mice at 12 weeks. Tissue isolation and preparation of single nuclei suspension was carried out in parallel for R6/2 and WT littermates to minimize batch effects. Additionally, to reduce the impact of individual animal variability, MCs were sampled from two animals with the same genotype for each experimental run.

Buffers for MC dissection were adapted from Saunders et al. (2018). Mice were anaesthetised by intra peritoneal injections of 200 mg/kg Ketamine and 40 mg/kg Xylazine. Mice were perfused by intra-cardiac injection of ice-cold cutting buffer (110 mM NaCl, 2.5 mM KCl, 10 mM HEPES, 7.5 mM $MgCl_2$, 25 mM Glucose, 75 mM Sucrose, pH 7.4). All following procedures were performed at 4°C. The brain was extracted, transferred into cutting buffer and the fresh brain was cut at a thickness of 300 µM in cutting buffer on a Leica VT 1200S vibratome at 0.2 mm/s. Brain slices were transferred into dissection buffer (82 mM Na_2SO_4, 30 mM K_2SO_4, 10 mM HEPES, 10 mM glucose and 5 mM $MgCl_2$), and the primary motor cortex was microdissected.

2.2.4 Nuclei isolation and snRNA-seq

The protocol and buffers for nuclei isolation were adapted from Mathys et al. (2019) and Wertz et al. (2020). MCs were transferred to a 2 ml KIMBLE tissue douncer with 600 µl homogenization buffer (320 mM sucrose, 5 mM $CaCl_2$, 3 mM $Mg(CH_3COO)_2$, 10 mM Tris HCl [pH 7.8], 0.1 mM EDTA [pH 8.0], 0.1% NP-40, 1 mM 2-mercaptoethanol, and 0.4 U/mL SUPERaseIn RNase Inhibitor). The tissue was dounced 15 times with a loose and 15 times with a tight pestle. The homogenized tissue was passed through a 30 µm cell strainer. The filtered suspension was mixed with an equal volume of working solution (50% OptiPrep density gradient medium, 5 mM $CaCl_2$, 3 mM $Mg(CH_3COO)_2$, 10 mM

Tris HCl [pH 7.8], 0.1m MEDTA [pH 8.0], and 1 mM 2-mercaptoethanol). The mixed suspension was transferred to a Sorenson microcentrifuge tube and underlaid first with 500 µl of 30% Optiprep solution (134 mM sucrose, 5 mM $CaCl_2$, 3 mM $Mg(CH_3COO)_2$, 10 mM Tris HCl [pH 7.8], 0.1 mM EDTA [pH 8.0], 1 mM 2-mercaptoethanol, 0.04% NP-40, and 0.17 U/mL SUPERase In RNase Inhibitor) and then with 300 µl of 35% Optiprep solution (96 mM sucrose, 5 mM $CaCl_2$, 3 mM $Mg(CH_3COO)_2$, 10 mM Tris HCl [pH 7.8], 0.1 mM EDTA [pH 8.0], 1 mM 2-mercaptoethanol, 0.04% NP-40, and 0.12 U/mL SUPERase In RNase Inhibitor). The gradient was centrifuged for 20 min at 3,000 g in an SH 3000 swing rotor in a Sorvall RC 6 plus superspeed centrifuge. Debris accumulating on top of the 30% Optiprep solution was removed. 200 µl of interface containing the nuclei were collected. For washing, the nuclei suspension was diluted in 1 ml 2% BSA in PBS, thoroughly mixed and centrifuged for 4 min at 300 g. The supernatant was removed and the washing step was repeated once. A 10 µl sample of the nuclei suspension was taken and stained with DAPI for counting. The integrity of nuclei was checked by making sure nuclei had well-resolved edges. The nuclei suspension was diluted to 300 nuclei/µl in 2% BSA in PBS.

For droplet-based snRNA-seq, a volume targeting for 12,000 nuclei was loaded onto a "10X Chromium controller". Sequencing libraries were prepared with the "Chromium Single Cell 3' reagent kit v3.1" according to manufacturer's protocol. Library indices were added with the "Single Index Kit T".

Sequencing was performed on a NovaSeq6000 Sequencing System (Illumina) at Core Facility Genomics of the Helmholtz Zentrum München. BCL files were demultiplexed to FASTQ files with Cell Ranger v4.0 (10X Genomics) using mkfastq(). Count matrices were generated by aligning FASTQ files to the mouse GRCm38 reference genome (NCBI: GCF_000001635.20) with cellranger count() with intronic reads being included.

2.2.5 Quality control and cell type annotation

Seurat v4.0.1 was used for subsequent data cleaning, normalization, dimensionality reduction, integration into the reference atlas and visualization. Nuclei with a higher UMI count than 30,000, with a lower UMI count than 250 or expressing less than 200 genes were

removed. Nuclei with more than 2% mitochondrial genes were removed. Normalization of UMI was done with NormalizeData() with a scale factor of 10,000 and “LogNormalize” as normalization method. Further, after cell type annotation, non-neuronal nuclei with less than 500 UMI and neuronal nuclei with less than 1,200 UMI were removed. Remaining doublets were removed using the doubletfinder package v2.0.3 assuming 6.1% of doublets. After quality control (QC), we retrieved 95,074 nuclei with a median of 5,303 UMI and 2,553 genes per nucleus.

For annotation, our data set was integrated into the mouse MC reference atlas published by the BICCN (Yao, Liu, et al., 2021). We used “snRNA-seq 10x v3 data set B” as a reference as it was generated with an improved nuclei isolation protocol and detected the most median genes per nucleus. Furthermore, it also used snRNA-seq with the "Chromium Next GEM Single Cell 3’ Kit v3.1". We integrated our data set into the reference atlas using the FindTransferAnchors() function with canonical correlation analysis as reduction method. Cell type annotation for each nucleus was predicted using TransferData() and cell type assigned according to the highest prediction score. Cell subclass annotation was retrieved by summarising the cell types according to the hierarchical BICCN annotation (Fig. 1.8) (Yao, Liu, et al., 2021).

2.2.6 Dimensionality reduction and marker identification

The top 4,000 highly variable genes were identified by FindVariableFeatures() with selection.method="vst". For principal component analysis (PCA), data was scaled with ScaleData(). PCA was done using RunPCA() with npcs = 35. Uniform manifold approximation and projection (UMAP) plotting was done with RunUMAP() with dims=1:30 and using otherwise standards settings of Seurat v4.0.1. For transcriptomic correlation between subclasses, the top 4,000 highly variable genes were utilized and correlation values were calculated with Pearson’s correlation. Hierarchical clustering was done with pheatmap() with "clustering_distance_rows=correlation" and standard settings of the pheatmap package v1.0.12. The top 100 subclass-specific marker genes were identified using FindAllMarkers() with min.pct = 0.2 and logfc.threshold = 0.2 for the normalized data.

2.2.7 Differential abundance testing

Differential abundance testing was performed with the miloR package v1.4.0. K-nearest neighbourhood graph was generated using k=28 and d=28 (Dann, Henderson, Teichmann, Morgan, & Marioni, 2022). Neighbourhoods were defined with makeNhoods() with randomly sampled neighbourhoods set to prop=0.05, k=28 and d=28 in PCA space. Neighbourhood connectivity was caluclated with calcNhoodDistance() d=28 in PCA space. Contrasts were defined between R6/2 nuclei of all ages and WT nuclei of all ages. Significantly different neighbourhoods between conditions were computed with testNhoods() and defined as having a false discovery rate (FDR) corrected p-value < 0.1. plotDAbeeswarm() was used to generate swarm plots and plotNhoodGraphDA() to plot neighbourhood graphs.

2.2.8 Differentially expressed genes analysis

Subclass-specific differentially expressed genes (DEGs) were identified with FindMarkers() using the Wilcoxon rank-sum test for the normalized data. DEGs were defined as having an adjusted p-value < 0.05, a |Log2(fold change (FC))| > 0.2 and being expressed in at least 5% of nuclei in the respective subclass.

Importantly, Seurat v4.0.1 was used for calculating Log2(FC) (Hao et al., 2021). With the introduction of Seurat v5, Seurat uses the presto package to calculate Log2(FC), which adds a pseudocount on the group level instead of the cell level (Hao et al., 2023). This results in higher, more biologically accurate, but less stable Log2(FC) according to the authors (Hao et al., 2023). Hence, Log2(FC) presented in this thesis, excluding Log2(FC) calculated with DESeq2, might be underestimated.

To confirm the results of the Wilcoxon rank-sum test at 8 and 12 weeks, we generated pseudobulk counts for each subclass from individual experiments and performed DEG analysis with DESeq2 v1.36.0 between WT and R6/2 with pseudobulk counts from 8 weeks and 12 weeks (Love, Huber, & Anders, 2014). Again, DEGs were defined as having an adjusted p-value < 0.05 and a |Log2(FC)| > 0.2.

For DEG subsampling analysis, 300 nuclei were chosen randomly from a cell subclass for an individual time point. Afterwards, DEGs were identified with the Wilcoxon rank-

sum test as described above. This process was repeated for 100 iterations.

2.2.9 Disease scores

For calculation of disease scores, we first used SCTransform() with standard settings for normalization and variance stabilization of the UMI counts. Afterwards, the Euclidean distance between the average expression of WT and R6/2 expression values was calculated for individual time points and individual subclasses. We excluded genes with an average expression higher than 10, like metastasis associated lung adenocarcinoma transcript 1 (*Malat1*), as their high absolute expression values heavily biased the analysis. Euclidean distances were then summed up to calculate the disease score.

2.2.10 Pseudotime trajectory analysis

Pseudotime trajectory analysis was conducted with slingshot v2.4.0 (Street et al., 2018). Nuclei were subset by their cell subclass or cell type (L5 IT and L6 IT neurons). Standard procedures for identification of variable genes and scaling of UMI counts were done. Nuclei were replotted using RunPCA() with npcs = 15 and UMAP with dims = 1:15. The pseudotime trajectory was generated by using slingshot() with the WT nuclei as starting point and R6/2 nuclei as end point, no breaks, curve approximation along 150 nuclei and extension of the curve being allowed.

2.2.11 Kyoto Encyclopedia of Genes and Genomes pathway over-representation analysis

Kyoto Encyclopedia of Genes and Genomes (KEGG) pathway over-representation analysis was performed with the clusterProfiler package, which uses one-sided Fisher's exact test (T. Wu et al., 2021). DEGs of individual subclasses were taken for over-representation analysis. Pathway analysis was done separately for down- and upregulated DEGs. Pathways were categorized as significantly enriched when having an adjusted p-value < 0.05 after Benjamini-Hochberg FDR correction.

2.2.12 scWGCNA

WGCNA for was performed using the scWGCNA package v0.1.0 (Feregrino & Tschopp, 2022). scWGCNA was conducted with all nuclei for all time points. For pseudonuclei generation, nuclei were subset by genotype and time point. Afterwards, PCA was done with npcs=25 and UMAP generated with dims=1:25. Then, pseudonuclei were generated using 20% of nuclei as seeds and 15 nearest neighbours in UMAP space.

scWGCNA was performed considering the top 2,000 highly variable genes and DEGs that occurred in at least 2 subclasses at one time points. Genes expressed in less than 1% of nuclei were filtered out. WGCNA threshold was chosen using pickSoftThreshold() with a cut-off power of 0.9 for a signed network. WGCNA was performed iteratively until all genes were assigned a to a module, topological overlap and adjacencies calculated as described in Feregrino and Tschopp (2022). Module eigengene expression for nuclei was calculated with moduleEigengenes() of the WGCNA package (Langfelder & Horvath, 2008). The module-trait relationships were calculated using Pearson's correlation with module eigengene expression of pseudocells and the corresponding trait.

Gene network representations were plotted using the igraph package v1.4.1 with Fruchterman-Reingold representation. The top 10% of hub genes from modules with a module-trait relationship > |0.15| for at least one time point were plotted. The vertex size is proportional to module eigengene values. Edges represent the top 20% highest absolute adjacencies.

P-values for the over-representation of neuronal essential genes and mHTT modifier genes in WGCNA gene modules were calculated using one-sided Fisher's exact test, following the same principal of KEGG pathway enrichment analysis. All neuronal essential genes and mHTT modifier genes expressed in at least 5% of neuronal nuclei were considered.

2.2.13 HEK cell culture

HEK-293T Cells (HEK cells) were cultured in HEK medium (88% DMEM with high glucose, 10% FBS, 1% non-essential amino acids, 1% Penicillin-Streptomycin). Stable ss-RFP-GFP-KDEL HEK cells were cultured in HEK medium with 0.5 ng/μL Puromycin.

Cells were kept at 37°C and 5% CO_2. Cell lines were split before surpassing 90% confluence. HEK cells were split 1:5 or 1:10 depending on their confluence every 2-3 days. For splitting, cells were washed once with PBS, covered with Trypsin and incubated for 5 min at 37 °C. Cells were resuspended in 5 ml HEK medium and centrifuged for 3 min at 300 g. The supernatant was discarded and the cell pellet taken up in 10 ml. For a 1:10 split, 1 ml was taken from the cell suspension and transferred to a new flask. HEK cells were used up to passage 25. Stable ss-RFP-GFP-KDEL HEK cells were used up to passage 20.

2.2.14 Generation of stable ss-RFP-GFP-KDEL HEK cell lines

HEK cells were seeded at a confluence of 30% on a 24-well plate in antibiotic-free HEK medium. Transfection was conducted when HEK cells reached a confluence of 70-80%. For each well of a 24-well plate, 0.5 μg of DNA were diluted in 100 μl of Opti-MEM. Then, 1.5 μl of Lipofectamine LTX per well were added, the solution gently mixed and incubated for 30 min at RT. Afterwards, 100 μl of the DNA-Lipofetamine LTX mix were added dropwise to each well. The medium was replaced with fresh HEK medium after 48 h. For the selection of cells with transfected ss-RFP-GFP-KDEL construct, 1 ng/μL Puromycin was added to the medium. HEK medium containing Puromycin was exchanged each 48 h. After 10 days of selection, the cells were brought into a cell suspension as described above at a concentration of 100 cells/ml. Then, through sequential dilution further suspensions with a concentration of 50 cells/ml, 25 cells/ml, 12.5 cells/ml, 6.25 cells/ml, 3.125 cells/ml were generated. From each cell suspension 5 times 100 μl were plated on a 96-well plate. From then on, transfected HEK cells were kept in HEK medium with 0.5 ng/μL Puromycin. After 10 days, single cell colonies were visible and were then transferred to a 6-well plate. From there on stable ss-RFP-GFP-KDEL HEK cells were expanded and kept in HEK medium with 0.5 ng/μL Puromycin.

2.2.15 Transfection

For experiments followed by ICC, HEK cells were seeded at a confluence of 30% on baked glass coverslip on a 24-well plate. Transfection was conducted as described in

chapter 2.2.14. For experiments with stable expressing ss-RFP-GFP-KDEL HEK cell lines, directly after transfection of HTTQ25-His or HTTQ72-His, Doxycycline at a concentration of 4 µg/ml was added to the medium. HEK cells were fixed 48 h after transfection by washing once with PBS and incubation in 4% PFA for 15 min. Afterwards, cells were washed with PBS and kept at 4°C in PBS with 0.02% NaN_3.

2.2.16 Lentivirus production

HEK cells were plated in a T175 cell culture flask at a confluence of 30% in antibiotic-free HEK medium. Cells were transfected 24 h later when a confluence of 70-80% was reached. Plasmid mix was prepared with 18.6 μg of plasmid of interest, 11 μg psPAXx and 6.4 μg in DMEM. TansIT mix was prepared by adding 108 μl TransIT-Lenti Transfection Reagent to 1398 μl DMEM. Plasmid mix and TransIT mix were mixed, incubated for 20 min at RT and added to the HEK cells. 24 h after transfection, the medium was removed and 30 ml fresh HEK medium added. 2 days later, the HEK medium containing the lentivirus was collected and debris spun down by centrifugation at 1200g for 20 min. The supernatant was filtered through a 0.45 μm filter. To 30 ml medium, 10 ml of Lenti-X Concentrator were added. The suspension was thoroughly mixed and incubated overnight at 4 °C. The suspension was centrifuged at 1500g for 45 min at 4 °C. The supernatant was discarded. The Falcon tube containing the pelleted virus was dried for 5 min at RT. The pellet was resuspended in 300 μl PBS and incubated for 4 h at 4°C. The virus was aliquoted and kept at -80°C until usage.

2.2.17 Coating of glass cover slips

Glass coverslips were baked for disinfection at 180°C overnight. Glass cover slips were placed in a 24-well format and washed with PBS. 400 μl of PDL 1 mg/ml in Borate buffer (3.1 g Boric acid, 4.75 g Borax in 1l water, adjusted to pH 8.5) were added and incubated overnight at 37°C. The next morning, cover slips were washed three times with PBS. After washing, glass coverslips were incubated with laminin 5 μg/ml in PBS for 4 h at 37°C. Before usage, coated cover slips were washed three times with PBS.

2.2.18 Preparation of primary cortical cultures

A WT CD-1 mouse with embryos at embryonic stage E15.5 was sacrificed through cervical dislocation. The abdomen was disinfected with 80% ethanol and the abdominal cavity was opened by a cut at the height of the uterus. The embryos were dissected from the uterus and transferred into ice-cold PBS. The embryos were removed from the amniotic sac and decapitated. The skulls were transferred into dissection medium (97% HBSS, 1% Pen/Strep, 1% HEPES 1M, 1% $MgSO_4$ 1M). The skull was opened, the whole brain removed and transferred into a petri dish with fresh pre-warmed dissection medium. The meninges were removed and the neocortex dissected. Neocortices were incubated in pre-warmed Trypsin with 0.05% DNase1 for 15 min at 37 °C. Afterwards, Trypsin was inactivated by adding 10 ml of Trypsin inactivation medium (95% neurobasal medium, 5% FBS). The Trypsin inactivation medium was removed and 2 ml of pre-warmed neuronal culture medium (96% neurobasal medium, 2% B27-supplement, 1% Pen/Strep, 1% L-Glutamine) added. The neocortices were homogenised by pipetting them 15 times with a P1000 pipette. The homogenised cells were pelleted by centrifugation at 130 g for 5 min. The cells were resuspended in 1 ml neuronal culture medium per dissected embryo. Cell were counted and diluted to a cell suspension of 250,000 cells/ml. 0.5 ml of the cell suspension were given into each well of a 24-well plate resulting in a density of 125,000 cells/well. Neuronal cultures were kept at 37 °C with 5% CO2.

2.2.19 Transduction with lentivirus

Primary cortical neurons were transduced at day in vitro (DIV) 7. For each well of a 24-well plate, a suspension was prepared with 100 μl pre-warmed neuronal culture medium and LV suspension in the range of 0.5 μl to 1 μl, depending on the virus titer. 100 μl of the suspension were added to individual wells. Primary cortical neurons were fixed with the same procedure as described for HEK cells 7 days after transduction.

2.2.20 Immunocytochemistry

Cells were kept in the dark at all times. Cells were washed with PBS for 5 min. Cells were incubated with 50 mM NH_4Cl in PBS for 10 min. For permeabilization, cells were treated with 0.25% Triton X-100 in PBS for 5 minutes. Cells were washed once with PBS. Cells were transferred to a humid chamber. Unspecific binding sites were blocked by incubating the cells with blocking solution (2% BSA, 4% normal donkey serum in PBS) for 30 min. Primary antibodies were diluted in blocking solution as described in table 2.3. Cells were incubated with 50 μl of primary AB solution for 1 h. Afterwards, cells were washed 3 times with PBS. DAPI (1:2,000) and secondary ABs were diluted in blocking solution as described in table 2.4. Cells were incubated with 50 μl of secondary AB solution for 30 min. Cells were washed 3 times for 5 min with PBS. Afterwards, cells were washed by shortly dipping the cover slip in distilled H_2O. 10 μl of ProLong Glass Antifade Mountant were given onto cover glasses and the coverslips were mounted. Slides were stored at 4°C until iamging. Images were taken of randomly chosen cells with a Leica TCS SP8 confocal microscope.

2.2.21 Statistics

Differences were considered statistically significant at a p-value < 0.05 and in cases of multiple comparisons at an adjusted p-value < 0.05. The method for calculating p-values is indicated in the figure caption of plots. In bar graphs, columns with error bars represent mean ± standard deviation. In box plots, boxes indicate median and interquartile range from the first (Q1) to the third quartile (Q3), and whiskers indicate Q1/Q3 -/+ 1.5 * interquartile range. In violin plots, the central dot indicates the median and the central line spans Q1 to Q3.

3 Results

3.1 Cell type annotation of a longitudinal snRNA-seq dataset of R6/2 mice and WT controls

To understand how HD affects different cell types with disease progression, we conducted a longitudinal snRNA-seq study with the R6/2 mice and WT littermate controls. We collected MC tissue at three distinct ages: at 5 weeks, which is an early time point with no observable symptoms; at 8 weeks, shortly before the onset of motor symptoms; and a final time point at 12 weeks, when the R6/2 mice are are a fully symptomatic stage (Fig. 3.1 A) (Menalled et al., 2009; Voelkl et al., 2022). Nuclei isolated from the MC were used to perform snRNA-seq with the droplet-based 10x Chromium system. For each time point, two experiments with MC from R6/2 mice and experiments with 2 WT littermate controls were conducted. An exception was the 8-week time point for which 3 experiments were conducted with WT mice.

To ensure the high quality of the dataset, several quality control metrics were applied to retain only nuclei derived from healthy cells. Nuclei with more than 2% mitochondrial RNA (mtRNA) were excluded, as elevated mtRNA levels are an indicator for leaky mitochondrial membranes of cells in a cytotoxic state (Osorio & Cai, 2021). Additionally, nuclei with fewer than 250 unique molecular identifier (UMI) were excluded in order to remove non-viable nuclei. Nuclei with more than 30,000 UMI were excluded to filter out potential doublets. Further, after cell type annotation, remaining doublets were removed by employing the doubletfinder package. After applying these common quality control metrics, 95,074 high-quality nuclei were obtained for further analysis (Fig. 1.8) (Fig. 3.1 B).

To determine the cell types and cell subclasses of the nuclei, we integrated nuclei from our dataset into the MC mouse reference atlas published by the Allen Brain institute (Yao, Liu, et al., 2021). Specifically, we integrated our data set into dataset “10x B” as it used an “improved collection method” and also utilized the 10x Chromium system. Visual

assessment confirmed that nuclei from both genotypes aligned well with the clusters in the reference atlas (Fig. 3.1 C, D, E). We then took over the cell type annotation from the reference atlas for our nuclei. Subsequently, cell subclasses of nuclei were assigned based on the cell type according to the BICCN hierarchical annotation (Yao, Liu, et al., 2021). Prediction scores for nuclei being assigned to the correct cell subclass (mean =0.82, sd=0.21) and cell type (mean =0.96, sd=0.1) were reliably high (Fig. 3.1 C, D). This demonstrated a high level of agreement between our dataset and the reference atlas. Importantly, we observed no significant impact of genotype on the quality of integration or cell type annotation (Fig. 3.1 D).

In total, we identified 12 neuronal and 7 non-neuronal cell subclasses. Among the neuronal subclasses, there were 7 glutamatergic excitatory and 5 GABAergic inhibitory subclasses. According to the BICCN nomenclature, the glutamatergic cell subclasses are named after the layer their soma is located in and their projection target. The glutamatergic neurons encompassed IT neurons from several cortical layers (L2/3 IT, L5 IT, L6 IT), CT neurons (L6 CT), layer 6b neurons (L6b neurons), NP neurons (L5/6 NP) and ET neurons (L5 ET, also known as pyramidal neurons). GABAergic neurons are annotated by the expression of specific marker genes, including Pv, Sst, Vip, Lamp5 and Sncg GABAergic neurons (Fig. 3.1 E, Fig.3.2 A).

For further statistical analyses, nuclei from cell subclasses with fewer than 200 nuclei per time point were excluded due to insufficient statistical power for robust analysis. Among neurons, this was the case for L6b neurons and Sncg GABAergic neurons, and among other cell subclasses for endothelial cells (Endo), pericytes (Peri) and vascular leptomeningeal cells (VLMC).

In summary, nuclei from our data set passed high quality control standards, exhibited high consistency with a reference atlas, and cell types and cell subclasses could be identified reliably through integration into the reference atlas.

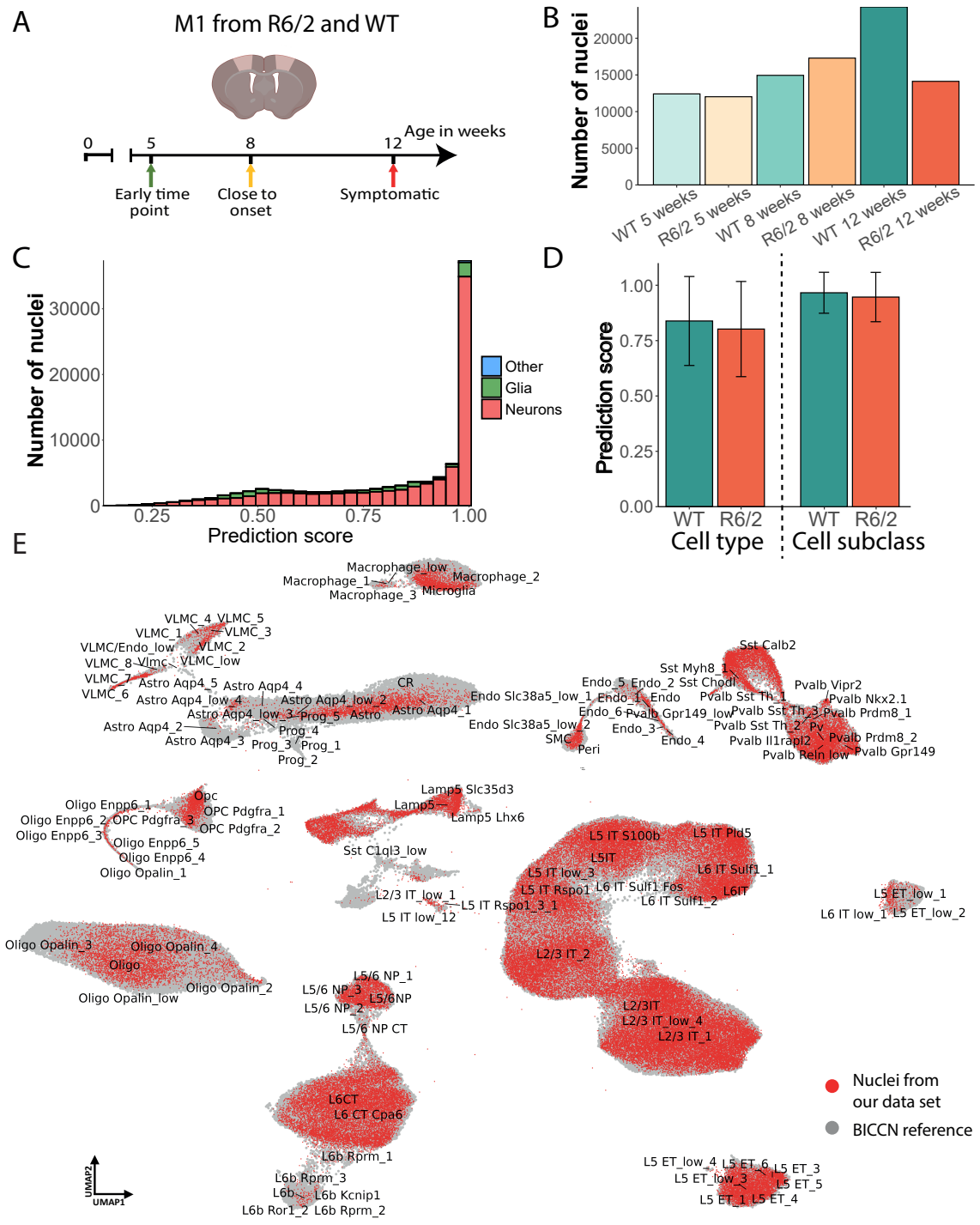

Fig. 3.1: Cell type annotation for our snRNA-seq dataset through integration into a reference atlas

A. Schematic representation of the experimental design

B. Total number of nuclei passing quality control for each condition.

C. Histogram displaying prediction scores, which represent the likelihood of nuclei being assigned to the correct cell type. Neurons, glia and other cell classes showed high levels of prediction scores.

D. Prediction scores for nuclei being assigned to the correct cell type and cell subclass categorized by genotype. Genotype had little effect on prediction score. Bar plot with error bars represent mean ± standard deviation.

E. UMAP plot depicting nuclei of our data set (red) from all time points and both genotypes integrated into the reference atlas (grey) published by the Allen Brain Institute (Yao, Liu, et al., 2021).

3.2 Longitudinal snRNA-seq analysis reveals changes in cellular composition in R6/2 mice

UMAP plotting of nuclei from all ages and both genotypes resulted in a clear separation of nuclei from distinct cell subclasses (Fig. 3.2 A). Among glutamatergic neurons, IT neuronal subclasses plotted within proximity, indicating their transcriptomic similarity. Deeper layer glutamatergic neurons, including L6 CT, L6b, and L5/6 NP neurons, also showed close proximity in UMAP space. L5 ET plotted seperatly from the other glutamatergic clusters, but localised closest to the other deep layer glutamatergic populations. GABAergic neurons plotted separately, forming two distinct groups. One group consisted of Sncg, Lamp5, and Vip neurons, while the other group comprised Pv and Sst neurons.

Examining the correlation between the WT transcriptomes of the individual cell subclasses revealed, as expected, a high correlation among glutamatergic neurons with each other and conversely, for GABAergic neurons (Fig. 3.2 B). Glia cells exhibited positive correlation values between each other, but negative correlation with neuronal subclasses (Fig. 3.2 B). Moreover, hierarchical clustering emphasized the high transcriptomic correlation among the IT neurons, which was also seen on the UMAP plot (Fig. 3.2 A, B). Also, the proximity of Pv and Sst, and on the other hand, Lamp5 and Vip neurons was reflected by the distance in the dendrogram of the hierarchical clustering.

The glutamatergic marker gene, solute carrier family 17 member 7 (*Slc17a7*), was expressed across all glutamatergic subclasses (Fig. 3.2 C). In addition, glutamatergic neurons expressed a combination of further marker genes. IT neurons exclusively expressed among the glutamatergic neurons solute carrier family 30 member 3 (*Slc30a3*). L5 ET and L5/6 NP neurons respectively expressed exclusively serpin family E member 2 (*Serpine2*) and teashirt zinc finger homeobox 2 (*Tshz2*). GABAergic neurons expressed the inhibitory marker genes glutamate decarboxylase 1 (*Gad1*) and glutamate decarboxylase 2 (*Gad2*). GABAergic neurons also expressed their cell subclass-specific marker, for instance, Vip neurons expressed *Vip* and Pv neurons expressed *Pvalb* (Fig. 3.2 C).

In summary, cell subclasses exhibited high transcriptomic correlation with other cell

subclasses of the same cell class. Additionally, they expressed marker genes consistent with those found by previous scRNAseq studies of the MC (Yao, Liu, et al., 2021; Yao et al., 2023).

For most cell subclasses, the fraction of nuclei remained constant with genotype and over age (Fig. 3.2 D, E). Interestingly though, 12-week-old R62 mice showed several changes in their cellular composition. Among neurons, L2/3 IT and L5 IT neurons showed a decrease of 3% and 2.5% of relative proportions respectively, corresponding to a loss of approximately 15% for these cell subtypes. The proportion of nuclei remained stable for other glutamatergic neurons and GABAergic neurons. This specific decrease in IT neurons suggests an increased vulnerability of IT neurons in R6/2 mice.

In addition to IT neurons, astrocytes (abbreviated by "Astros" on figures) and oligodendrocytes (abbreviated by "Oligos" on figures) also showed changes in their proportions. The number of astrocytes doubled at 12 weeks in R6/2 mice relative to the 8 week and 5 week time point (Fig. 3.2 E). Furthermore, the proportion oligodendrocytes increased from 4.9% to 7.2% percent from 8 weeks to 12 weeks in R62 mice (Fig. 3.2 E). Oligodendrocyte precursor cells (OPC) and microglia proportions remained stable with disease progression in R6/2 mice. This increase of astrocytes and oligodendrocytes might be attributed to a increased proliferation or recruitment mechanism for these glia cells to affected brain areas in R6/2 mice.

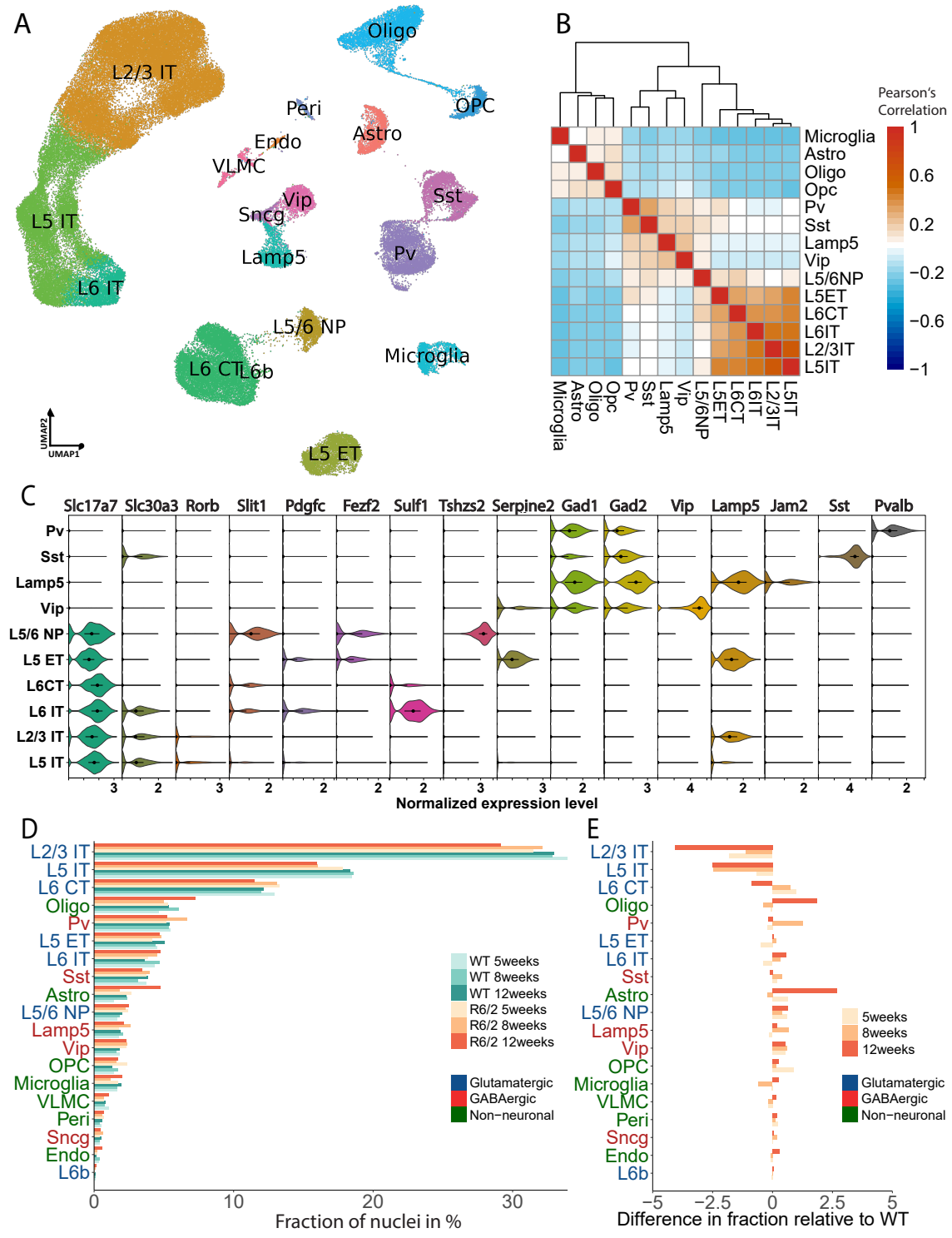

Fig. 3.2: Transcriptomic characteristics of MC cell populations and their change in fraction in R6/2 mice

A. UMAP plot showing nuclei labelled by their cell subclass. Nuclei of all time points, and of WT and R6/2 mice are included.

B. Heatmap showing the Pearson's correlation for the expression level of variable genes between the cell subclasses. The results of hierarchical clustering are depicted as a dendrogram.

C. Violin plot depicting the normalized expression of well established marker genes of neuronal cell subclasses. Points mark the median and the central line ranges the 2nd and 3rd quartile.

D. Fraction of nuclei for the individual cell subclasses for each condition.

E. The absolute difference in the fraction of nuclei from R6/2 for each time point relative

3.3 Glutamatergic neurons undergo a strong transcriptomic shift in R6/2 mice

The observed decrease in the relative fraction of L2/3 IT and L5 IT neurons constituted an initial indication that glutamatergic neurons might be more affected by the pathology in the R6/2 mouse model. UMAP plotting revealed a striking difference between glutamatergic and GABAergic neurons (Fig. 3.3 A). Nuclei from GABAergic neurons of both, WT and R6/2 mice, overlapped on the UMAP (Fig. 3.3 A, C). In stark contrast, nuclei from glutamatergic neurons from 8- and 12-week-old R6/2 mice separated from their WT counterparts (Fig. 3.3 A, B). This suggested a severe change in the transcriptome at 8 and 12 weeks in R6/2 mice, specifically among glutamatergic neurons. Among the glutamatergic neurons, the most notable shift was observed for IT neurons, reflecting the prominent involvement in HD pathology (Fig. 3.3 A).

To further examine this observation, DA testing was utilized to quantify this transcriptomic shift. DA analysis groups nuclei which are within proximity in PCA space into groups of around 50 to 200 nuclei, called "neighbourhoods" (Fig. 3.3 D). DA analysis then calculates whether there is an over-representation of WT or R6/2 nuclei in individual neighbourhoods. DA analysis revealed an increased number of neighbourhoods enriched for R6/2 nuclei and WT nuclei in most glutamatergic neuronal populations (Fig. 3.3 D, E). In particular, most neighbourhoods from IT neurons were significantly enriched and showed high over-representation values (Fig. 3.3 D, E). In contrast, for GABAergic neurons, few neighbourhoods were enriched for WT or R6/2 nuclei and these neighbourhoods showed only slight over-representations. This further supported our hypothesis that glutamatergic neurons undergo a strong transcriptomic shift in R6/2 mice.

To further explore at what age this transcriptomic shift occurs, we used two additional methods to quantify the difference in WT and R6/2 transcriptome at different time points. For the first approach, we corrected for a possible bias due to the varying amount of nuclei for each cell subclass by randomly subsampling 300 nuclei from each cell subclass.

Then, the amount of differentially expressed genes (DEGs) was calculated. This was repeated 100 times and the amount of DEGs taken as measurement of transcriptomic change between WT and R6/2 cell subclasses (Fig. 3.3 F). Neurons showed the highest amount of DEGs, with glutamatergic neurons having more DEGs than GABAergic neurons. In particular, IT neurons showed the highest number of DEGs, consistent with previous results from DA analysis. Also, an increase of DEGs with age was observed in most cell subtypes, demonstrating that the progressive characteristic of HD is also reflected on the transcriptomic level in R6/2 mice. Here, a particularly strong increase in the amount of DEGs was seen from 5 to 8 weeks, suggesting that at this time point the transcriptome changes significantly in neurons of R6/2 mice.

Moreover, we calculated the transcriptome-wide distance between WT and R6/2 nuclei for the individual cell subclasses ("Disease score", (Pineda et al., 2024)). Again, glutamatergic neurons exhibited higher disease scores than GABAergic neurons (Fig. 3.3 G). Particularly, IT and L6 CT neurons showed the highest disease scores, which was in line with the results from DA analysis, DEG subsampling and the observed cell loss at 12 weeks for IT and CT neurons. Again, similarly to the DEGs subsampling analysis, disease scores increased notably at 8 weeks.

In conclusion, transcriptomic changes affect MC cell populations to varying degrees, with glutamatergic neurons showing stronger transcriptomic alterations than GABAergic neurons and glial cells. Interestingly, neuronal populations identified as undergoing significant transcriptomic alterations are particularly affected by selective vulnerability. Finally, this substantial transcriptomic shift appears to occur between 5 and 8 weeks of age.

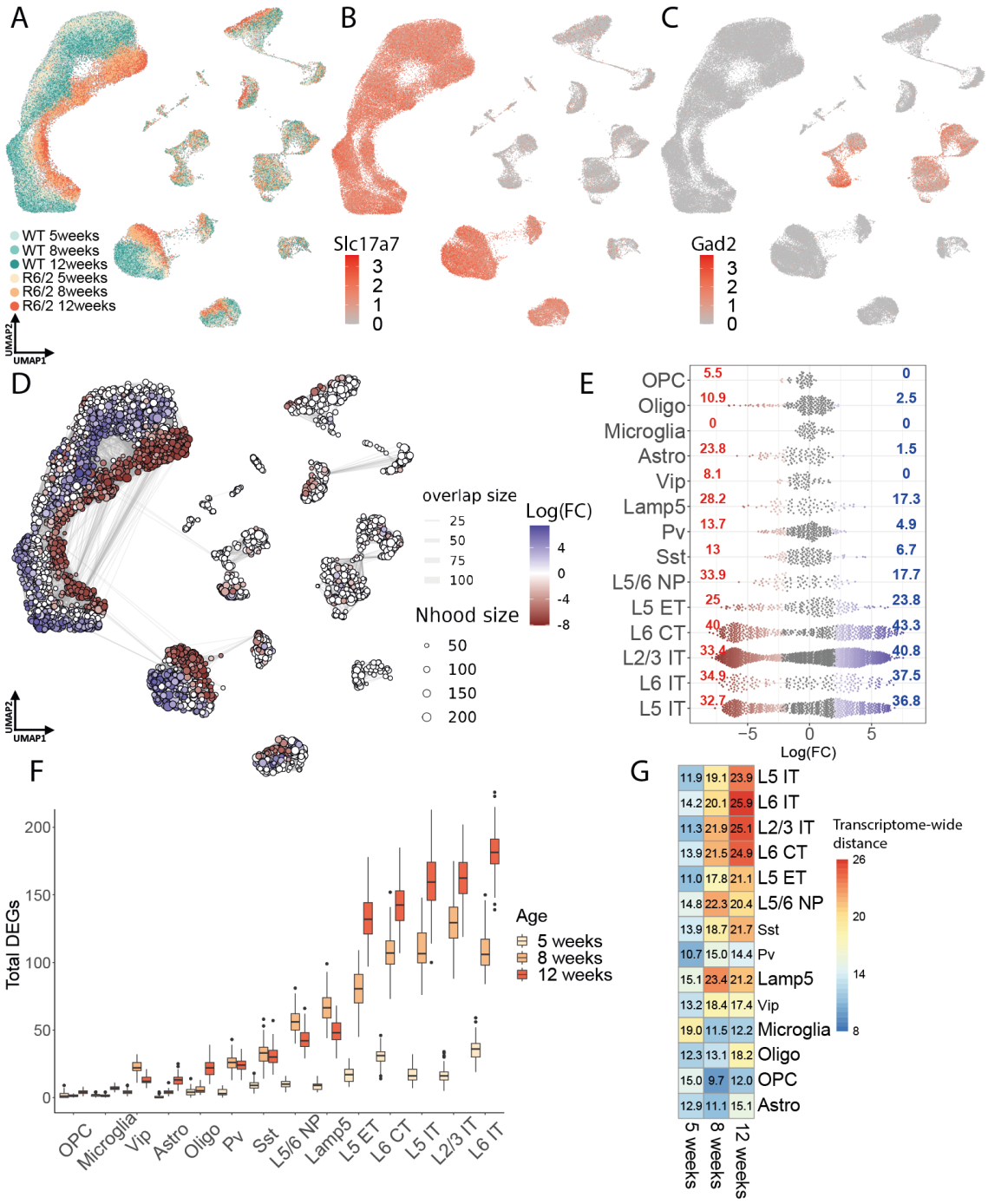

Fig. 3.3: Glutamatergic neurons undergo a strong transcriptomic shift in R6/2 mice

A. UMAP plot with colour-coded nuclei by genotype and age.
B. UMAP plot showing the normalized expression of *Slc17a7*.
C. UMAP plot showing the normalized expression of *Gad2*.
D. UMAP plot with nuclei grouped as neighbourhoods. Neighbourhoods with a significant enrichment for WT (blue) or R6/2 nuclei (red) are coloured.
E. Swarm plot depicting neighbourhoods and their Log(FC) enrichment for WT (blue) or R6/2 nuclei (red). Neighbourhoods with no significant over-representation are shown in white.
F. Box plot with the number of DEGs identified after subsampling 300 nuclei for each cell subclass across different time points. This process was repeated for 100 iterations.
G. Transcriptome-wide distance between R6/2 and WT nuclei.

3.4 A set of genes undergoes bidirectional expression changes during disease progression

Our previous analysis showed a notable increase in transcriptomic changes from 5 to 8 weeks in R6/2 mice (3.3 D-G). To investigate these age-dependent transcriptomic changes, we focused on glutamatergic IT neurons, as they consistently exhibited the strongest transcriptomic changes across various analysis approaches. For this, IT neurons from all time points were individually subplotted on UMAP plots. Afterwards, nuclei were ordered on a pseudotime trajectory with the Slingshot package (Fig. 3.4 A). Pseudotime trajectory analysis aims to sort nuclei along a trajectory that represents a continuous transcriptomic change. In our case, this trajectory represents the change of the transcriptome occurring with disease progression.

WT nuclei of L2/3 IT_ 1 cell type exhibited no discernible differences in their pseudotime values, indicating that there is no considerable transcriptomic change between WT controls of different ages. However, R6/2 nuclei were markedly shifted. The pseudotime trajectory showed a continuous trajectory from WT, to 8-week R6/2 nuclei and ending with the 12-week nuclei (Fig. 3.4 A-C). This demonstrated the progressive effect of the disease on the transcriptome. Surprisingly though, 5-week R6/2 nuclei displayed lower pseudotime values than WT nuclei and were positioned at the opposite end of trajectory to nuclei from 8 and 12 weeks old R6/2 (Fig. 3.4 B-C). A similar pattern of a continuous trajectory from WT to 8-week nuclei to 12-week nuclei and 5-week nuclei laying at the beginning of the trajectory was observed for the other IT cell types, L6 CT neurons, L5 ET neurons (Examples shown for L6 IT in Fig. 3.4 D-F). In contrast, GABAergic neurons and glial cells did not follow a continuous trajectory and did not exhibit a comparable distribution (Fig. 3.4 G).

This indicated that glutamatergic neurons undergo transcriptomic changes, which differ between the presymptomatic and symptomatic stage. To explore this hypothesis, we correlated the total of transcriptomic changes between the different time points. The

correlation of transcriptomic changes between 8 and 12 weeks was high, confirming a similar set of genes being altered in the same direction at these two ages (Fig. 3.4 H). Also, most transcriptomic changes between different glutamatergic cell subclasses showed Pearson's correlation values greater than 0.8, indicating a high overlap of transcriptomic changes between glutamatergic neurons. This could explain the similarity in pattern of pseudotime trajectories among glutamatergic neurons (Fig. 3.4 A-F). However, there was little correlation of transcriptomic changes between 5 and 8 weeks (Fig. 3.4 I). This further supports our hypothesis that transcriptomic changes during the early and late stages of the disease are distinct.

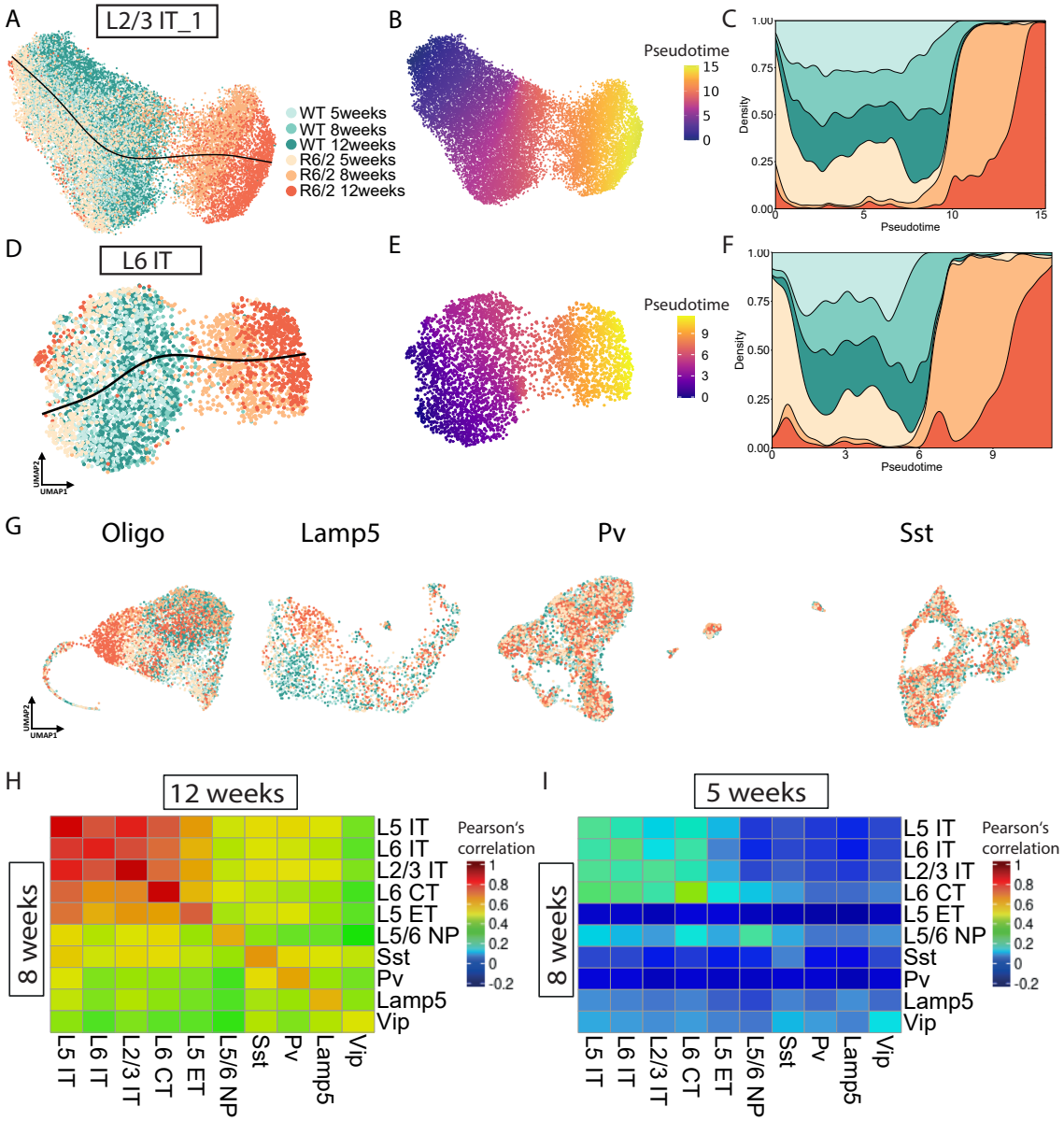

Fig. 3.4: Nuclei of glutamatergic neurons lay on a trajectory from early to late stages of the disease

A. UMAP plot of L2/3 IT_1 reveals a trajectory from 5-week R6/2 nuclei to WT nuclei, and then coninuing to nuclei from 8- and 12-week-old R6/2 mice.
B. UMAP plot depicting pseudotime values for L2/3 IT_1.
C. Density plot with the pseudotime values of L2/3 IT_1 shows low pseudtime values for 5-week nuclei from R6/2 and the increased pseudotime values for 8-week nuclei, which further increases for 12-week-old R6/2 nuclei.
D-F. Plots as in A-C with L6 IT.
G. Oligogdendrocytes, Lamp5, Pv and Sst neurons do not align on pseudotime trajectories on UMAP plots.
H. Heatmap showing the correlation of transcriptome-wide changes from WT to R6/2 between 8 weeks and 12 weeks. Transcriptomic changes from 8 and 12 weeks are highly correlated for the same cell subclass. Further, transcriptomic changes between subclasses of glutamatergic neurons are highly correlated.
I. Transcriptomic changes of 5 and 8 weeks show little correlation.

Next, we investigated which genes give rise to this temporal dynamics seen with pseudotime trajectories. To identify these genes, we hierarchically clustered DEGs from 5-weeks of L2/3 IT and their changes in expression at 8 and 12 weeks. Hierarchical clustering and subsequent k-means clustering separated these genes into three gene sets (Fig. 3.5 A). Two sets contained genes for which the expression changes at 5 weeks correlated to the changes at 8 and 12 weeks. Kyoto Encyclopedia of Genes and Genomes (KEGG) pathway analysis showed that genes upregulated at both, early and late stages, were genes of categories such as "Glutamatergic synapse", "Long-term potentiation" and "Gap junctions". Genes that were downregulated at both time points were linked to categories like "Circadian rhythm" and "Glucagon signalling" (Fig. 3.5 B). However, we also found a prominent set containing genes that were downregulated at 5 weeks but upregulated at 8 and 12 weeks (Fig. 3.5 A). Interestingly, KEGG pathways analysis for this set of genes showed that these genes were involved in "Oxidative phosphorylation", "Ribosomes" and also involved in "Pathways of NDs- multiple diseases" like "AD", "PD" and "HD" (Fig. 3.5 B).

Among the genes with a clear age-dependent bidirectional regulation were ATPase H+ transporting V0 subunit c (*Atp6v0c*), cytochrome c oxidase subunit 8A (*Cox8a*), defender against cell death 1 (*Dad1*), calcyon neuron specific vesicular protein (*Caly*), Ubiquitin B (*Ubb*) and ribosomal protein L41 (*Rpl41*) (3.5 C). *Atp6v0c* and *Cox8a* are mitochondrial genes involved in the respiratory chain. *Ubb* is crucial for marking proteins for degradation via the proteasome pathway. *Caly* was shown to interact with dopamine receptors at the post-synapse and enhance the release of calcium ions upon dopamine receptor activation (Bergson, Levenson, Goldman-Rakic, & Lidow, 2003). *Rpl41* is one of the ribosomal genes for which KEGG pathway analysis showed significant over-representation. Similar patterns were observed in L5 ET and L5 IT neurons, with comparable genes showing bidirectional regulation and alterations in similar pathways, suggesting a common mechanism (3.5 C).

In conclusion, these results demonstrate that the progression of transcriptional dysregulation in HD is not linear, with some genes exhibiting expression changes in opposite

directions at different stages of disease. KEGG pathway analysis indicated that these bidirectionally altered genes are involved in pathways relevant for HD.

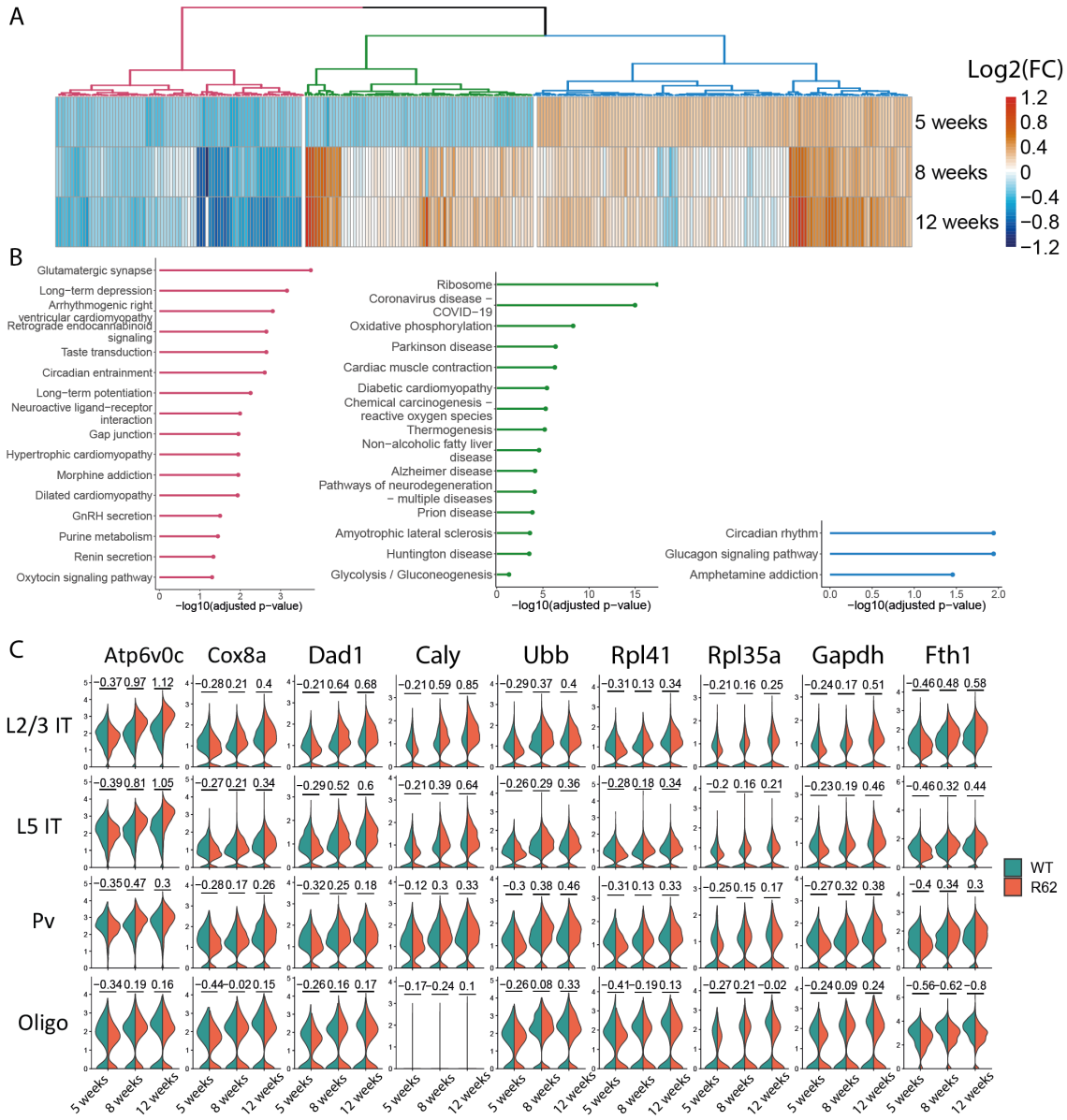

Fig. 3.5: A cluster of genes is differentially regulated before disease onset and during disease progression

A. Heat map with each column depicting a significant DEG of the 5-week time point of L2/3 IT and their Log2(FC) at 5, 8 and 12 weeks. Genes were hierarchically clustered according to their similarity in the temporal pattern. Afterwards, they were separated into clusters with k-means clustering (k=3).

B. KEGG pathways analysis for gene clusters from A, showing that bidirectionally regulated genes fit categories such as "Ribosomes" "Oxidative phosphorylation", "AD", "PD" and "HD".

C. Violin plots showing the normalized expression and Log2(FC) changes in expression gene between WT and R6/2 for all time points. The genes were chosen from the pathways identified with KEGG pathway analysis for the bidirectionally regulated gene cluster in A.

3.5 Neurons lose marker gene expression in R6/2 mice

After identifying dysregulated genes preceding disease onset, our focus shifted to transcriptomic alterations occurring at later disease stages. Notably, as shown in Fig. 3.4 H, transcriptomic changes at 8 and 12 weeks were highly correlated. This was also evident in the overlap of DEGs between the two time points, which was 49% percent for upregulated DEGs and 42% percent for downregulated DEGs for L2/3 IT neurons (Fig. 3.6 A, B). For most DEGs, the expression changes observed at 8 weeks persisted and became more pronounced at 12 weeks. Furthermore, the amount of DEGs increased from 8 to 12 weeks (Fig. 3.6 A, B). This observation aligns with the previous finding of nuclei lying on a continuous disease trajectory from 8 to 12 weeks, indicating the disease progression on a transcriptomic level.

Given the high overlap between 8 and 12 week time points, we focused our subsequent analyses on the 12-week time point. The result from the analysis for the 12-week time point were seen similarly at 8 weeks. Of note, DEGs were defined as having an absolute Log2 fold change greater than 0.2 and an adjusted p-value of less than 0.05. P-values were calculated using the Wilcoxon rank sum test with each nucleus as statistical unit. This has proven to be a reliable method in the field of scRNAseq but can produce inflated p-values (Heumos et al., 2023). To further support the DEGs identified with Wilcoxon rank sum test, we used DEseq2 to replicate our findings. DEseq2 is based on pseudobulk counts from individual experiments as the statistical unit. As the transcriptomic changes between WT and R6/2 mice at 8 and 12 weeks were highly correlated, pseudobulk counts from both time points were used for DESeq2 to strengthen the statistical power. With this method, most DEGs identified with Wilcoxon rank sum test were also found with DEseq2 (Fig. 3.6 C). For cell subclasses with fewer nuclei, like GABAergic neurons, we found that there was a tendency for a decreased overlap between DEseq2 and the Wilcoxon rank sum test. However, the most significant DEGs were found with both methods. All DEGs discussed in this thesis from later time points were identified with both methods and DEGs

that encouraged further investigation are shown for both methods (e.g. Fig. 3.9 C, D).

To further explore transcriptomic changes at late time points, we examined which DEGs are shared between cell subclasses and which are exclusive to specific cell subclasses. An intriguing observation was that many upregulated DEGs were shared among glutamatergic populations, whereas downregulated genes were more specific for individual glutamatergic cell subclass (Fig. 3.6 D, E). At 12 weeks, 400 DEGs were commonly upregulated in at least 5 of the 6 glutamatergic cell subclasses, whereas only 50 downregulated genes were shared (Fig. 3.6 D). Of the downregulated genes around 44% were specific for a specific for a subclass, while for upregulated DEGs only 32% were subclass-specific (Fig. 3.6 E). This suggests that glutamatergic neurons upregulate a common set of genes in response to the R6/2 pathology. In contrast, downregulation of genes is more cell type-specific and each cell subclass decreases expression for a more specific set of genes.

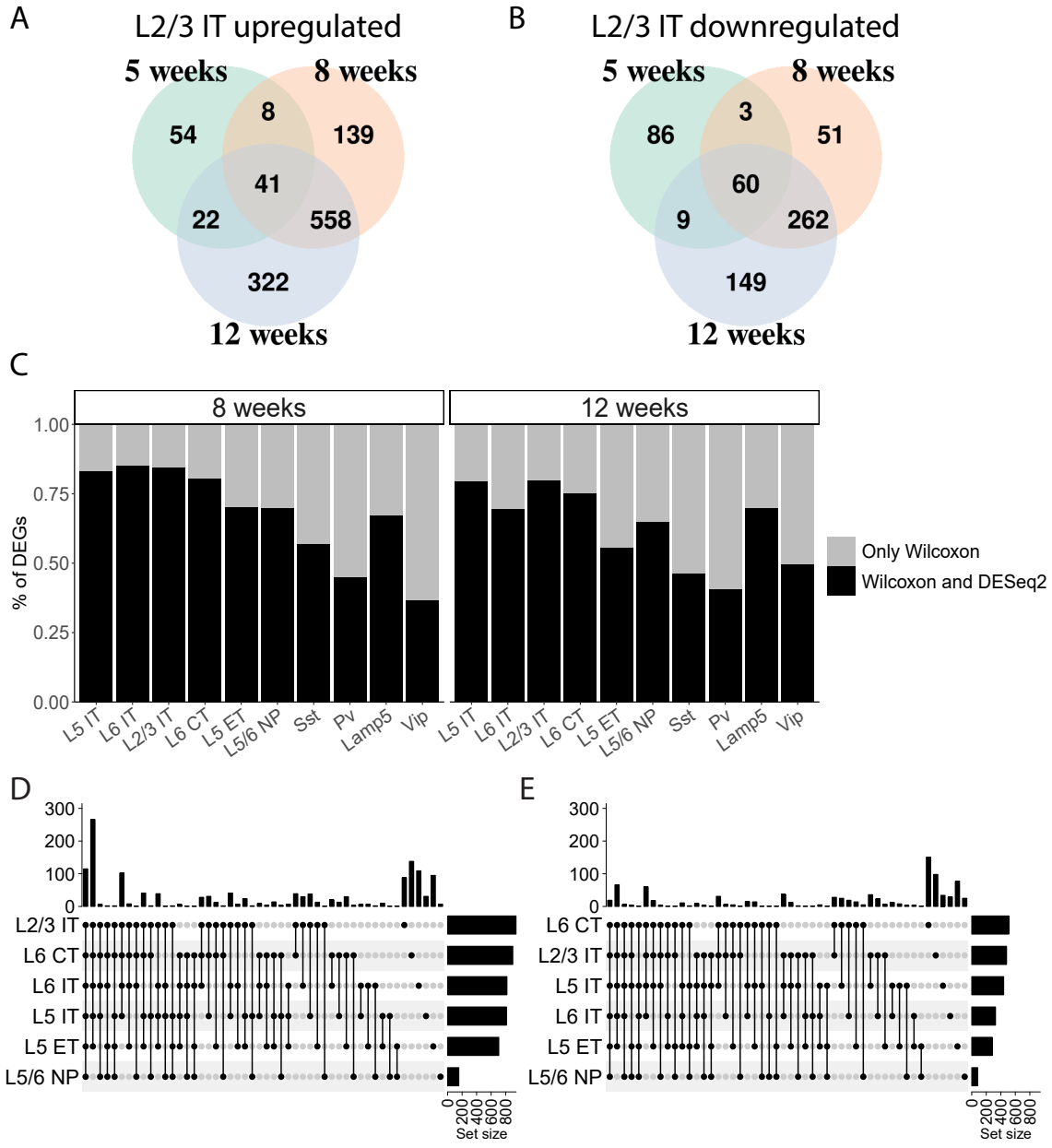

Fig. 3.6: Upregulated genes are shared between glutatmatergic populations, whereas downregulated genes have a tendency of being subclass-specific

A. Venn diagramm of upregulated DEGs for the different time points of L2/3 IT neurons.
B. Venn diagramm of downregulated DEGs for the different time points of L2/3 IT neurons.
C. Stacked barplot showing the percentage of DEGs identified with both Wilcoxon rank sum test and DESeq2 method, and percentage of DEGs only identified with Wilcoxon rank sum test.
D. UpSet plot for the overlap of upregulated DEGs between individual glutamatergic subclasses at 12 weeks. Connected points and the corresponding bar above indicate the total amount of DEGs shared between the connected subclasses. Set sizes correspond to the total amount of upregulated DEGs for the subclass. The highest amount of DEGs were shared between 5 and 6 out of the 6 glutamatergic subclasses.
E. UpSet plot for the overlap of downregulated DEGs between individual glutamatergic subclasses at 12 weeks. The highest amount of DEGs were specific for glutamatergic subclasses.

To further investigate cell type-specific downregulated genes, we examined previous findings. Previous publications from our lab had demonstrated that the cell subclass-defining marker genes of Vip and Sst neurons are downregulated in HD mouse models at the protein level (Voelkl et al., 2022). This loss of marker expression was also reflected on the transcriptomic level, both GABAergic subclasses investigated in the previous study showing marked downregulation of their markers on the transcriptomic level (Fig. 3.7 A). Consistent with the finding by Voelkl et al. (2022), the decrease in marker expression in Pv neurons was less pronounced. Additionally, also Lamp5 neurons, which were not investigated in the previous study, showed a decrease in *Lamp5* expression (Fig. 3.7 A). Moreover, also well-established marker genes of the glutamatergic subclasses, such as Neurogranin (*Nrgn*), neural EGFL like 1 (*Nell1*), RNA binding fox-1 homolog 1 (*Rbfox1*) and TAFA chemokine like family member 1 (*Tafa1*) were decreased in expression (Fig. 3.7 A).

To assess whether marker loss was a more widespread phenomenon affecting other cell subclasses and more marker genes, we identified the top 100 marker genes for each cell subclass and calculated their average change in expression across all ages (Fig. 3.7 B). At 5 weeks, the marker expression did not differ strongly between WT and R6/2 mice. However, at 8 weeks, a substantial decrease in marker gene expression was observed in all neuronal clusters in R6/2 mice. Particularly glutamatergic neurons and Lamp5 neurons exhibited a substantial reduction in marker expression at 8 weeks, which continued to 12 weeks. A decrease in marker expression was also observed in Oligodendrocytes and Astrocytes, but not Microglia and OPCs. These findings are consistent with previous publications implicating oligodendrocytes and astrocytes in HD pathology (Al-Dalahmah et al., 2020; R. G. Lim et al., 2022).

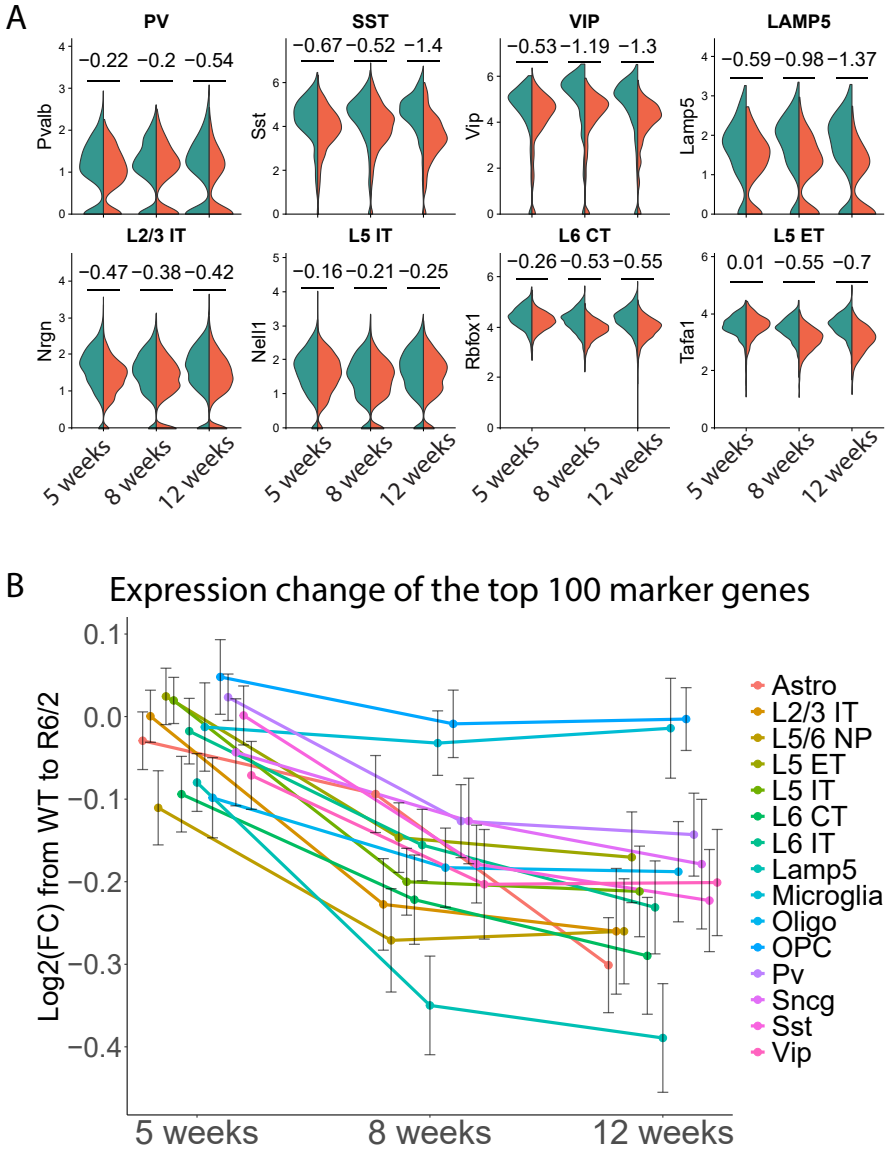

Fig. 3.7: A multitude of cell subclass marker genes is downregulated in various cell populations of R6/2 mice

A. Violin plots showing the normalized expression and Log2(FC) in expression for marker genes of several glutamatergic and GABAergic neuronal subclasses.
B. Quantification of the average change in expression for the top 100 marker genes for the individual neuronal subclasses. Error bars indicate the 95% confidence interval.

To investigate a potential cause for the decrease in marker expression, we turned our attention to transcription factors (TFs) which likely regulate cell identity. In a recent publication, the BICCN published a data set of TFs which are cell class-specific, and are

likely crucial to define and maintain the cell type characteristics of neurons (Yao et al., 2023). Specifically, Yao et al. (2023) identified TFs, which are specficially expressed in glutamatergic neurons derived from the pallium, as well as TFs exclusive expressed in the subpallium-derived GABAergic neurons. We calculated the average expression change for TFs specifically expressed in glutamatergic neurons and GABAergic neurons. Glutamatergic-specific TFs showed a notable decrease in expression (Fig. 3.8 A.). This decrease in glutamatergic-specific TFs then might cause the loss of maker expression in glutamatergic neurons.

Several Glutamatergic-specific TFs, which were particularly strongly downregulated in glutamatergic cell subclasses included *Neurod1*, FEZ family zinc finger 2 (*Fezf2*), JunB proto-oncogene (*Junb*), FosB proto-oncogene (*Fosb*), zinc finger E-box binding homeobox 2 (*Zeb2*), inhibitor of DNA binding 2 (*Id2*) and nuclear factor I X (*Nfix2*) (Fig. 3.8 B). To our surprise, for GABAergic neurons, the decrease in expression was limited to few cell class-specific TFs which showed only slight downregulation (Fig. 3.8 A, B).

In summary, marker genes showed a widespread downregulation across neuronal populations. In glutamatergic neurons, the decrease in marker genes is paralleled by the downregulation of TFs which are likely responsible for defining cell class identity. The reduced expression of these TFs may result in a decreased expression of cell subclass-defining genes and, in consequence, to a deficit in cell identity.

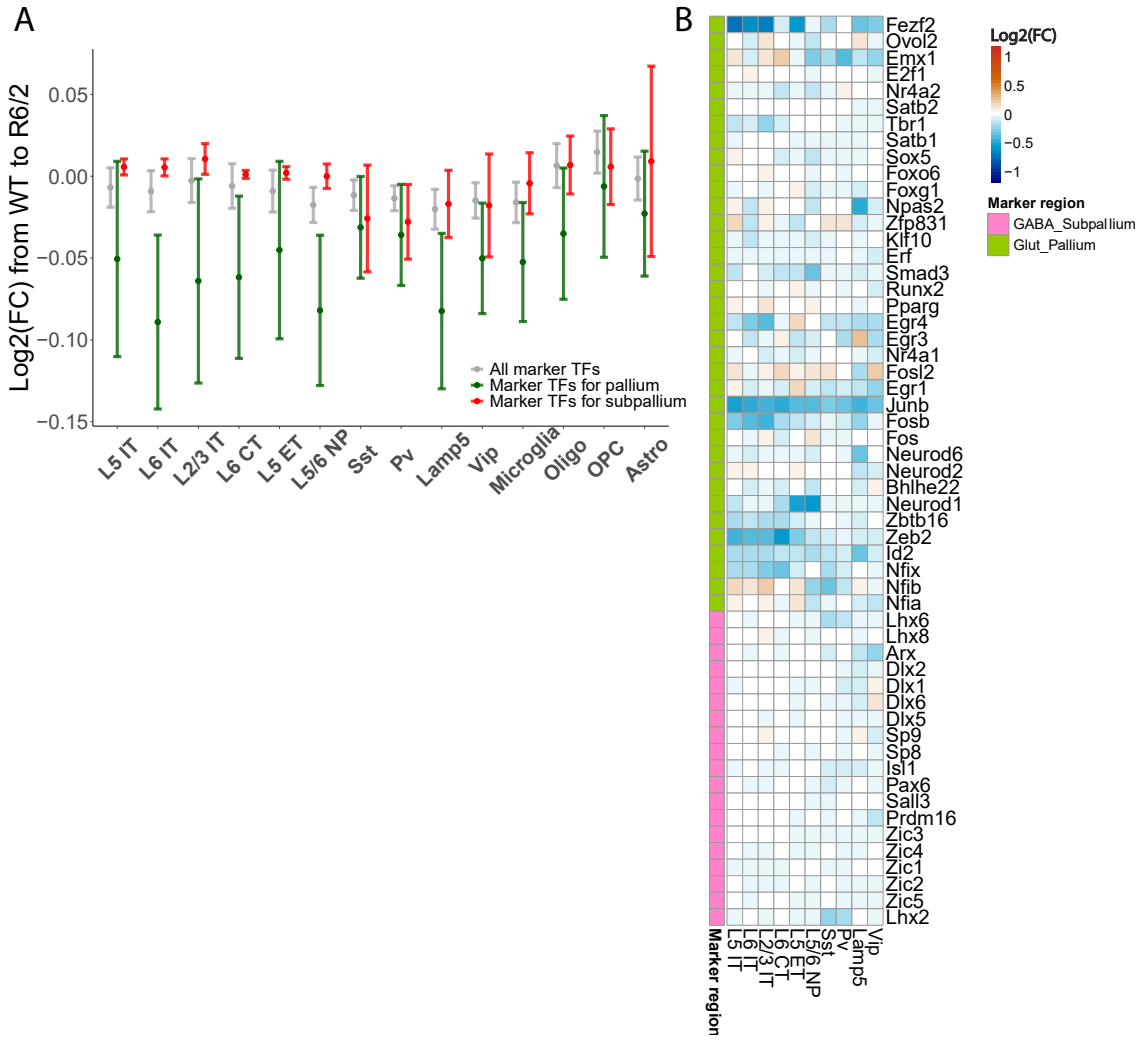

Fig. 3.8: Glutamatergic-specific TFs are downregulated in R6/2 glutamatergic populations

A. Quantification of the average change in expression for TFs specific for glutamatergic neurons (marker TFs for pallium) and GABAergic neurons (maker TFs for subpallium). Error bars indicate the 95% confidence interval. Particularly marker TFs for the glutamatergic neurons exhibited downregulation in glutamatergic neurons. GABAergic marker TFs showed little downregulation.
B. Heatmap depicting the change in expression for subclass-specific TFs in the individual neuronal subclasses.

3.6 Pathway analysis suggests a vital role of ER stress response in HD

After exploring subclass-specific transcriptomic changes, we investigated pathways commonly altered among glutamatergic neurons, aiming to identify pathways, which are crucial for the response to mHTT.

As shown in Fig. 3.6 D and E, fewer genes are commonly downregulated than upregulated across multiple glutamatergic neuronal subclasses. KEGG pathway analysis revealed that commonly downregulated pathways are involved in "Glutamatergic synapse", "Circadian entrainment", "Calcium signalling", "Axon guidance" and "Long-term potentiation" (Fig. 3.9 A). These downregulated pathways primarily revolved around neuronal signalling, with several DEGs fitting into multiple categories (Fig. 3.10). The "Glutamatergic synapse" pathway was particularly interesting, as "GABAergic synapse" was identified as one of the upregulated pathways (Fig. 3.9 B). Most of the "Glutamatergic synapse" genes were post-synaptic genes. For instance, calcium voltage-gated channel subunit alpha1 AC (*Cacna1a*) is a subunit of a voltage-dependent calcium channel and glutamate ionotropic receptor NMDA type subunit 2A (*Grin2a*) is a subunit of NMDA receptors (Fig. 3.9 C, D, Fig. 3.10). Both play crucial disease-related roles. *Cacna1a* mutations are known to cause ataxias, familial hemiplegic migraine and intellectual disabilities. *Grin2a* mutations have been linked with epilepsy (Travaglini et al., 2017; Strehlow et al., 2019). Additionally, homer scaffold protein 1 (*Homer1*), an important scaffolding protein of glutamatergic post-synapses, was downregulated (Fig. 3.9 C, D, Fig. 3.10). Among "GABAergic synapse" genes, for instance, subunits of GABA receptors such as gamma-aminobutyric acid type A receptor subunit alpha2 (*Gabra2*) and Gamma-Aminobutyric Acid Type A Receptor Subunit Gamma2 (*Gabrg2*) were downregulated.

Excitotoxicity was shown to be involved in the pathology of HD (Sánchez, Mejía-Toiber, & Massieu, 2008). Thus, the downregulation of glutamatergic post-synaptic genes

might serve as a compensatory mechanism to reduce excitatory input and prevent further excitotoxicity. Conversely, the upregulation of GABAergic post-synaptic genes could aim to increase inhibitory input and render glutamatergic neurons less excitable.

For upregulated pathways, KEGG pathway analysis identified several pathways involved in NDs like "AD", "PD" and "HD" (Fig. 3.9 B). Several DEGs of the ND pathways were also part of the "Oxidative phosphorylation" and "Protein processing in the ER" pathways (Fig. 3.10).

Of the "Oxidative phosphorylation" pathway, a multitude of structural mitochondrial genes and mtRNAs were upregulated. The increase in mtRNAs might be attributed to the release of mtRNAs from mitochondria through leaky mitochondrial membranes. The released mtRNA could adhere to the nuclear envelope and be detected with snRNA-seq, which was already demonstrated by a previous study (H. Lee et al., 2020).

Moreover, the "Lysosome" pathway was significantly upregulated in all glutamtergic neuronal populations (Fig. 3.9 B). Lysosomal genes included lysosomal-associated membrane protein (*Lamp1*) and *Lamp2*, and the lysosomal protease Cathepsin D (*Ctsd*) (Fig. 3.9 C, D, Fig. 3.10). This is consistent with previous observations of increased lysosome numbers in HD patients (Sapp et al., 1997).

One pathway that stood out as by far most significantly upregulated was "Protein processing in the ER" (Fig. 3.9 B). Upregulated genes of this pathway included a variety of structural ER genes, UPR signalling and UPR genes. For example, the expression of several structural ER genes was increased including OS9 Endoplasmic Reticulum Lectin (*Os9*), calreticulin (*Calr*), and calnexin (*Canx*) (Fig. 3.9 C, D). *Os9* is commonly known as a marker for the ER-derived quality control compartment of the ER (Alcock & Swanton, 2009). The ER-derived quality control compartment was shown to be swollen in cellular HD models (Leitman et al., 2013). Furthermore, increased expression was observed for *Hspa5*, which senses unfolded proteins in the ER lumen and activates the UPR pathway upon ER stress. Additionally, the expression of the TF *Xbp1* was increased. *Xbp1* is activated via *Hspa5* upon ER stress and upregulates the expression of UPR genes.

Moreover, several ER-resident chaperones were upregulated, including heat shock protein 90 alpha family class A member 1 (*Hsp90aa1*), heat shock protein 90 alpha class B member 1 (*Hsp90ab1*), heat shock protein 8 (*Hspa8*) (Fig. 3.9 C, D).

In conclusion, these findings suggest the occurrence of ER stress in R6/2 mice, triggering the UPR pathway via *Hspa5* and *Xbp1*, leading to the upregulation of UPR genes and structural ER genes.

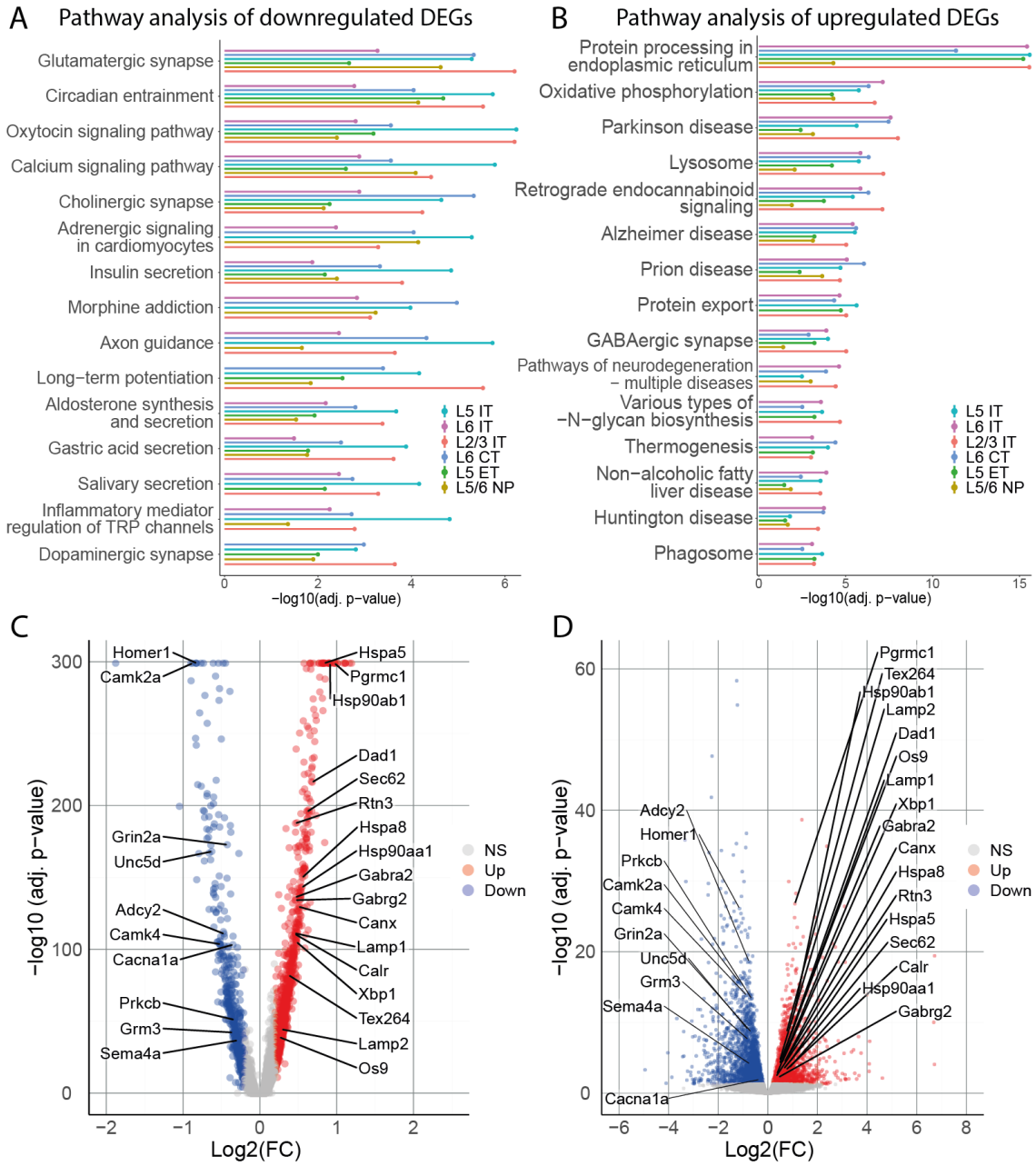

Fig. 3.9: Commonly differentially expressed pathways among glutamatergic neurons

A. KEGG pathway analysis for downregulated DEGs of glutamatergic neurons at 12 weeks.

B. KEGG pathway analysis for upregulated DEGs of glutamatergic neurons at 12 weeks.

C. Volcano plot for transcriptome-wide changes of L2/3 IT neurons at 12 weeks. Adjusted p-values were calculated with the Wilcoxon rank sum test.

D. Volcano plot for transcriptome-wide changes of L2/3 IT neurons at 8 and 12 weeks. Adjusted p-values and Log2(FC) were calculated with DESeq2 from pseudobulk counts from 8 and 12 weeks.

Downregulated Pathways	
Glutamatergic synapse	Homer1,Plcb1,Grin2a,Adcy2,Cacna1a,Dlgap1,Itpr1,Prkca,Gria3,Prkcb,Ppp3ca,Grm3,Grm8,Gls,Plcb4
Circadian entrainment	Camk2a,Plcb1,Grin2a,Adcy2,Itpr1,Prkca,Nos1ap,Gria3,Per3,Prkcb,Per1,Gucy1a1,Plcb4
Oxytocin signaling pathway	Camk2a,Plcb1,Cacna2d3,Adcy2,Camk4,Cacng3,Itpr1,Prkca,Cacnb4,Rock2,Camkk2,Prkcb,Ppp3ca,Camk1g,Gucy1a1,Eef2k,Plcb4
Calcium signaling pathway	Camk2a,Plcb1,Chrm3,Grin2a,Adcy2,Camk4,Cacna1a,Itpka,Ntrk2,Itpr1,Prkca,Prkcb,Ppp3ca,Ntrk3,Camk1g,Htr2a,Phka2,Plcb4
Cholinergic synapse	Camk2a,Plcb1,Chrm3,Adcy2,Camk4,Cacna1a,Kcnq5,Itpr1,Prkca,Prkcb,Kcnq3,Plcb4
Upregulated Pathways	
Protein processing in endoplasmic reticulum	Hspa5,Hsp90ab1,Tusc3,Dad1,Sec62,Pdia6,Sar1b,Rpn1,Pdia3,Hspa8,Hsp90aa1,Erp29,Canx,Bcap31,Hsp90b1,Ddost,Calr,Ssr2,Xbp1,Amfr,Rpn2,Erlec1,Ssr4,Ssr1,Herpud1,Ubxn4,Pdia4,Prkcsh,Ssr3,Ckap4,Man1a,Sar1a,Ubxn8,Selenos,Hyou1,Tram1l1,Os9,Dnaja1,Prkn,Dnajb11
Oxidative phosphorylation	Ndufc2,Atp6v0c,Atp6v0a1,Ndufa4,Atp6ap1,Ndufa13,Ndufa1,Ndufa3,Ndufb11,Ndufa11,Cox8a,Ndufb5,Cox6c,Ndufs7,Cox4i1,Cox6a1,Atp6v1e1,Atp6v0e2,Atp6v1h,Cyc1,Atp5k,Ndufb6,Atp6v1d,Ndufb8
Parkinson disease	Hspa5,Ndufc2,Ndufa4,Ndufa13,Gnas,Ndufa1,Ndufa3,Ndufb11,Xbp1,Ubb,Klc1,Ndufa11,Tubb2a,Cox8a,Ndufb5,Cox6c,Psmd3,Ndufs7,Sncaip,Cox4i1,Gnai2,Slc39a6,Cox6a1,Slc39a3,Psmb1,Tuba1a,Slc39a7,Tubb5,Cyc1,Uchl1,Camk2d,Ndufb6,Slc25a4,Vdac3,Ndufb8,Prkn,Psma3,Rps27a
Lysosome	Psap,Laptm4a,Atp6v0c,Ctsb,Ctsl,Atp6v0a1,Atp6ap1,Gaa,Ctsd,Lamp1,Lgmn,Smpd1,Hgsnat,Atp6v1h,M6pr,Lamp2,Ctsf,Abca2,Ids,Ppt1,Scarb2,Hexb,Ap4s1,Slc17a5,Gnptg
Retrograde endocannabinoid signaling	Ndufc2,Ndufa4,Ndufa13,Gria1,Ndufa1,Gabrb1,Gabra2,Ndufa3,Gabrg2,Ndufb11,Ndufa11,Gria2,Ndufb5 Ndufs7,Kcnj3,Gnai2,Cacna1d,Gabra1,Gabrb3,Gng3,Gnao1,Ndufb6,Cacna1b,Gabra3,Ndufb8,Gabrg3

Fig. 3.10: List of significantly changed KEGG pathways and their DEGs
List of the top 5 KEGG pathways most significantly enriched for downregulated and upregulated DEGs, and the DEGs of these pathways. DEGs are exemplary shown for L2/3 IT neurons.

3.7 ER-phagy is increased in presence of mHTT aggregates

The process of ER-phagy has received increasing interest for its role in starvation response, ER reshaping and ER stress response in recent years (Yang et al., 2021). As KEGG pathway analysis indicated an important role of ER stress response in R6/2 mice, we explored whether ER-phagy might also be involved as a response to ER stress in R6/2 mice.

To date, six porteins are known to function as membrane-anchored mammalian ER-phagy receptors. Interestingly, five out of six of those ER-phagy receptors were significantly upregulated: cell cycle progression 1 (*Ccpg1*), reticulophagy regulator 1 (*Retreg1*), *Tex264*, *Sec62* and *Rtn3* . Of the 5 upregulated ER-phagy receptors, especially *Tex264*, *Sec62* and *Rtn3* exhibited particularly strong upregulation (Fig. 3.9 C, D, Fig. 3.11 A). Additionally, genes previously shown to facilitate ER-phagy and cargo recognition, like progesterone receptor membrane component 1 (*Pgrmc1*) and *Canx* were upregulated (Fig. 3.9 C, D). Furthermore, lysosomal genes previously mentioned like *Lamp1*, *Lamp2* and

Ctsd were upregulated (Fig. 3.9 C, D). Hence, ER-phagy might be a response to mitigate ER stress and restore ER homeostasis in R6/2 mice.

Next, we investigated whether the process of ER-phagy is increased in response to mHTT in cellular models. For this, we utilized the ER-phagy sensor ss-RFP-GFP-KDEL (Chino & Mizushima, 2020). This sensor localizes to the ER lumen due to the presence of a signal sequence (ss) and contains a KDEL sequence for ER retention (Fig. 3.11 B). If ss-RFP-GFP-KDEL is in the ER at neutral pH, both GFP and RFP, emit fluorescence. However, during ER-phagy, the sensor is engulfed into lysosomes along with ER fragments. In lysosomes, the pH is more acidic and GFP gets quenched, leaving only RFP fluorescence (Fig. 3.11 B).

We generated a stable HEK cell line expressing ss-RFP-GFP-KDEL. To test the functionality of the sensor in HEK cells, we starved the stable ss-RFP-GFP-KDEL HEK cells for 4 hours in Earle's Balanced Salt Solution (EBSS), which triggers ER-phagy (Y. Lim, Kim, & Kim, 2021). Starvation led to an increased amount of acidified ER (Fig. 3.11 D). Next, we transfected the stable ss-RFP-GFP-KDEL HEK cells with non-toxic HTTQ25-His or toxic HTTQ72-His, and fixed the cells after 48 hours. ss-RFP-GFP-KDEL HEK cells showed a significant increase of acidified ER, when transfected with HTTQ72-His compared to the non-toxic HTTQ25-His 48h after transfection (Fig. 3.11 C, D). This was also true, when we normalized the amount of acidified ER to the total intensity of GFP, as an indicator for the expression level of ss-RFP-GFP-KDEL (Fig. 3.11 E). This indicated an increase in ER-phagy in the presence of mHTT.

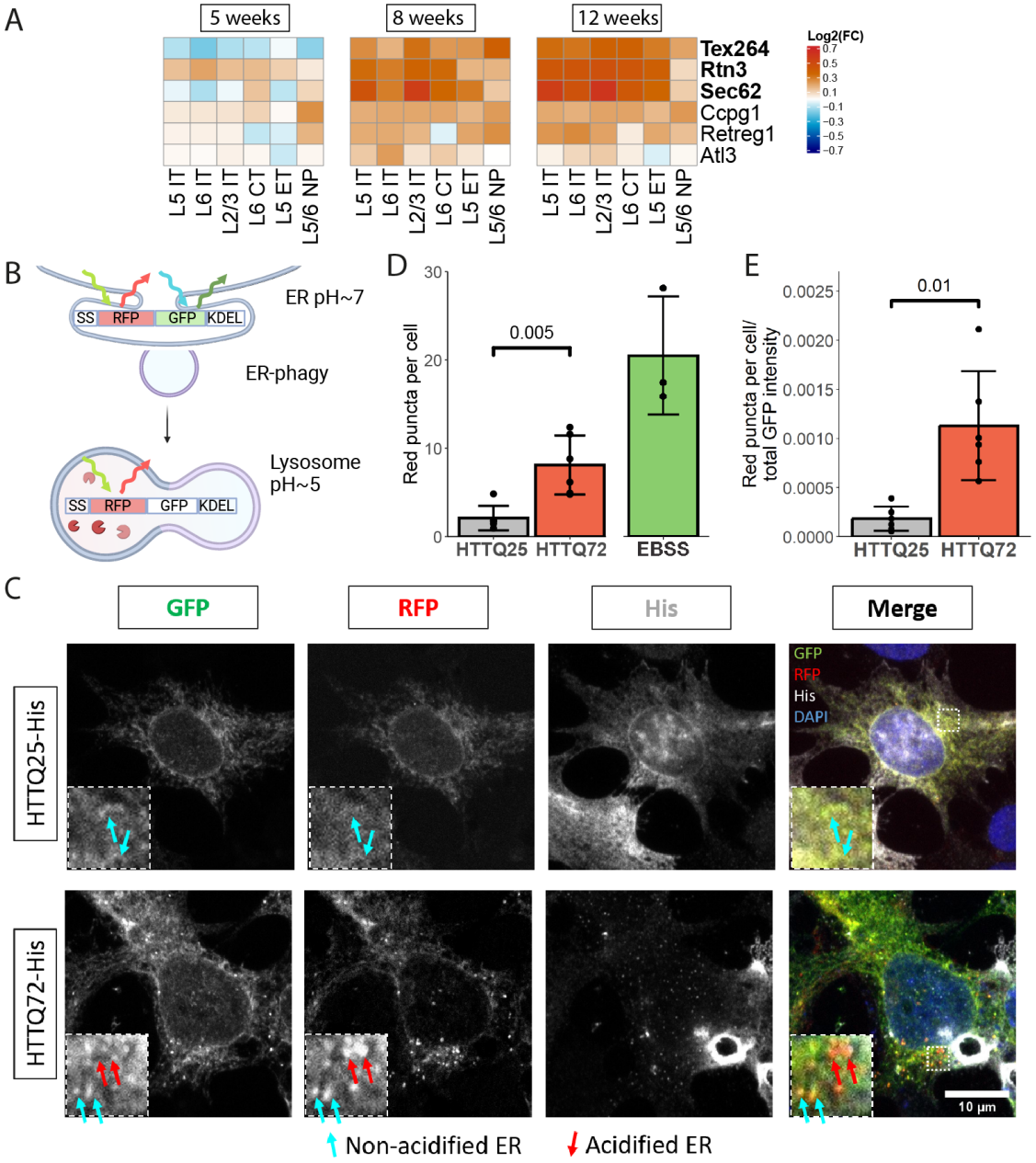

Fig. 3.11: An ER-phagy sensor detects an increase in acidified ER in the presence of mHTT

A. Several of the ER-phagy receptors are upregulated in R6/2 mice from 8 weeks on.
B. ss-RFP-GFP-KDEL exhibits RFP and GFP fluorescence in the ER. Upon ER-phagy, the sensor gets transported to lysosomes where the pH is more acidic and GFP is quenched.
C. Representative images of stable ss-RFP-GFP-KDEL HEK cells transfected with HTTQ25-His or HTTQ72-His. Cells transfected with HTTQ72-His showed an increased amount of acidified ER (red arrows). Stable ss-RFP-GFP-KDEL HEK cells were transfected with HTTQ25-His or HTTQ72-His, fixed after 48 hours and stained with immunocytochemistry.
D. Quantification of acidified ER per cell for stable ss-RFP-GFP-KDEL HEK293T transfected with HTTQ25-His or HTTQ72-His for 48 hours (n=6 biological replicates, with $\sim$ 15 cells per replicate). Starvation with EBSS for 4 h is used as a positive control for demonstrating the functionality of the sensor in stable expressing HEK293T cells.
E. To make sure differences in acidified ER were not caused by a difference in expression level of the ss-RFP-GFP-KDEL reporter, we normalized the acidified ER per cell to the total amount of GFP.

3.8 Upregulated gene modules of R6/2 mice have a higher expression in WT GABAergic neurons

After identifying differentially expressed pathways, we focused on identifying gene networks that are differentially expressed in R6/2 mice and genes that are central to these networks, so-called "hub genes". For identifying co-expression networks, we applied weighted gene co-expression network analysis (WGCNA), a method which groups genes into modules based on their co-expression across genotypes and time points. For WGCNA, we used the "scWGCNA" package by Feregrino and Tschopp (2022). ScWGCNA averages the transcriptome of 15 neighboring nuclei in UMAP space to pseudocells. These pseudocells enable a more robust analysis with WCGNA (Feregrino & Tschopp, 2022; Morabito et al., 2021). We ran scWGCNA on variable genes and DEGs that occurred at least at one time point and for at least 2 cell subclasses. ScWGCNA separated these genes into 20 co-expression modules, each containing between 65 and 431 genes (Fig. 3.12 A, B).

Next, we correlated the expression of these modules, in form of module eigengene expression, with their expression in WT or R6/2 nuclei at each time point (Fig. 3.12 B). Modules with a positive correlation correspond to modules with a set of genes that are mostly upregulated in R6/2 mice. Modules with a negative correlation correspond to modules, where genes are mostly downregulated in R6/2 mice. Correlation values at 8 and 12 weeks were relatively similar, being in line with our observation of a high correlation of transcriptomic changes at 8 and 12 weeks (Fig. 3.5 H, I). The turquoise module exhibited a negative correlation at 5 weeks but a positive correlation at 8 and 12 weeks. This module also included genes with bidirectional regulation discussed in chapter 3.4.

Following this, we examined the expression level of the module eigengenes in WT glutamatergic neurons and WT GABAergic neurons. A positive correlation corresponds to a higher expression in WT GABAergic neurons relative to glutamatergic neurons,

and a negative correlation with a higher expression in glutamatergic neurons relative to GABAergic neurons. To our surprise, most modules with upregulated genes in R6/2 mice were correlated with a higher expression in WT GABAergic neurons (Fig. 3.12 B, C). Moreover, modules with downregulated genes in R6/2 mice are higher expressed in WT glutamatergic neurons. For instance, the turquoise module showed an upregulation in all neuronal cell subclasses starting at 8 weeks in R6/2 mice. This is shown by an increase in module eigengene expression in neuronal subclasses at 8 and 12 weeks in R6/2 nuclei (Fig. 3.12 D). However, WT GABAergic neurons displayed higher turquoise module eigengene expression compared to the WT glutamatergic neurons, indicating a higher baseline expression in WT GABAergic neurons.

This phenomenon was also reflected by the average expression values. The average expression of turquoise module genes in WT GABAergic neurons and WT glutamatergic neurons remained stable with age, but was 24% higher in WT GABAergic neurons ($1.24 = 2^{(2.028-1.714)} = 2^{(average.WT.expression.GABA - average.WT.expression.glutamate)}$) (Fig. 3.12 E). At 8 weeks, expression increased in both neuronal classes in R6/2 mice. However, expression values in R6/2 glutamatergic neurons only reached average expression values of WT GABAergic neurons (Fig. 3.12 D).

Considering the pattern of selective vulnerability, with GABAergic neurons being relatively spared from HD while glutamatergic neurons are more affected, we hypothesized that this gene module could contain genes protective against HD pathology. The upregulation of these genes could be a compensatory or protective response to the disease. The increased baseline expression of these genes in GABAergic neurons could render them less vulnerable to HD pathology.

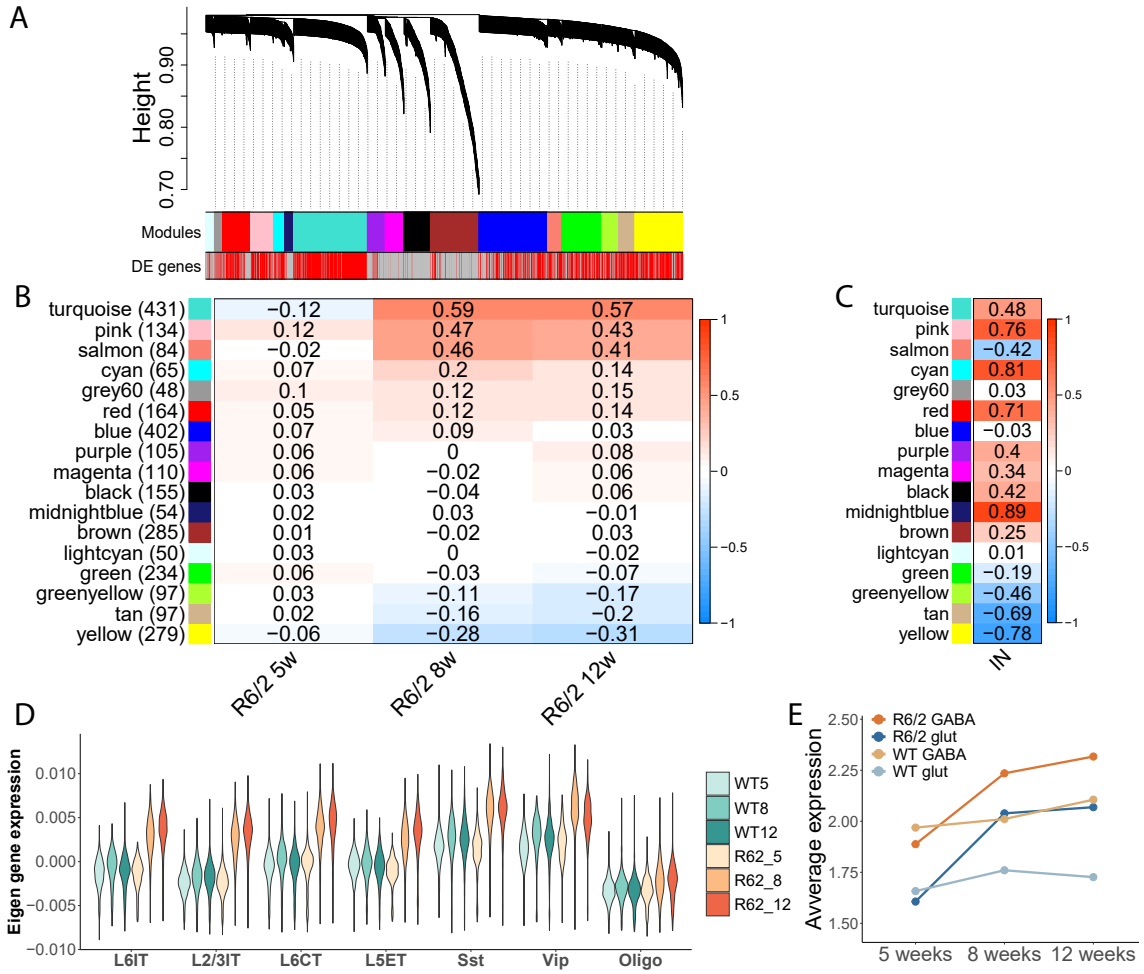

Fig. 3.12: A module of genes upregulated in R6/2 mice and intrinsically higher expressed in GABAergic neurons

A. Gene dendrogram showing gene modules identified with scWGCNA. The height represents 1-Topological overlap, a measurement for co-expression of the individual gene with other genes of the module. Modules are indicated by colour coding, and DEGs are marked in red.

B. Module-trait relationship showing the correlation of module expression with R6/2 nuclei from different ages. A positive correlation signifies an upregulation of the module in R6/2 mice at the time point, whereas a negative correlation a downregulation.

C. Module-trait relationship showing the correlation of module expression with WT GABAergic neurons. A positive correlation signifies a higher expression of the module in WT GABAergic neurons, whereas a negative correlation a higher expression in WT glutamatergic neurons.

D. Module eigengene expression for the turquoise module in several cell subclasses across time points. Module eigengene expression is a measurement for the combined expression of the 431 genes of the turquoise module. Turquoise eigengene expression is higher in WT GABAergic neurons compared to WT glutamatergic neurons. At 8 weeks, the expression increases in all neuronal subclasses.

E. Average expression of the 431 genes of the turqouise module in GABAergic and glutamatergic neurons. The 431 genes showed a higher baseline expression in WT GABAergic neurons compared to WT glutamtergic neurons.

To test our hypothesis, we investigated whether genes of these modules could be vital for neuronal survival or protective against HD pathology. We used data from a genome-wide screen, which identified genes that modify neuronal survival in striatum of WT mice and R6/2 mice (Wertz et al., 2020). In this study, the authors identified 3875 genes which caused neuronal cell death upon knock-down in WT mice ("neuronal essential genes"). Furthermore, they identified 554 genes that lead to increased neuronal death in R6/2 mice upon knock-down, indicating their protective role in R6/2 mice ("mHtt toxicity modifier genes"). Out of the 3875 neuronal essential genes, 3009 were expressed in the MC. Interestingly, neuronal essential genes were significantly overrepresented in the turquoise module (Fig. 3.13 A). Hence, a module with genes that are essential for neuronal survival, is upregulated in R6/2 mice and exhibits a higher baseline expression in WT GABAergic neurons compared to WT glutamatergic neurons. However, no modules showed significant over-representation of mHTT toxicity modifying genes (Fig. 3.13 B).

In summary, we identified a module of genes upregulated in R6/2 mice, potentially representing an adaptive response to the disease, as this module was significantly enriched for neuronal essential genes. Interestingly, genes of this module are intrinsically more highly expressed in GABAergic neurons, which could potentially render them less vulnerable compared to glutamatergic neurons.

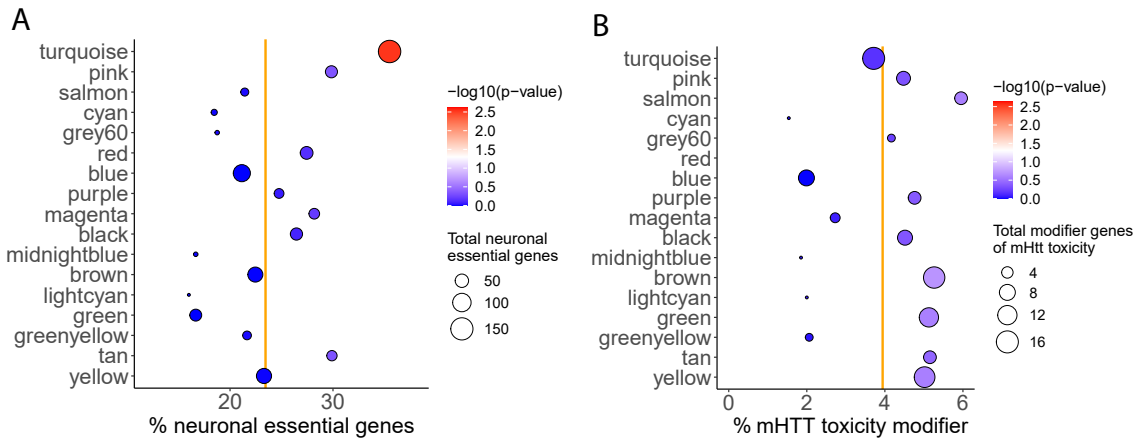

Fig. 3.13: A module of genes upregulated in R6/2 mice and intrinsically higher expressed in GABAergic neurons is enriched for neuronal essential genes

A. Gene modules were tested for the over-representation of 3009 neuronal essential genes identified by Wertz et al. (2020) that were expressed in the MC. P-values for over-representation were calculated using Fisher's exact test.
B. Same plot as A. with testing for the over-representation of mHTT toxicity modifier genes.

3.9 Identification of potentially protective hub genes in R6/2 mice

To pinpoint specific genes within modules that could render neurons more resilient to mHTT, we constructed the gene network with its hub genes. For this, we plotted the top 10% of hub genes from modules showing a correlation greater than absolute 0.15 for at least one time point. Further, we plotted the 20% highest absolute adjacencies within the network. The closer two genes are in the network, the more tightly they are co-expressed. Additionally, also all neuronal essential genes and mHTT modifier genes were highlighted (Fig. 3.14).

From the network, several hub genes emerged as particularly noteworthy. Among the upregulated hub genes, again, ER chaperones such as *Hspa5*, *Hsp90aa1*, *Hsp90ab1* and heat shock protein 90 beta family member 1 (*Hsp90b1*) stood out exhibiting a high

centrality. Furthermore, *Hspa8*, which was already shown to prevent formation of polyQ aggregates, was a central hub gene which was also a neuronal essential gene and mHTT modifier gene (Novoselova et al., 2005). Additionally, the ER-phagy receptors *Sec62*, *Tex264* and *Rtn3* were identified as hub genes. Furthermore, two genes encoding for secreted chaperones, *Pcsk1n* and *Scg5*, showed high centrality, with *Pcsk1n* being among the neuronal essential genes.

From the downregulated modules, calcium/calmodulin dependent protein kinase II alpha (*Camk2a*) stood out as having a high centrality while also being a neuronal essential gene and a mHTT modifier gene (Fig. 3.14). Decreased *Camk2a* activity has been associated with synaptic deficits in HD models, caused by an impaired BDNF–tyrosine receptor kinase B (TRKB)-CAMK2A signalling pathway (Zhang et al., 2018). Several other genes associated with synaptic signalling and calcium signalling like *Grin2a*, ryanodine receptor 2 (*Ryr2*), potassium voltage-gated channel interacting protein 4 (*Kcnip4*) and calcium voltage-gated channel auxiliary subunit alpha2delta 1 (*Cacna2d1*) were central to the network. Interestingly, the TF human immunodeficiency virus type I enhancer binding protein 2 (*Hivep2*) was among the central hub genes. *Hivep2* was previously not associated with HD, but *Hivep2* was shown to promote the expression of glutamate receptors, and *Hivep2* KO in mice caused decreased PV and GAD1 expression levels, a thinner cortex and a mild chronic inflammation of the brain (Zhou et al., 2022; Takao et al., 2013). Thus, *Hivep2* might constitute a TF that is involved in the loss of neuronal identity in R6/2 mice and the downregulation of glutamatergic synaptic genes observed in R6/2 mice.

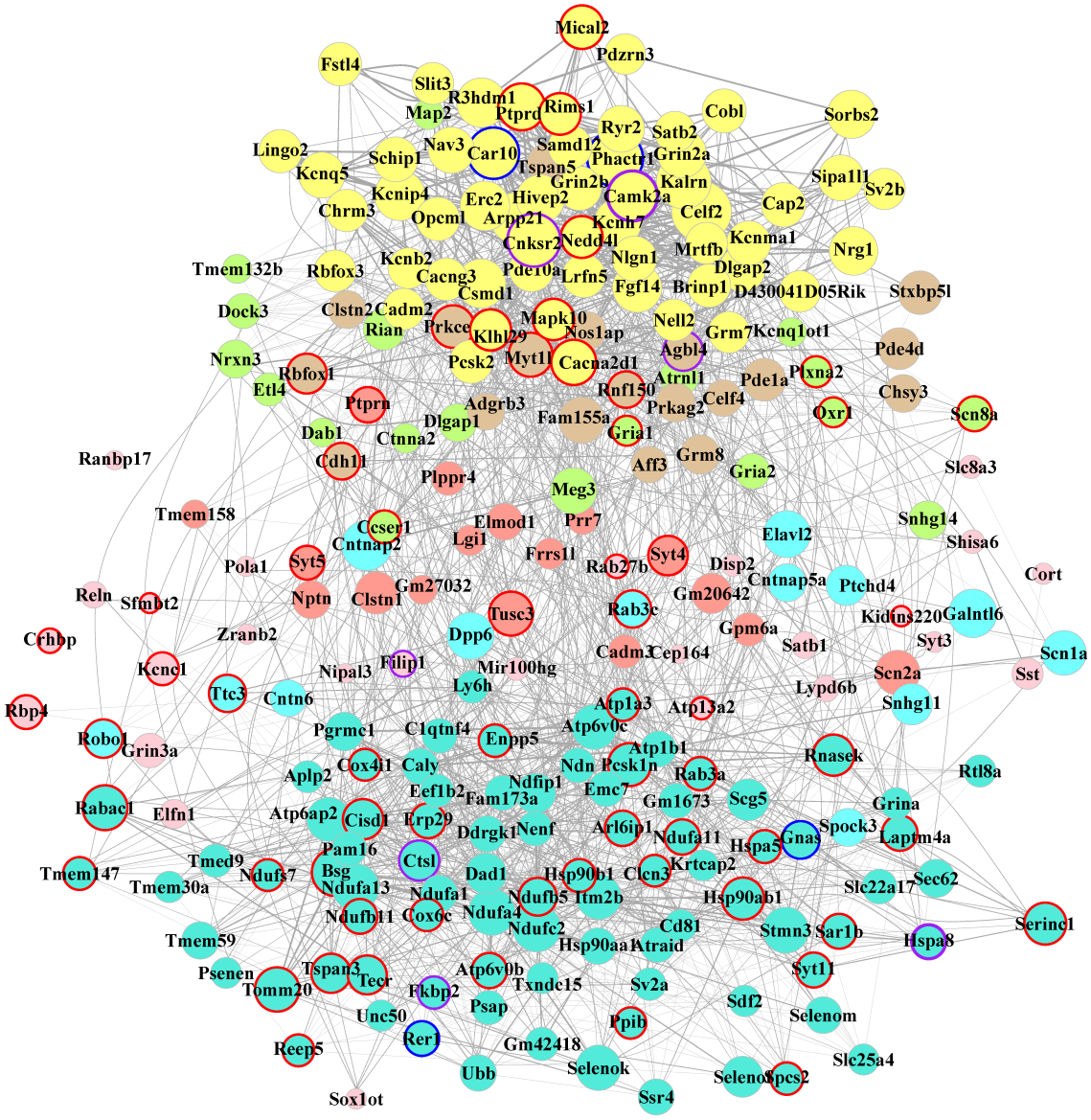

Fig. 3.14: Co-expression gene network with hub genes of the R6/2 transcriptome
Visualization of the co-expression gene network with hub genes of modules that differentially expressed in R6/2 mice. Vertices are coloured by the module the gene is part of. Yellow, tan and green yellow genes are from downregulated modules and turquoise, pink, salmon and cyan genes are from upregulated modules. The size of the vertices are proportional to the centrality of a gene, meaning the larger a vertex, the more tightly the gene is co-expressed with the other genes of the module. The size of the edges and distance between vertices represent the adjacency of genes, meaning the closer two genes are, the more tightly those two genes are co-expressed. Neuronal essential genes are marked by a red, mHTT toxicity modifier genes by a blue, and genes that fit both categories by a purple border.

In a second, complementary approach, we plotted all neuronal essential genes and

their relative expression between WT glutamatergic and WT GABAergic neurons (Fig. 3.15). To calculate the relative expression, we used DESeq2 to avoid possible biases due to the varying amount of neurons for the neuronal classes and due to normalization methods. We then looked for neuronal essential genes, which showed a higher expression in GABAergic neurons compared to glutamatergic neurons and could render them more resistant. As indicated by the correlation values, neuronal essential genes of the turquoise module were higher expressed in the GABAergic neurons. To these also belonged the aforementioned chaperones *Hspa8*, *Dnajb9*, *Hspab1* and protein disulfide isomerase A3 (*Pdia3*) (Fig. 3.15). Furthermore, several mitochondrial genes like NADH:ubiquinone oxidoreductase subunit A3 (*Ndufa3*), translocase of outer mitochondrial membrane 20 (*Tomm20*) and *Cox8a* which were among the bidirectionally regulated genes were more highly expressed in GABAergic neurons. Of particular interest was *Pcsk1n*, which was among the neuronal essential genes with the highest relative expression in GABAergic neurons (Fig. 3.15). Furthermore, *Pcsk1n* had already shown a high centrality in the gene network (Fig. 3.14).

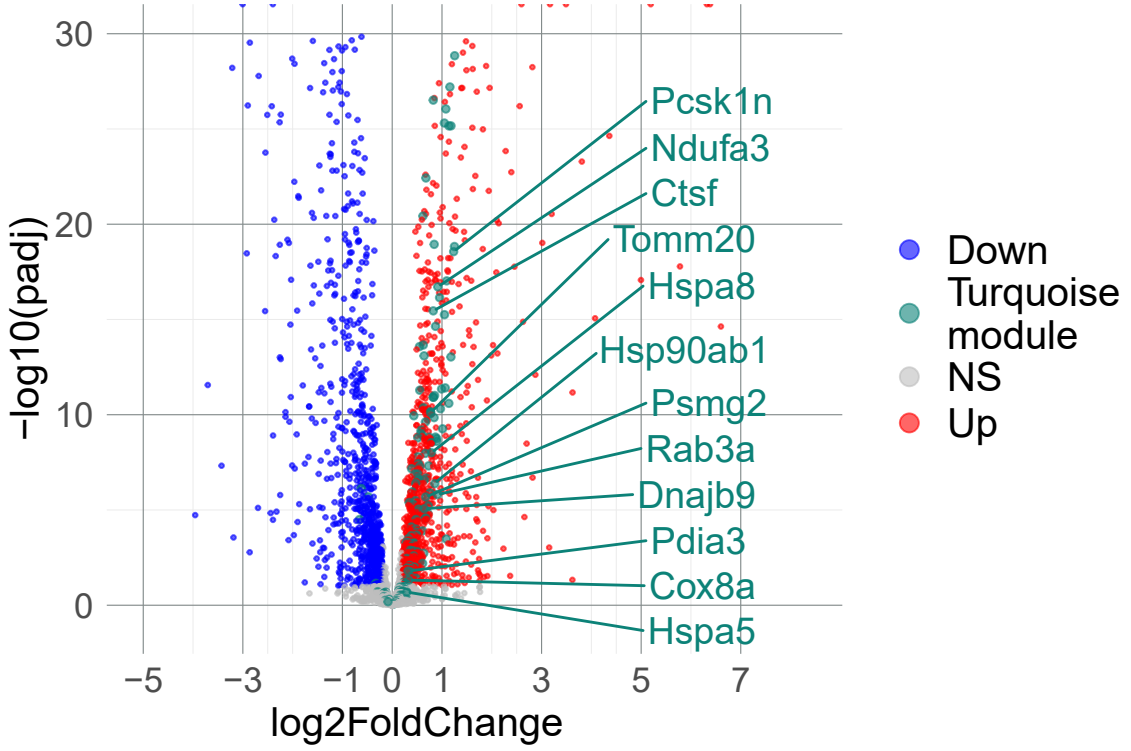

Fig. 3.15: Neuronal essential genes from the turquoise module have a higher expression in WT GABAergic neurons

Volcano plot showing the relative expression of neuronal essential genes between WT GABAergic and WT glutamatergic neurons. Genes from the turquoise module were particularly highly expressed in GABAergice neurons. One of the most significant DEGs was *Pcsk1n*, a chaperone which was previously mainly associated with a function as secretory chaperone. Log2(FC) and adjusted p-values were calculated with pseudobulk counts for WT glutamatergic neurons and WT GABAergic neurons from all time points (n=7).

To investigate the potential involvement of *Pcsk1n* in HD, we stained primary cortical neurons transduced with HTTQ25-myc or HTTQ72-myc for proSAAS. In neurons expressing HTTQ25-myc, proSAAS expression was detected thoughout the soma of neurons. To our surprise, in neurons expressing HTTQ72-myc, proSAAS exhibited a distinct nuclear localization, a phenomenon not previously reported for proSAAS (Fig. 3.16 A, B). This nuclear formation of spheres was significantly increased in neurons expressing HTTQ72-myc (Fig. 3.16 B). However, the proSAAS spheres did not colocalize with HTT-Q72 aggregates (Fig. 3.16 C). It is intriguing to think about a possible chaperon function of

proSAAS helping to mitigate proteotoxic stress upon the formation of mHTT aggregates.

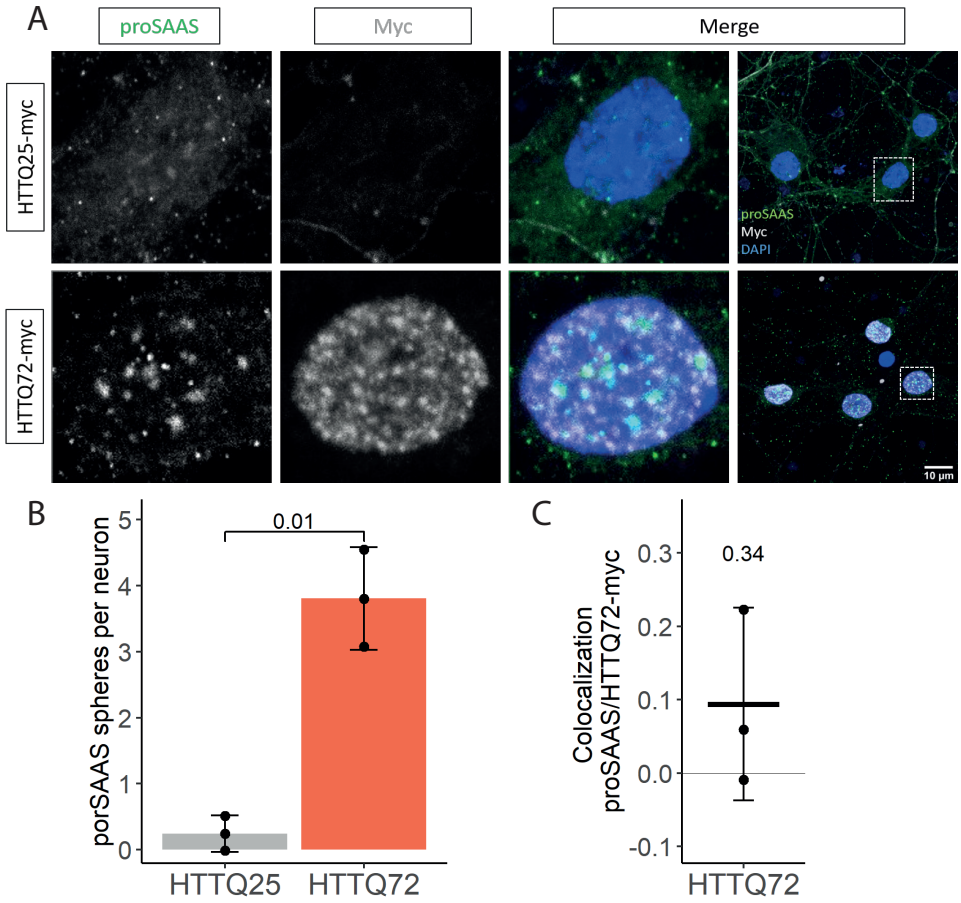

Fig. 3.16: proSAAS translocates to the nucleus in the presence of nuclear mHTT

A. Representative images of primary neurons transduced with HTTQ25-myc or HTTQ72-myc, fixed after 7 DIV post-transduction and stained for proSAAS with ICC. In HTTQ25-myc transduced primary neurons, proSAAS is distributed evenly across the soma. In the presence of nuclear HTTQ72-myc aggregates, proSAAS translocates to the nucleus and formes spheres.
B. The formation of proSAAS spheres was significantly increased in primary neurons expressing HTTQ72-myc.
C. ProSAAS spheres did not show a colocalization with HTTQ72-myc aggregates in primary neurons.

In summary, our analysis revealed that gene modules upregulated in R6/2 mice have a tendency of a higher expression in WT GABAergic neurons. In contrast, genes that are widely downregulated in R6/2 mice have a higher expression in WT glutamatergic neurons. An upregulated module with a higher expression in WT GABAergic neurons was enriched

for neuronal essential genes. We hypothesized that genes of this module could render GABAergic neurons more resistant to the toxicity of mHTT. We investigated whether one of these genes, the chaperone proSAAS, could play a role in HD. Surprisingly, proSAAS translocated to the nucleus in neurons expressing HTTQ72-myc, suggesting a potential mechanism linking proSAAS and mHTT.

4 Discussion

While the genetic cause of HD has been identified in 1983 and mHTT aggregates were discovered in 1997, to date, the molecular pathways driving neurodegeneration in HD remain to be uncovered (Gusella et al., 1983; Davies et al., 1997). Identification of pathways giving rise to neurodegeneration might result in novel opportunities for therapeutic approaches. Moreover, the pattern of selective vulnerability in the MC, with glutamatergic CPNs being particularly affected, lacks explanation. Unraveling the mechanism giving rise to the pattern of selective vulnerability could provide insights into which factors render certain neuronal populations more resilient, and how to protect vulnerable populations.

In this study, we conducted a snRNA-seq study with the R6/2 mouse model across multiple time points. Our findings reveal that vulnerable neuronal populations of the MC undergo a strong transcriptomic shift in contrast to non-vulnerable populations. Interestingly, transcriptomic changes during disease progression are not linear, and some genes are bidirectionally regulated at early and late time points. Moreover, we observed that the expression of marker genes for ER stress is increased in R6/2 mice and ER-phagy is increased in the presence of mHTT. Finally, we discovered that the chaperone proSAAS, which was previously only found to be secreted and located in the soma, translocates to the nucleus in presence of nuclear mHTT aggregates suggesting a possible interaction.

4.1 SnRNA-seq identifies a transcriptomic shift in vulnerable populations in the MC of R6/2 mice

In the cortex of HD patients, the pattern of selective vulnerability is characterized by the loss of CPNs, while GABAergic neurons remain relatively spared (Thu et al., 2010; Macdonald & Halliday, 2002; Han et al., 2010). Initially, the R6/2 mouse model of HD was perceived as lacking neuronal cell death (Turmaine et al., 2000). However, our study

reveals neuronal loss occurring in the MC of R6/2 mice with similar neuronal populations being lost as observed in HD patients (Bunner & Rebec, 2016; Rebec, 2018). Specifically, a reduction in the proportions was observed particularly for L2/3 IT and L5 IT neurons at 12 weeks (Fig. 3.2 D, E).

Notably, this loss of neurons was preceded by a pronounced transcriptomic shift in these populations. The transcripomic shift was present in the more vulnerable glutamatergic neurons, but not in the more resilient GABAergic neurons, as demonstrated by multiple analytical approaches (Fig. 3.3 A-G). These findings align with observations from the striatum of another HD mouse model, where the vulnerable MSNs, but not the locally projecting interneurons, undergo a transcriptomic shift (Malaiya et al., 2021).

Furthermore, IT neurons exhibited increased transcriptomic changes compared to other glutamatergic populations (Fig. 3.3 D-G). Loss of cortico-striatal connectivity has been observed in a knock-in HD mouse model and precedes the death of striatal neurons (Deng, Wong, Bricker-Anthony, Deng, & Reiner, 2013). As IT neurons mainly project to the striatum, potentially, the loss of synaptic innervation with striatal neurons might affect IT neurons, leading to transcriptomic alterations and an increased vulnerability.

Moreover, we observed an increase in the abundance of astrocytes and oligodendrocytes (Fig. 3.2 D, E). Previous studies have reported a similar increase in oligodendrocytes in the cortex of HD patients and HD mouse models (Myers et al., 1991; R. G. Lim et al., 2022). Astrocytes were shown to be in a reactive state in the cingulate cortex of HD patients (Al-Dalahmah et al., 2020). Further, lowering mHTT expression in astrocytes had beneficial effects on behaviour and rescued metabolic functions in R6/2 mice (Gangwani et al., 2023). Hence, the prominent involvement of astrocytes and oligodendrocytes is reflected by an increase in numbers, overall transcriptomic alterations and a decrease in marker gene expression (Fig. 3.2 D, E, Fig. 3.3 D-G, Fig. 3.7 B). Their increase in numbers might be attributed to an increased proliferation or a recruitment mechanism to the particularly affected brain regions.

One potential explanation for these transcriptomic alterations is that transcriptomic disturbances are directly caused by mHTT and add to the disease pathogenesis. This disruption may stem from nuclear mHTT aggregates sequestering TFs, thereby interfering

with transcriptomic regulation. Notably, mHTT was shown to sequester several TFs, potentially giving rise to the observed transcriptomic changes (Cong et al., 2005; Steffan et al., 2000; Takano & Gusella, 2002; Marcora et al., 2003; Dunah et al., 2002; Zuccato et al., 2003; Malaiya et al., 2021). Additionally, sequestration of proteins of the small interfering RNA (siRNA) machinery and alterations in enhancer RNA expression might further exacerbate transcriptomic dysregulation (Nalavade, Griesche, Ryan, Hildebrand, & Krauss, 2013; Le Gras et al., 2017).

On the other hand, transcriptomic alterations might represent an adaptive response employed by affected neuronal populations to counteract mHTT toxicity. Neurons more susceptible to mHTT toxicity could exhibit stronger transcriptomic changes in an attempt to develop a more robust protective response. An argument for this could be, that upregulated genes included several chaperones, genes of the UPR and protein degradation, which likely aid in mitigating the proteotoxic stress (Fig. 3.9 C, D, Fig. 3.14). Furthermore, it could be a well-defined response program, which is common across neuronal populations, as transcriptomic changes and upregulated genes were highly correlated and shared between glutamatergic subclasses (Fig. 3.4 H, Fig. 3.6 D). Possibly, both transcriptomic dysregulation caused by disturbances in the transcriptional regulation machinery and an adaptive response to mHTT toxicity, are reflected by these transcriptomic alterations.

4.2 Temporal dynamics of transcriptomic changes in R6/2 mice show a bidirectional pattern

To date, few studies have investigated early transcriptomic changes in HD and how they evolve with disease progression, also due to the limitation of human HD samples only being available post-mortem. Additionally, to our knowledge, no study with single-cell resolution at an early time point has yet been published. Leveraging the advantages of snRNA-seq and our longitudinal approach, we further delved into transcriptomic changes occurring at early time points and their development with time.

Pseudotime trajectory analysis revealed a distinct shift for R6/2 nuclei of L2/3 IT neurons, which formed a continuous trajectory from WT to 8-week R6/2 nuclei, ending

with the 12-week nuclei (Fig. 3.4 A-C). This trajectory underscored the progressive impact of mHTT on the transcriptome in symptomatic animals. Surprisingly, 5-week R6/2 nuclei displayed lower pseudotime values compared to WT nuclei and were positioned at the opposite end of the trajectory from 8 and 12-week R6/2 nuclei (Fig.3.4 A-C). This temporal pattern was consistent across IT, L6 CT and LE ET neurons (Fig. 3.4 D-F). In contrast, inhibitory neurons and glial cells did not exhibit a similar continuous trajectory, suggesting that excitatory neurons undergo distinct transcriptomic changes before and during disease onset (Fig. 3.4 G).

To further explore these temporal dynamics, we conducted a correlation analysis of transcriptomic changes at different ages (Fig. 3.4 H, I). The high correlation between 8 and 12 weeks validated, that a shared set of genes is altered in the same direction at the two late time points of the disease. However, the low correlation between 5 and 8 weeks supported the hypothesis that early and late disease stages involve distinct transcriptomic changes (Fig. 3.4 I).

Further investigation into the underlying genes responsible for these temporal dynamics revealed a set of genes that was downregulated at 5 weeks but upregulated at 8 and 12 weeks (Fig. 3.5 A). These genes, including *Atp6v0c*, *Cox8a*, *Dad1*, *Caly*, *Ubb*, and *Rpl41*, exhibited age-dependent bidirectional regulation, consistent across different neuronal subclasses (Fig. 3.5 C). KEGG pathway analysis highlighted the involvement of these genes in "Ribosomes", "Oxidative phosphorylation", and "Various NDs" including "HD" (Fig. 3.5 B). This bidirectional regulation of genes suggests a non-linear progression of transcriptional alterations in HD.

How these expression changes are involved in disease onset and progression remains to be explored. For instance, early in the disease, ribosomal genes might be downregulated to slow down the synthesis of further proteins that might be prone to aggregation. It was shown that ribosomal protein synthesis is stalled by mHTT in HD models (Eshraghi et al., 2021). Further, factors promoting translation were shown to be sequestered by mHTT aggregates, causing deficits in protein synthesis (Joag et al., 2020) Possibly, with disease progression, this stalling of ribosomal protein synthesis then is counteracted through the upregulation of ribosomal genes.

H. Lee et al. (2020) demonstrated the release of mtRNA from mitochondria due to ruptures in the mitochondrial membrane in HD patients and HD mouse models. However, this study was limited to a single, late-stage time point. Our findings further support this hypothesis and add a temporal dynamic to it, where mitochondrial genes and structural mitochondrial genes are initially downregulated. Possibly, this early downregulation may contribute to a defective mitochondrial structure, subsequently leading to the release of mtRNA from mitochondria with disease progression.

In conclusion, our findings provide valuable insights into the temporal dynamics of transcriptomic changes in glutamatergic neurons during HD progression. The non-linear nature of transcriptional dysregulation is characterized by distinct gene sets being dysregulated in opposite directions at different disease stages. These findings highlight the importance of identifying age-resolved molecular pathogenesis, as therapeutics targeting late molecular changes of HD might have adverse effects at early disease stages.

4.3 Loss of marker gene expression across cell populations

DEGs at later disease stages exhibited an interesting pattern, with upregulated DEGs being shared across various glutamatergic subclasses, while downregulated genes were more specific for the individual glutamatergic subclasses (Fig. 3.6 D, E). We hypothesized that these downregulated subclass-specific genes could be marker genes, based on a previous publication from our lab by Voelkl et al. (2022). Voelkl et al. (2022) demonstrated a downregulation of the interneuron type-specific markers SST and VIP in the corresponding GABAergic neuronal populations on the protein level in the MC of R6/2 mice.

In line with the observations on the protein level, we also observed a downregulation of these marker genes at the transcriptional level (Fig. 3.7 A). Moreover, we observed the same pattern as Voelkl et al. (2022), with *Sst* and *Vip* showing pronounced downregulation. This finding aligns with human post-mortem studies, which showed a decrease in calbindin-positive neurons, which highly overlap with the SST-positive neuron population (E. H. Kim et al., 2014; Gonchar, Wang, & Burkhalter, 2008). While Voelkl et al. (2022) did not observe a decrease in PVALB-positive neurons, we found a downregulation of *Pvalb*,

although less pronounced than that of *Sst* and *Vip* (Fig. 3.7 A). Possibly, the less pronounced transcriptional change of *Pvalb* precedes alterations at the protein level and is not yet detectable at the protein level. Additionally, we also observed downregulation of the marker gene *Lamp5* for the Lamp5 GABAergic neurons (Fig. 3.7 A). Interestingly, the phenomenon of marker gene downregulation was also seen for glutamatergic neurons, suggesting a more widespread mechanism of marker gene downregulation (Fig. 3.7 A).

Next, we investigated whether marker gene downregulation not only extended across several subclasses, but also affected multiple marker genes (Fig. 3.7 B). We observed a widespread marker downregulation of the top 100 marker genes for all neuronal subclasses. Moreover, marker gene downregulation was not limited to neuronal populations, but also affected astrocytes and oligodendrocytes, which have been previously implicated in HD (Myers et al., 1991; R. G. Lim et al., 2022; Al-Dalahmah et al., 2020). In conclusion, the downregulation of marker genes affects multiple cell subclasses involved in HD and impacts a multitude of marker genes.

Similar loss of marker genes has been observed in other NDs such as PD, ALS, or AD (Liguz-Lecznar, Urban-Ciecko, & Kossut, 2016; Offen et al., 2000). For instance, in AD, *Sst* and *Vip* are downregulated in their respective GABAergic neuronal subclasses (Liguz-Lecznar et al., 2016; Offen et al., 2000). Moreover, a meta-analysis of 22 AD large-scale gene expression datasets found downregulation of *Gad1* and *Gad2*, and replicated the downregulation of *Sst* (Hill & Gammie, 2022). In PD models, rescuing VIP expression had neuroprotective effects and in AD models, rescuing VIP expression decreased aggregate formation (Offen et al., 2000; M. Song et al., 2012). Moreover, restoration of GABAergic signalling was already proposed as a potential treatment in AD and PD (Shetty & Bates, 2016). It would be intriguing to explore whether rescuing *Vip* expression or the expression of other marker genes would also exert beneficial effects in HD.

Despite being observed across several NDs, the underlying cause of the marker gene downregulation remains elusive. Studies with induced pluripotent stem cells (iPSCs) derived from juvenile HD patients found a delayed differentiation of these iPSCs into striatal-like neurons (Mathkar, Suresh, Dunn, Tom, & Mattis, 2019). However, in our study, neurons from R6/2 mice at 5 weeks showed little change in marker expression, suggesting

that marker dysregulation occurs with disease progression and is not a direct result of developmental deficits (Fig. 3.7 B).

To investigate possible causes for the decrease in marker gene expression, we hypothesized that cell marker gene expression could be perturbed by a dysregulation of TFs, which regulate cell type identity (Yao et al., 2023). Indeed, marker TFs for glutamatergic neurons showed downregulation in glutamatergic neurons (Fig. 3.8 A, B). Specifically, the marker TFs *Neurod1*, *Zeb2*,*Junb* and *Fezf2* were downregulated (Fig. 3.8 B). However, downregulation of marker TFs for GABAergic neurons was limited to a few marker TFs, such as LIM Homeobox 2 (*Lhx2*) and LIM Homeobox 2 (*Lhx6*) (Fig. 3.8 B). Possibly, marker downregulation in GABAergic neurons is not caused by dysregulation of marker TFs, or the marker TFs for GABAergic neurons were not captured in the reference used for the analysis.

Another TF that could play a role maintaining cell identity and functional synapses is *Hivep2*, which was identified as a downregulated hub gene of the gene network (Fig. 3.14). *Hivep2* increases the expression of glutamate receptors, and *Hivep2* KO in mice leads to reduced PVALB and GAD1 expression (Zhou et al., 2022; Takao et al., 2013). Hence, the decreased expression of *Hivep2* might contribute to decreased marker expression in R6/2 mice.

In conclusion, the decrease in marker gene expression is not limited to the GABAergic populations identified previously, but is common among neuronal subclasses, and affects even astrocytes and oligodendrocytes. Moreover, the loss of marker gene expression affects a multitude of marker genes, possibly caused by the decreased expression of marker TFs. Rescue of marker gene expression could be protective, as seen in AD and PD (Offen et al., 2000; M. Song et al., 2012; Shetty & Bates, 2016). Rescuing marker gene expression by restoring marker TF expression could be an approach to target more upstream transcriptional regulators and achieve a more widespread effect.

4.4 Pathways altered at late stages in R6/2 mice

We investigated commonly altered pathways across glutamatergic populations, given their increased susceptibility observed with previous analyses. Common pathways with downregulated DEGs were mostly associated with neuronal signalling, including pathways like "glutamatergic synapse" and "Calcium signalling" (Fig. 3.9 A). Notably, the "Glutamatergic synapse" pathway encompassed DEGs from both, the glutamatergic pre-synapse and post-synapse. There are several potential explanations for the downregulation of glutamatergic synaptic genes (Fig. 3.10). One possibility is that the decrease in expression of glutamatergic pre-synaptic genes serves as a response to mitigate excitotoxicity mediated by cortical neurons onto striatal neurons (Sánchez et al., 2008). Another potential cause could be that the downregulation of glutamatergic synaptic genes follows the loss of corticostriatal connections, or conversely, it could be the cause for the loss of this connectivity (Deng et al., 2013; Cepeda & Levine, 2022). It remains to be explored whether the downregulation of synaptic genes is a cause or a consequence of this loss of connectivity.

Moreover, genes from the glutamatergic post-synapse are implicated in HD. In HD mouse models, there is an increased excitatory drive and a decreased inhibitory drive onto CPNs in the cortex (D. M. Cummings et al., 2009; Cepeda & Levine, 2022). The downregulation of post-synaptic glutamatergic genes and the upregulation of GABAergic post-synaptic genes could represent an adaptive response to restore normal network function. Furthermore, gene variations in the glutamate receptor subunit *Grin2a* and *Grin2b*, which are both downregulated in R6/2 mice at 12 weeks, have been found to account for 7.1% of the variation in the age of onset in HD patients (Arning et al., 2007).

Additionally, loss of synaptic connectivity might contribute to the decrease in neuronal marker genes, as several of them like *Vip*, *Gad1* and *Gad2* are neurotransmitters or are located at the synapse, such as solute carrier family 24 member 2 (*Slc24a2*), a marker for L5 IT neurons or glutamate ionotropic receptor kainate type subunit 3 (*Grik3*), a marker for L6 CT neurons and other lower cortical layer glutamatergic neurons. This could also explain why marker loss occurs in several NDs, as the loss of synaptic connectivity is a common phenomenon across NDs (Henstridge, Pickett, & Spires-Jones, 2016).

Moreover, calcium transients were found to be reduced in amplitude in R6/2 mice (Donzis et al., 2020). Additionally, cortical neurons of R6/2 mice exhibited increased synchrony in calcium spiking (Burgold et al., 2019). From the "Calcium signalling" pathway, the calcium/calmodulin-dependant kinase *Camk2a* stood out and was identified as hub gene, and is a neuronal essential gene, as well as a mHTT toxicity modifier gene (Fig. 3.14). Protein levels of CAMK2A were decreased in HD mouse models, and additionally, post-translational modification in the form of phosphorylation was decreased (Mees et al., 2022). An impaired BDNF–TRKB-CAMK2A signalling pathway has been linked with synaptic deficits in HD (Zhang et al., 2018). In summary, abnormal calcium signalling is likely to be a central mechanism contributing to neuronal death (Kolobkova, Vigont, Shalygin, & Kaznacheyeva, 2017).

In contrast to downregulated DEGs, more upregulated DEGs were shared across glutamatergic neuronal subclasses. Pathways enriched for upregulated DEGs included "Lysosome", "Oxidative phosphorylation", "Protein processing in the ER" and "Pathways of neurodegeneration - multiple diseases", and "HD" (Fig. 3.9 B).

The upregulation of genes related to the "Lysosome" pathway is consistent with previous observations of increased lysosome numbers in HD patients (Sapp et al., 1997). However, lysosomes were found to be mispositioned and have a decreased amount of cytosolic cargo in HD models (Erie et al., 2015; Martinez-Vicente et al., 2010). The upregulation of lysosomal genes, such as *Lamp1*, *Lamp2* and lysosomal protein transmembrane 4 alpha (*Laptm4a*) explains the increase of lysosomes in HD and might be a compensatory response caused by the lack of lysosomal degradation (Fig. 3.9 C, D, Fig. 3.10). Nevertheless, lysosomes were still found to have a normal turnover and possess normal proteolytic function (Martinez-Vicente et al., 2010). It was suggested that HTT is a receptor for selective autophagy and mHTT fails to fulfil this function, causing cargo-deprived lysosomes (Martinez-Vicente et al., 2010; Rui et al., 2015). Hence, cargo recognition mediated by HTT might be decreased in HD, possibly though, cargo recognition might be mediated by other autophagy receptors, like the ER-phagy receptors discussed in chapter 3.5.

In summary, downregulated pathways shared between glutamatergic subclasses were mostly associated with neuronal signalling and might be a response to excitotoxicity.

Furthermore, downregulation of synaptic genes might be a cause or a consequence of the loss of synaptic connectivity in HD. Upregulated pathways included pathways previously implicated in HD (Irfan et al., 2022). The upregulation of lysosomal genes might be an effort to increase autophagy and restore lysosomal function in HD (Martinez-Vicente et al., 2010; Rui et al., 2015). The detected increase in mitochondrial RNA might be a consequence of disrupted mitochondrial membranes causing their release (H. Lee et al., 2020). Further, the upregulation of structural ER and structural mitochondrial genes might be an attempt to restore proper function and also potentially, physical contact sites between the two organelles.

4.5 ER stress and ER-phagy are increased in R6/2 mice

Of all pathways, "Protein processing in the ER" showed the most significant enrichment for upregulated DEGs (Fig. 3.9 A). Genes of "Protein processing in the ER" included structural ER genes (e.g. *Os9*, *Rtn1*, *Canx*), genes of UPR signalling (e.g. *Hspa5*, *Xbp1*, *Hsp90b1*), and UPR target genes (e.g. *Hspa5*, *Hsp90b1*, *Pdia3*). The upregulation of marker genes for ER stress and UPR signalling, such as *Os9*, *Hspa5*, and *Xbp1*, suggested the occurrence of ER stress and the subsequent response in the form of UPR in R6/2 mice (Fig. 3.9 C, D). ER stress was already shown to be increased in HD patients and HD models, triggering UPR as a consequence (Vidal, Caballero, Couve, & Hetz, 2011; Leitman et al., 2013). Interestingly, the expression of UPR genes correlated with CAG-repeat length in HD model mice (Kalathur et al., 2015). As mHTT is mostly located in the cytosol and nucleus, ER stress is not caused by mHTT aggregates directly. It was suggested that mHTT sequesters proteins relevant for ERAD, leading to an increase in unfolded proteins in the ER (Duennwald & Lindquist, 2008; Leitman et al., 2013).

UPR has been found to be protective in HD models and the overexpression of *Xbp1* led to a decrease in mHTT aggregates (Zuleta, Vidal, Armentano, Parsons, & Hetz, 2012). However, if chronic activation of the UPR does not restore proteostasis, UPR can trigger apoptotic pathways (Sano & Reed, 2013; Kalathur et al., 2015). A meta-analysis found six genes, which potentially connect the UPR pathway and apoptotic pathway in HD (Kalathur

et al., 2015). One of these, *Hsp90b1*, was significantly upregulated across glutamatergic neurons starting at 8 weeks and was still upregulated at 12 weeks (Fig. 3.9 C, D, Fig. 3.14). Hence, this data suggests the occurrence of chronic ER stress, followed by UPR and possibly a link to apoptotic signalling. Lowering ER stress could therefore be protective against cell death in HD.

Interestingly, five out of the six known membrane-anchored ER-phagy receptors were upregulated in R6/2 mice (Fig. 3.9 C, D). Especially, *Tex264*, *Sec62* and *Rtn3* were strongly upregulated at 8 and 12 weeks, with *Rtn3* already showing upregulation at 5 weeks (Fig. 3.11 A). To date, only one study has linked ER-phagy to NDs. Recently, D. Y. Kim et al. (2023) showed that ER-phagy via *Canx* and *Retreg1* was able to degrade α-Syn located in the ER. Furthermore, elevation of ER-phagy had neuroprotective effects and beneficial effects for motor behaviour in PD mouse models (D. Y. Kim et al., 2023). We hypothesized that ER-phagy could be a response to elevated ER stress and could aid in the restoration of proteostasis in the ER. Thereby, chronic activation of UPR could be mitigated, and it could be prevented that chronic UPR activation triggers apoptosis.

To investigate whether ER-phagy is involved in HD, we utilized the sensor ss-RFP-GFP-KDEL which detects the uptake of ER into lysosomes (Fig. 3.11 B). We generated a HEK cell line stably expressing ss-RFP-GFP-KDEL and confirmed the functionality of the sensor (Fig. 3.11 C, D). Interestingly, ss-RFP-GFP-KDEL HEK cell expressing toxic HTTQ72-His exhibited an increase in acidified ER compared to cells expressing non-toxic HTTQ25-His (Fig. 3.11 C, D). This finding suggested an increase in ER-phagy upon mHTT expression.

In conclusion, our findings support the occurrence of ER stress and UPR in HD. Genes of the UPR were upregulated at both later time points, indicating a chronic activation of the UPR, which possibly might also trigger apoptotic pathways via *Hsp90b1* (Fig. 3.9 B, C, D). Moreover, the upregulation of several ER-phagy receptors was observed (Fig. 3.11 A). We were able to demonstrate that ER-phagy is increased in the presence of mHTT (Fig. 3.11 C, D). As snRNA-seq captures only transcriptomic changes, further experiments should be conducted on a functional, protein level. Further investigation should aim at determining which of these ER-phagy receptors mediates increased ER-phagy and what segments

of the ER are subject to ER-phagy upon mHTT aggregation. Additionally, determining whether ER-phagy aids in mitigating ER stress and whether the upregulation of ER-phagy is beneficial in HD would be needed to uncover the potential for a therapeutic strategy.

4.6 A gene module enriched for neuronal essential genes is upregulated in R6/2 mice and higher expressed in WT GABAergic neurons

To explore further genes which might contribute to mHTT toxicity or might be protective in HD, we identified the underlying gene network of R6/2 mice using scWGCNA. In total, we identified 20 distinct gene modules with 65 to 431 genes in each module (Fig. 3.12 A). Among these modules, four exhibited a correlation greater than 0.15 with R6/2 nuclei, while three showed a correlation more negative than -0.15 (Fig. 3.12 B). Notably, several gene modules with a heightened expression in R6/2 nuclei showed an increased expression in WT GABAergic neurons compared to WT glutamatergic neurons (Fig. 3.12 C). Conversely, modules with a decreased expression in R6/2 nuclei showed a higher expression in WT GABAergic neurons (Fig. 3.12 C). This pattern was also observed with analyses utilizing module eigengene expression, as well as average expression values (Fig. 3.12 D, E).

We hypothesised that modules, which are upregulated in R6/2 mice and higher expressed in WT GABAergic neurons could contain genes of an adaptive response to mHTT and might potentially be neuroprotective. Further, the higher intrinsic expression of these modules could render WT GABAergic neurons more resilient to HD. To test this hypothesis, we examined the over-representation of neuronal essential genes and mHTT toxicity modifying genes (Fig. 3.13 A, B). No module exhibited an over-representation of mHTT toxicity modifying genes (Fig. 3.13 B). This might be explained by either mHTT toxicity modifiers not being differentially expressed in R6/2 mice, the upregulation of mHTT modifier genes being masked by other transcriptional changes, or mHTT toxicity modifier genes not being co-expressed and contained within the same gene module (Wertz et al.,

2020).

However, we identified a module significantly enriched for neuronal essential genes, which was upregulated in R6/2 mice and showed increased expression in WT GABAergic neurons compared to WT glutamatergic neurons (Fig. 3.12 C, Fig. 3.13 A). Potentially, these neuronal essential genes render neurons more vital and contribute to an increased survival of neurons also in the context of mHTT expression. Moreover, this finding may also explain the pattern of selective vulnerability, as this module was expressed higher in WT GABAergic neurons.

To identify specific genes, which could be protective in HD, we applied two approaches. For the first approach, we visualized the gene network with vertex size of genes correlating with their centrality to the gene network and with edge length and size indicating the adjacency of the two connected genes. Furthermore, we highlighted neuronal essential genes and mHTT toxicity modifier genes (Fig. 3.14 A).

This approach highlighted genes from previous analyses, such as *Camk2a*, *Grin2a*, *Grin2b*, *Ryr2* among the downregulated genes, and *Laptm4a*, *Tomm20*, *Hspa5*, *Xbp1*, *Hsp90b1* and *Sec62* among the upregulated genes (Fig. 3.9 C, D, Fig. 3.14).

Additionally, the chaperones *Hspa8* and FKBP prolyl isomerase 2 (*Fkbp2*) exhibited a high centrality and constituted both, neuronal essential genes and mHTT toxicity modifier genes (Fig. 3.14). Intriguingly, *Hspa8* was shown to disentangle polyQ aggregates and was able to translocate from the cytosol to the nucleus under proteotoxic stress (Novoselova et al., 2005; F. Wang et al., 2018). *Fkbp2* functions as an ER chaperone involved in the *Xbp1*-dependent UPR and serves as a key regulator for lowering ER stress (Jeong et al., 2017).

In a second approach, we calculated the differential expression of all neuronal essential genes between WT GABAergic neurons and WT glutamatergic neurons (Fig. 3.15). Interestingly, as already observed in (Fig. 3.12 C, D), genes of the turquoise module were higher expressed in WT GABAergic neurons. Notably, among these genes were several chaperones like *Hspa8*, *Hsp90ab1* and the ER chaperone *Dnajb9*.

Further, this method also identified genes of the previously discussed pathway of "Oxidative phosphorylation", including *Tomm20* and *Cox8a*, and "Lysosomes", like the

lysosomal proteases cathepsin F (*Ctsf*), *Ctsd*, and *Lamp1*. Interestingly, also *Pcsk1n*, which was previously identified as a hub gene, showed an 2.35-fold higher expression in WT GABAergic neurons compared to glutamatergic neurons (Fig. 3.15).

In summary, gene modules comprising genes upregulated in R6/2 mice demonstrated a higher baseline expression in GABAergic neurons, whereas gene modules with genes downregulated in R6/2 mice are higher expressed in glutamatergic neurons. Notably, one of the modules with a higher expression in GABAergic neurons was enriched for neuronal essential genes, including several chaperones, genes of lysosomes, and mitochondria.

4.7 The chaperone proSAAS translocates to the nucleus in the presence of nuclear mHTT aggregates

The previous analyses identified *Pcsk1n* as a hub gene, neuronal essential gene and significantly higher expressed in WT GABAergic neurons. proSAAS, previously thought of as a chaperone secreted into the extracellular matrix, has already been implicated in other NDs (Fricker et al., 2000). In post-mortem AD brains, proSAAS co-localized with amyloid deposits and prevented the fibrillization of Aβ_{1-42} oligomers *in vitro* (Hoshino et al., 2014). Additionally, proSAAS colocalized with α-Syn, prevented its aggregation and prevented α-Syn aggregate mediated neurotoxicity in cellular PD models (Jarvela et al., 2016). A recent publication demonstrated that proSAAS can also form spheres in the cytoplasm and encapsulate TDP-43 aggregates, preventing its further aggregation (Peinado et al., 2022). Interestingly, this study also tested whether proSAAS was also able to encapsulate mHTT. For this, the study used HA-HTT-Q74, which aggregates in the cytoplasm of HEK cells. proSAAS did not form spheres encapsulating cytoplasmic mHTT-Q74 (Peinado et al., 2022). However, in HD patients mHTT mostly aggregates in the nucleus.

To investigate a potential interplay between proSAAS and mHTT, we transduced primary neurons with lentivirus inducing the expression of either non-toxic HTT-Q25 or toxic mHTT-Q72, which aggregates in the nucleus. To our surprise, proSAAS translocated

to the nucleus in neurons expressing mHTT-Q72 suggesting a potential interplay between proSAAS and mHTT-Q72 (Fig. 3.16 A, B). Notably, a nuclear localisation of endogenous proSAAS has not been demonstrated previously. However, we did not find a colocalization of proSAAS spheres and mHTT aggregates (Fig. 3.16 C).

Subsequent investigations could delve into the mechanism, which proSAAS fulfills upon mHTT aggregation. proSAAS translocating to the nucleus could be a consequence of proteotoxic stress in the nucleus, where it acts to restore proteostasis. Further, understanding the mechanism by which proSAAS translocates to the nucleus would be of interest. One potential mechanism could be related to the four lysines for which the substitution for arginins caused proSAAS to exhibit nuclear localisation (Peinado et al., 2022). Furthermore, there might be a mechanistic link between the ER stress we observed and the nuclear localisation of proSAAS, as proSAAS was shown to undergo cellular retention upon ER stress (Shakya et al., 2020).

Moreover, investigating whether proSAAS can prevent the formation of mHTT aggregates, similar to its effect on Aβ_{1-42} oligomers and α-Syn aggregates, would be valuable (Hoshino et al., 2014). Further experiments elucidating the interplay of proSAAS and mHTT, and examining whether proSAAS is protective against mHTT toxicity will be needed. Finally, assessing whether the modulation of proSAAS expression would be beneficial in HD would be an important avenue for further investigation.

4.8 Concluding remarks

In summary, this study provides novel insights into the transcriptomic changes occurring in the R6/2 mouse model of HD in a time-resolved manner. We demonstrate that the more vulnerable glutamatergic neurons are more severely affected by these transcriptomic changes than the more resilient GABAergic neurons. Additionally, while previous studies primarily focused on late disease time points in HD, we were also able to identify early transcriptomic changes. Surprisingly, a subset of these early transcriptomic changes were in the opposite direction of those seen at later stage, underscoring the importance of considering divergent early and late-stage effects in drug studies targeting early therapeutic intervention.

We show that the loss of cell subclass-specific marker genes affects a multitude of marker genes and cell populations. This is potentially caused by the dysregulation of TFs responsible for giving rise to and maintaining cell identity, suggesting that more upstream regulators of cell identity are dysregulated than previous implicated.

Furthermore, we highlight two mechanisms, which could play important roles in neuronal vulnerability in HD. First, we show that the expression of ER-phagy receptors is upregulated in R6/2 mice by 8 weeks of age, and ER-phagy is increased in cellular HD models. To our knowledge, no study has explored the role of ER-phagy in HD. Future studies should investigate whether modifying the activity of ER-phagy could enhance neuronal resilience in the context of HD. Uncovering the relevance of ER-phagy in HD could help to understand the role of the ER in protecting against proteotoxic stress in HD and other NDs.

Secondly, the chaperone proSAAS shows increased expression in R6/2 mice by 8 weeks of age and translocates to the nucleus in the presence of nuclear mHTT aggregates. Interestingly, proSAAS has been shown to co-localize with aggregates in other NDs such as ALS, PD and AD, highlighting its role across NDs. Protein aggregates in these diseases are located in different cellular compartments or even extracellularly. In our study, proSAAS did not colocalize with mHTT aggregates, but could play a role in mitigating proteotoxic stress occurring in the nucleus. Investigating how proSAAS is recruited to

these different sites and what role proSAAS fulfills in the individual diseases could enhance our understanding of the importance of proSAAS.

In conclusion, this study elucidates several disease mechanisms in HD model mice and highlights two pathways for a potential intervention point for a disease-modifying therapy.

References

Acosta-Alvear, D., Zhou, Y., Blais, A., Tsikitis, M., Lents, N. H., Arias, C., ... Dynlacht, B. D. (2007). Xbp1 controls diverse cell type-and condition-specific transcriptional regulatory networks. *Molecular cell*, *27*(1), 53–66.

Alcock, F., & Swanton, E. (2009). Mammalian os-9 is upregulated in response to endoplasmic reticulum stress and facilitates ubiquitination of misfolded glycoproteins. *Journal of molecular biology*, *385*(4), 1032–1042.

Al-Dalahmah, O., Sosunov, A. A., Shaik, A., Ofori, K., Liu, Y., Vonsattel, J. P., ... Goldman, J. E. (2020). Single-nucleus rna-seq identifies Huntington disease astrocyte states. *Acta neuropathologica communications*, *8*(1), 1–21.

Arning, L., & Nguyen, H. P. (2022). Huntington disease update: New insights into the role of repeat instability in disease pathogenesis. *Medizinische Genetik*, *33*(4), 293–300.

Arning, L., Saft, C., Wieczorek, S., Andrich, J., Kraus, P. H., & Epplen, J. T. (2007). Nr2a and nr2b receptor gene variations modify age at onset in Huntington disease in a sex-specific manner. *Human genetics*, *122*, 175–182.

Bakels, H. S., Roos, R. A., van Roon-Mom, W. M., & de Bot, S. T. (2022). Juvenile-onset Huntington disease pathophysiology and neurodevelopment: a review. *Movement Disorders*, *37*(1), 16–24.

Bakken, T. E., Hodge, R. D., Miller, J. A., Yao, Z., Nguyen, T. N., Aevermann, B., ... others (2018). Single-nucleus and single-cell transcriptomes compared in matched cortical cell types. *PloS one*, *13*(12), e0209648.

Bates, G. P., Dorsey, R., Gusella, J. F., Hayden, M. R., Kay, C., Leavitt, B. R., ... others (2015). Huntington disease. *Nature reviews Disease primers*, *1*(1), 1–21.

Beitz, J. M., et al. (2014). Parkinson's disease: a review. *Front Biosci (Schol Ed)*, *6*(1), 65–74.

Benn, C. L., Gibson, K. R., & Reynolds, D. S. (2021). Drugging dna damage repair pathways for trinucleotide repeat expansion diseases. *Journal of Huntington's Disease*, *10*(1), 203–220.

Bergson, C., Levenson, R., Goldman-Rakic, P. S., & Lidow, M. S. (2003). Dopamine

receptor-interacting proteins: the ca2+ connection in dopamine signaling. *Trends in pharmacological sciences*, *24*(9), 486–492.

Bertolotti, A., Zhang, Y., Hendershot, L. M., Harding, H. P., & Ron, D. (2000). Dynamic interaction of bip and er stress transducers in the unfolded-protein response. *Nature cell biology*, *2*(6), 326–332.

Blokhuis, A. M., Groen, E. J., Koppers, M., van den Berg, L. H., & Pasterkamp, R. J. (2013). Protein aggregation in amyotrophic lateral sclerosis. *Acta neuropathologica*, *125*, 777–794.

Blumenstock, S., & Dudanova, I. (2020). Cortical and striatal circuits in Huntington's disease. *Frontiers in neuroscience*, *14*, 82.

Braak, H., Rüb, U., Gai, W., & Del Tredici, K. (2003). Idiopathic parkinson's disease: possible routes by which vulnerable neuronal types may be subject to neuroinvasion by an unknown pathogen. *Journal of neural transmission*, *110*, 517–536.

Briggs, F., & Usrey, W. M. (2008). Emerging views of corticothalamic function. *Current opinion in neurobiology*, *18*(4), 403–407.

Browne, S. E., Bowling, A. C., Macgarvey, U., Baik, M. J., Berger, S. C., Muquit, M. M., ... Beal, M. F. (1997). Oxidative damage and metabolic dysfunction in Huntington's disease: selective vulnerability of the basal ganglia. *Annals of Neurology: Official Journal of the American Neurological Association and the Child Neurology Society*, *41*(5), 646–653.

Bunner, K. D., & Rebec, G. V. (2016). Corticostriatal dysfunction in Huntington's disease: the basics. *Frontiers in Human neuroscience*, *10*, 317.

Burgold, J., Schulz-Trieglaff, E. K., Voelkl, K., Gutiérrez-Ángel, S., Bader, J. M., Hosp, F., ... others (2019). Cortical circuit alterations precede motor impairments in Huntington's disease mice. *Scientific reports*, *9*(1), 6634.

Carlozzi, N. E., Stout, J. C., Mills, J. A., Duff, K., Beglinger, L. J., Aylward, E. H., ... others (2011). Estimating premorbid iq in the prodromal phase of a neurodegenerative disease. *The Clinical Neuropsychologist*, *25*(5), 757–777.

Carmo, C., Naia, L., Lopes, C., & Rego, A. C. (2018). Mitochondrial dysfunction in Huntington's disease. *Polyglutamine disorders*, 59–83.

Carnemolla, A., Fossale, E., Agostoni, E., Michelazzi, S., Calligaris, R., De Maso, L., ... Persichetti, F. (2009). Rrs1 is involved in endoplasmic reticulum stress response in Huntington disease. *Journal of Biological Chemistry*, *284*(27), 18167–18173.

Caron, N., Wright, G., Hayden, M., Adam, M., Ardinger, H., Pagon, R., ... Amemiya, A. (2020). Genereviews®.

Cepeda, C., & Levine, M. S. (2022). Synaptic dysfunction in Huntington's disease: lessons from genetic animal models. *The Neuroscientist*, *28*(1), 20–40.

Chaplot, K., Jarvela, T. S., & Lindberg, I. (2020). Secreted chaperones in neurodegeneration. *Frontiers in aging neuroscience*, *12*, 268.

Chen, S., Berthelier, V., Yang, W., & Wetzel, R. (2001). Polyglutamine aggregation behavior in vitro supports a recruitment mechanism of cytotoxicity. *Journal of molecular biology*, *311*(1), 173–182.

Cherubini, M., Lopez-Molina, L., & Gines, S. (2020). Mitochondrial fission in Huntington's disease mouse striatum disrupts ER-mitochondria contacts leading to disturbances in Ca2+ efflux and reactive oxygen species (ROS) homeostasis. *Neurobiology of Disease*, *136*, 104741.

Chino, H., & Mizushima, N. (2020). Er-phagy: quality control and turnover of endoplasmic reticulum. *Trends in Cell Biology*, *30*(5), 384–398.

Colin, E., Zala, D., Liot, G., Rangone, H., Borrell-Pagès, M., Li, X.-J., ... Humbert, S. (2008). Huntingtin phosphorylation acts as a molecular switch for anterograde/retrograde transport in neurons. *The EMBO journal*, *27*(15), 2124–2134.

Cong, S.-Y., Pepers, B. A., Evert, B. O., Rubinsztein, D. C., Roos, R. A., van Ommen, G.-J. B., & Dorsman, J. C. (2005). Mutant Huntingtin represses cbp, but not p300, by binding and protein degradation. *Molecular and Cellular Neuroscience*, *30*(1), 12–23.

Cummings, D. M., Alaghband, Y., Hickey, M. A., Joshi, P. R., Hong, S. C., Zhu, C., ... others (2012). A critical window of cag repeat-length correlates with phenotype severity in the r6/2 mouse model of Huntington's disease. *Journal of neurophysiology*, *107*(2), 677–691.

Cummings, D. M., André, V. M., Uzgil, B. O., Gee, S. M., Fisher, Y. E., Cepeda, C., &

Levine, M. S. (2009). Alterations in cortical excitation and inhibition in genetic mouse models of Huntington's disease. *Journal of Neuroscience*, *29*(33), 10371–10386.

Cummings, J. L. (1995). Behavioral and psychiatric symptoms associated with Huntington's disease. *Advances in neurology*, *65*, 179–186.

Dann, E., Henderson, N. C., Teichmann, S. A., Morgan, M. D., & Marioni, J. C. (2022). Differential abundance testing on single-cell data using k-nearest neighbor graphs. *Nature Biotechnology*, *40*(2), 245–253.

Danoudis, M., & Iansek, R. (2014). Gait in Huntington's disease and the stride length-cadence relationship. *BMC neurology*, *14*, 1–8.

Davies, S. W., Turmaine, M., Cozens, B. A., DiFiglia, M., Sharp, A. H., Ross, C. A., ... Bates, G. P. (1997). Formation of neuronal intranuclear inclusions underlies the neurological dysfunction in mice transgenic for the hd mutation. *Cell*, *90*(3), 537–548.

Deng, Y., Wong, T., Bricker-Anthony, C., Deng, B., & Reiner, A. (2013). Loss of corticostriatal and thalamostriatal synaptic terminals precedes striatal projection neuron pathology in heterozygous Q140 Huntington's disease mice. *Neurobiology of disease*, *60*, 89–107.

Djousse, L., Knowlton, B., Hayden, M., Almqvist, E., Brinkman, R., Ross, C., ... others (2003). Interaction of normal and expanded cag repeat sizes influences age at onset of Huntington disease. *American journal of medical genetics Part A*, *119*(3), 279–282.

Dodds, L., Chen, J., Berggren, K., & Fox, J. (2014). Characterization of striatal neuronal loss and atrophy in the r6/2 mouse model of Huntington's disease. *PLoS currents*, *6*.

Donaldson, J., Powell, S., Rickards, N., Holmans, P., & Jones, L. (2021). What is the pathogenic cag expansion length in Huntington's disease? *Journal of Huntington's Disease*, *10*(1), 175–202.

Donzis, E. J., Estrada-Sánchez, A. M., Indersmitten, T., Oikonomou, K., Tran, C. H., Wang, C., ... Levine, M. S. (2020). Cortical network dynamics is altered in mouse models of Huntington's disease. *Cerebral Cortex*, *30*(4), 2372–2388.

Dragatsis, I., Levine, M. S., & Zeitlin, S. (2000). Inactivation of hdh in the brain and testis results in progressive neurodegeneration and sterility in mice. *Nature genetics*, *26*(3), 300–306.

Duennwald, M. L., & Lindquist, S. (2008). Impaired erad and er stress are early and specific events in polyglutamine toxicity. *Genes & development*, *22*(23), 3308–3319.

Dunah, A. W., Jeong, H., Griffin, A., Kim, Y.-M., Standaert, D. G., Hersch, S. M., ... Krainc, D. (2002). Sp1 and tafii130 transcriptional activity disrupted in early Huntington's disease. *Science*, *296*(5576), 2238–2243.

Duyao, M. P., Auerbach, A. B., Ryan, A., Persichetti, F., Barnes, G. T., McNeil, S. M., ... others (1995). Inactivation of the mouse Huntington's disease gene homolog hdh. *Science*, *269*(5222), 407–410.

Epping, E. A., & Paulsen, J. S. (2011). Depression in the early stages of Huntington disease. *Neurodegenerative disease management*, *1*(5), 407–414.

Erie, C., Sacino, M., Houle, L., Lu, M. L., & Wei, J. (2015). Altered lysosomal positioning affects lysosomal functions in a cellular model of Huntington's disease. *European journal of neuroscience*, *42*(3), 1941–1951.

Eshraghi, M., Karunadharma, P. P., Blin, J., Shahani, N., Ricci, E. P., Michel, A., ... others (2021). Mutant Huntingtin stalls ribosomes and represses protein synthesis in a cellular model of Huntington disease. *Nature Communications*, *12*(1), 1461.

Fan, H.-C., Ho, L.-I., Chi, C.-S., Chen, S.-J., Peng, G.-S., Chan, T.-M., ... Harn, H.-J. (2014). Polyglutamine (polyq) diseases: genetics to treatments. *Cell transplantation*, *23*(4-5), 441–458.

Farrer, L., Cupples, L., Kiely, D. K., Conneally, P. M., & Myers, R. H. (1992). Inverse relationship between age at onset of Huntington disease and paternal age suggests involvement of genetic imprinting. *American journal of Human genetics*, *50*(3), 528.

Feregrino, C., & Tschopp, P. (2022). Assessing evolutionary and developmental transcriptome dynamics in homologous cell types. *Developmental Dynamics*, *251*(9), 1472–1489.

Folstein, S. E. (1989). *Huntington's disease: a disorder of families.* Johns Hopkins

University Press.

Foroud, T., Gray, J., Ivashina, J., & Conneally, P. M. (1999). Differences in duration of Huntington's disease based on age at onset. *Journal of Neurology, Neurosurgery & Psychiatry*, *66*(1), 52–56.

Frakes, A. E., & Dillin, A. (2017). The uprer: sensor and coordinator of organismal homeostasis. *Molecular cell*, *66*(6), 761–771.

Fricker, L. D., McKinzie, A. A., Sun, J., Curran, E., Qian, Y., Yan, L., ... others (2000). Identification and characterization of proSAAS, a granin-like neuroendocrine peptide precursor that inhibits prohormone processing. *Journal of Neuroscience*, *20*(2), 639–648.

Fu, H., Hardy, J., & Duff, K. E. (2018). Selective vulnerability in neurodegenerative diseases. *Nature neuroscience*, *21*(10), 1350–1358.

Gangwani, M. R., Soto, J. S., Jami-Alahmadi, Y., Tiwari, S., Kawaguchi, R., Wohlschlegel, J. A., & Khakh, B. S. (2023). Neuronal and astrocytic contributions to Huntington's disease dissected with zinc finger protein transcriptional repressors. *Cell reports*, *42*(1).

Gauthier, L. R., Charrin, B. C., Borrell-Pagès, M., Dompierre, J. P., Rangone, H., Cordelières, F. P., ... others (2004). Huntingtin controls neurotrophic support and survival of neurons by enhancing bdnf vesicular transport along microtubules. *Cell*, *118*(1), 127–138.

Goedert, M., Spillantini, M. G., Jakes, R., Rutherford, D., & Crowther, R. (1989). Multiple isoforms of Human microtubule-associated protein tau: sequences and localization in neurofibrillary tangles of alzheimer's disease. *Neuron*, *3*(4), 519–526.

Gofflot, F., Chartoire, N., Vasseur, L., Heikkinen, S., Dembele, D., Le Merrer, J., & Auwerx, J. (2007). Systematic gene expression mapping clusters nuclear receptors according to their function in the brain. *Cell*, *131*(2), 405–418.

Gonchar, Y., Wang, Q., & Burkhalter, A. H. (2008). Multiple distinct subtypes of gabaergic neurons in mouse visual cortex identified by triple immunostaining. *Frontiers in neuroanatomy*, *2*, 93.

Gonzalez-Alegre, P., & Afifi, A. K. (2006). Clinical characteristics of childhood-onset

(juvenile) Huntington disease: report of 12 patients and review of the literature. *Journal of child neurology*, *21*(3), 223–229.

Goold, R., Hamilton, J., Menneteau, T., Flower, M., Bunting, E. L., Aldous, S. G., ... others (2021). Fan1 controls mismatch repair complex assembly via mlh1 retention to stabilize cag repeat expansion in Huntington's disease. *Cell Reports*, *36*(9).

Goto, S., Hirano, A., & Rojas-Corona, R. R. (1989). An immunohistochemical investigation of the Human neostriatum in Huntington's disease. *Annals of Neurology: Official Journal of the American Neurological Association and the Child Neurology Society*, *25*(3), 298–304.

Gray, M., Shirasaki, D. I., Cepeda, C., André, V. M., Wilburn, B., Lu, X.-H., ... others (2008). Full-length Human mutant Huntingtin with a stable polyglutamine repeat can elicit progressive and selective neuropathogenesis in bachd mice. *Journal of Neuroscience*, *28*(24), 6182–6195.

Gusella, J. F., Wexler, N. S., Conneally, P. M., Naylor, S. L., Anderson, M. A., Tanzi, R. E., ... others (1983). A polymorphic dna marker genetically linked to Huntington's disease. *Nature*, *306*(5940), 234–238.

Gutekunst, C.-A., Li, S.-H., Yi, H., Mulroy, J. S., Kuemmerle, S., Jones, R., ... Li, X.-J. (1999). Nuclear and neuropil aggregates in Huntington's disease: relationship to neuropathology. *Journal of Neuroscience*, *19*(7), 2522–2534.

Habib, N., Avraham-Davidi, I., Basu, A., Burks, T., Shekhar, K., Hofree, M., ... others (2017). Massively parallel single-nucleus RNA-seq with DroNc-seq. *Nature methods*, *14*(10), 955–958.

Halliday, G., McRitchie, D., Macdonald, V., Double, K., Trent, R., & McCusker, E. (1998). Regional specificity of brain atrophy in Huntington's disease. *Experimental neurology*, *154*(2), 663–672.

Han, I., You, Y., Kordower, J. H., Brady, S. T., & Morfini, G. A. (2010). Differential vulnerability of neurons in Huntington's disease: the role of cell type-specific features. *Journal of neurochemistry*, *113*(5), 1073–1091.

Hao, Y., Hao, S., Andersen-Nissen, E., Mauck, W. M., Zheng, S., Butler, A., ... others (2021). Integrated analysis of multimodal single-cell data. *Cell*, *184*(13), 3573–

3587.

Hao, Y., Stuart, T., Kowalski, M. H., Choudhary, S., Hoffman, P., Hartman, A., ... others (2023). Dictionary learning for integrative, multimodal and scalable single-cell analysis. *Nature Biotechnology*, 1–12.

Haque, A., Engel, J., Teichmann, S. A., & Lönnberg, T. (2017). A practical guide to single-cell rna-sequencing for biomedical research and clinical applications. *Genome medicine*, *9*(1), 1–12.

He, L., Qian, X., & Cui, Y. (2021). Advances in er-phagy and its diseases relevance. *Cells*, *10*(9), 2328.

Helwig, M., Hoshino, A., Berridge, C., Lee, S.-N., Lorenzen, N., Otzen, D. E., ... Lindberg, I. (2013). The neuroendocrine protein 7B2 suppresses the aggregation of neurodegenerative disease-related proteins. *Journal of Biological Chemistry*, *288*(2), 1114–1124.

Henstridge, C. M., Pickett, E., & Spires-Jones, T. L. (2016). Synaptic pathology: a shared mechanism in neurological disease. *Ageing research reviews*, *28*, 72–84.

Heumos, L., Schaar, A. C., Lance, C., Litinetskaya, A., Drost, F., Zappia, L., ... others (2023). Best practices for single-cell analysis across modalities. *Nature Reviews Genetics*, *24*(8), 550–572.

Hill, M. A., & Gammie, S. C. (2022). Alzheimer's disease large-scale gene expression portrait identifies exercise as the top theoretical treatment. *Scientific Reports*, *12*(1), 17189.

Hoffner, G., & Djian, P. (2015). Polyglutamine aggregation in Huntington disease: does structure determine toxicity? *Molecular neurobiology*, *52*, 1297–1314.

Hoshino, A., Helwig, M., Rezaei, S., Berridge, C., Eriksen, J. L., & Lindberg, I. (2014). A novel function for pro saas as an amyloid anti-aggregant in alzheimer's disease. *Journal of neurochemistry*, *128*(3), 419–430.

Huang, Z. J. (2014). Toward a genetic dissection of cortical circuits in the mouse. *Neuron*, *83*(6), 1284–1302.

Illarioshkin, S., Klyushnikov, S., Vigont, V., Seliverstov, Y. A., & Kaznacheyeva, E. (2018). Molecular pathogenesis in Huntington's disease. *Biochemistry (moscow)*,

83, 1030–1039.

Irfan, Z., Khanam, S., Karmakar, V., Firdous, S. M., El Khier, B. S. I. A., Khan, I., … Khan, A. (2022). Pathogenesis of Huntington's disease: An emphasis on molecular pathways and prevention by natural remedies. *Brain Sciences*, *12*(10), 1389.

Jarosińska, O. D., & Rüdiger, S. G. (2021). Molecular strategies to target protein aggregation in Huntington's disease. *Frontiers in Molecular Biosciences*, *8*, 1068.

Jarvela, T. S., Lam, H. A., Helwig, M., Lorenzen, N., Otzen, D. E., McLean, P. J., … Lindberg, I. (2016). The neural chaperone proSAAS blocks α-synuclein fibrillation and neurotoxicity. *Proceedings of the National Academy of Sciences*, *113*(32), E4708–E4715.

Jason, G. W., Pajurkova, E. M., Suchowersky, O., Hewitt, J., Hilbert, C., Reed, J., & Hayden, M. R. (1988). Presymptomatic neuropsychological impairment in Huntington's disease. *Archives of Neurology*, *45*(7), 769–773.

Jeong, M., Jang, E., Choi, S. S., Ji, C., Lee, K., & Youn, J. (2017). The function of FK506-binding protein 13 in protein quality control protects plasma cells from endoplasmic reticulum stress-associated apoptosis. *Frontiers in Immunology*, *8*, 222.

Joag, H., Ghatpande, V., Desai, M., Sarkar, M., Raina, A., Shinde, M., … Majumdar, A. (2020). A role of cellular translation regulation associated with toxic Huntingtin protein. *Cellular and Molecular Life Sciences*, *77*, 3657–3670.

Johri, A., Chandra, A., & Beal, M. F. (2013). Pgc-1α, mitochondrial dysfunction, and Huntington's disease. *Free Radical Biology and Medicine*, *62*, 37–46.

Joshi, A., Newbatt, Y., McAndrew, P. C., Stubbs, M., Burke, R., Richards, M. W., … others (2015). Molecular mechanisms of Human ire1 activation through dimerization and ligand binding. *Oncotarget*, *6*(15), 13019.

Jurcau, A., & Jurcau, C. M. (2022). Mitochondria in Huntington's disease: implications in pathogenesis and mitochondrial-targeted therapeutic strategies. *Neural Regeneration Research*.

Kalathur, R. K. R., Giner-Lamia, J., Machado, S., Barata, T., Ayasolla, K. R., & Futschik, M. E. (2015). The unfolded protein response and its potential role in Huntington's disease elucidated by a systems biology approach. *F1000Research*, *4*.

Kaltenbach, L. S., Romero, E., Becklin, R. R., Chettier, R., Bell, R., Phansalkar, A., ... others (2007). Huntingtin interacting proteins are genetic modifiers of neurodegeneration. *PLoS genetics*, *3*(5), e82.

Kaufman, R. J., Scheuner, D., Schröder, M., Shen, X., Lee, K., Liu, C. Y., & Arnold, S. M. (2002). The unfolded protein response in nutrient sensing and differentiation. *Nature reviews Molecular cell biology*, *3*(6), 411–421.

Kim, D. Y., Shin, J. Y., Lee, J. E., Kim, H. N., Chung, S. J., Yoo, H. S., ... others (2023). A selective er-phagy exerts neuroprotective effects via modulation of α-synuclein clearance in parkinsonian models. *Proceedings of the National Academy of Sciences*, *120*(37), e2221929120.

Kim, E. H., Thu, D. C., Tippett, L. J., Oorschot, D. E., Hogg, V. M., Roxburgh, R., ... Faull, R. L. (2014). Cortical interneuron loss and symptom heterogeneity in Huntington disease. *Annals of neurology*, *75*(5), 717–727.

Kim, E. J., Juavinett, A. L., Kyubwa, E. M., Jacobs, M. W., & Callaway, E. M. (2015). Three types of cortical layer 5 neurons that differ in brain-wide connectivity and function. *Neuron*, *88*(6), 1253–1267.

Kirkwood, S. C., Su, J. L., Conneally, P. M., & Foroud, T. (2001). Progression of symptoms in the early and middle stages of Huntington disease. *Archives of neurology*, *58*(2), 273–278.

Kolobkova, Y. A., Vigont, V., Shalygin, A., & Kaznacheyeva, E. (2017). Huntington's disease: calcium dyshomeostasis and pathology models. *Acta Naturae*, *9*(2 (33)), 34–46.

Kuhn, P.-H., Wang, H., Dislich, B., Colombo, A., Zeitschel, U., Ellwart, J. W., ... Lichtenthaler, S. F. (2010). Adam10 is the physiologically relevant, constitutive α-secretase of the amyloid precursor protein in primary neurons. *The EMBO journal*, *29*(17), 3020–3032.

Landles, C., & Bates, G. P. (2004). Huntingtin and the molecular pathogenesis of Huntington's disease: Fourth in molecular medicine review series. *EMBO reports*, *5*(10), 958–963.

Langfelder, P., & Horvath, S. (2008). Wgcna: an r package for weighted correlation

network analysis. *BMC bioinformatics*, *9*(1), 1–13.

Lanoue, E., & Day, R. (2001). Coexpression of proprotein convertase SPC3 and the neuroendocrine precursor proSAAS. *Endocrinology*, *142*(9), 4141–4149.

Lee, A.-H., Iwakoshi, N. N., & Glimcher, L. H. (2003). Xbp-1 regulates a subset of endoplasmic reticulum resident chaperone genes in the unfolded protein response. *Molecular and cellular biology*, *23*(21), 7448–7459.

Lee, H., Fenster, R. J., Pineda, S. S., Gibbs, W. S., Mohammadi, S., Davila-Velderrain, J., ... others (2020). Cell type-specific transcriptomics reveals that mutant Huntingtin leads to mitochondrial rna release and neuronal innate immune activation. *Neuron*, *107*(5), 891–908.

Lee, J.-M., Correia, K., Loupe, J., Kim, K.-H., Barker, D., Hong, E. P., ... others (2019). Cag repeat not polyglutamine length determines timing of Huntington's disease onset. *Cell*, *178*(4), 887–900.

Lee, J.-M., Huang, Y., Orth, M., Gillis, T., Siciliano, J., Hong, E., ... others (2022). Genetic modifiers of Huntington disease differentially influence motor and cognitive domains. *The American Journal of Human Genetics*, *109*(5), 885–899.

Lee, J.-M., Pinto, R. M., Gillis, T., St. Claire, J. C., & Wheeler, V. C. (2011). Quantification of age-dependent somatic cag repeat instability in hdh cag knock-in mice reveals different expansion dynamics in striatum and liver. *PLoS One*, *6*(8), e23647.

Lee, J.-M., Wheeler, V. C., Chao, M. J., Vonsattel, J. P. G., Pinto, R. M., Lucente, D., ... others (2015). Identification of genetic factors that modify clinical onset of Huntington's disease. *Cell*, *162*(3), 516–526.

Leeflang, E. P., Tavaré, S., Marjoram, P., Neal, C. O., Srinidhi, J., MacFarlane, H., ... others (1999). Analysis of germline mutation spectra at the Huntington's disease locus supports a mitotic mutation mechanism. *Human Molecular Genetics*, *8*(2), 173–183.

Le Gras, S., Keime, C., Anthony, A., Lotz, C., De Longprez, L., Brouillet, E., ... Merienne, K. (2017). Altered enhancer transcription underlies Huntington's disease striatal transcriptional signature. *Scientific reports*, *7*(1), 42875.

Leitman, J., Ulrich Hartl, F., & Lederkremer, G. Z. (2013). Soluble forms of polyq-

expanded Huntingtin rather than large aggregates cause endoplasmic reticulum stress. *Nature communications*, *4*(1), 2753.

Li, J.-L., Hayden, M. R., Almqvist, E. W., Brinkman, R. R., Durr, A., Dodé, C., ... others (2003). A genome scan for modifiers of age at onset in Huntington disease: The hd maps study. *The American Journal of Human Genetics*, *73*(3), 682–687.

Liguz-Lecznar, M., Urban-Ciecko, J., & Kossut, M. (2016). Somatostatin and somatostatin-containing neurons in shaping neuronal activity and plasticity. *Frontiers in neural circuits*, *10*, 48.

Lim, R. G., Al-Dalahmah, O., Wu, J., Gold, M. P., Reidling, J. C., Tang, G., ... others (2022). Huntington disease oligodendrocyte maturation deficits revealed by single-nucleus rnaseq are rescued by thiamine-biotin supplementation. *Nature Communications*, *13*(1), 7791.

Lim, Y., Kim, S., & Kim, E.-K. (2021). Palmitate reduces starvation-induced er stress by inhibiting er-phagy in hypothalamic cells. *Molecular Brain*, *14*(1), 65.

Love, M. I., Huber, W., & Anders, S. (2014). Moderated estimation of fold change and dispersion for rna-seq data with deseq2. *Genome biology*, *15*(12), 1–21.

Luo, S., Vacher, C., Davies, J. E., & Rubinsztein, D. C. (2005). Cdk5 phosphorylation of Huntingtin reduces its cleavage by caspases: implications for mutant Huntingtin toxicity. *The Journal of cell biology*, *169*(4), 647–656.

MacDonald, M. E., Ambrose, C. M., Duyao, M. P., Myers, R. H., Lin, C., Srinidhi, L., ... others (1993). A novel gene containing a trinucleotide repeat that is expanded and unstable on Huntington's disease chromosomes. *Cell*, *72*(6), 971–983.

Macdonald, V., & Halliday, G. (2002). Pyramidal cell loss in motor cortices in Huntington's disease. *Neurobiology of disease*, *10*(3), 378–386.

Macosko, E. Z., Basu, A., Satija, R., Nemesh, J., Shekhar, K., Goldman, M., ... others (2015). Highly parallel genome-wide expression profiling of individual cells using nanoliter droplets. *Cell*, *161*(5), 1202–1214.

Maiuri, T., Woloshansky, T., Xia, J., & Truant, R. (2013). The Huntingtin n17 domain is a multifunctional crm1 and ran-dependent nuclear and cilial export signal. *Human molecular genetics*, *22*(7), 1383–1394.

Malaiya, S., Cortes-Gutierrez, M., Herb, B. R., Coffey, S. R., Legg, S. R., Cantle, J. P., ... Ament, S. A. (2021). Single-nucleus rna-seq reveals dysregulation of striatal cell identity due to Huntington's disease mutations. *Journal of Neuroscience*, *41*(25), 5534–5552.

Mangiarini, L., Sathasivam, K., Seller, M., Cozens, B., Harper, A., Hetherington, C., ... others (1996). Exon 1 of the HD gene with an expanded CAG repeat is sufficient to cause a progressive neurological phenotype in transgenic mice. *Cell*, *87*(3), 493–506.

Marcora, E., Gowan, K., & Lee, J. E. (2003). Stimulation of neurod activity by Huntingtin and Huntingtin-associated proteins hap1 and mlk2. *Proceedings of the National Academy of Sciences*, *100*(16), 9578–9583.

Martin, D. D., Heit, R. J., Yap, M. C., Davidson, M. W., Hayden, M. R., & Berthiaume, L. G. (2014). Identification of a post-translationally myristoylated autophagy-inducing domain released by caspase cleavage of Huntingtin. *Human molecular genetics*, *23*(12), 3166–3179.

Martinez-Vicente, M., Talloczy, Z., Wong, E., Tang, G., Koga, H., Kaushik, S., ... others (2010). Cargo recognition failure is responsible for inefficient autophagy in Huntington's disease. *Nature neuroscience*, *13*(5), 567–576.

Masters, C. L., Multhaup, G., Simms, G., Pottgiesser, J., Martins, R., & Beyreuther, K. (1985). Neuronal origin of a cerebral amyloid: neurofibrillary tangles of alzheimer's disease contain the same protein as the amyloid of plaque cores and blood vessels. *The EMBO journal*, *4*(11), 2757–2763.

Mathkar, P. P., Suresh, D., Dunn, J., Tom, C. M., & Mattis, V. B. (2019). Characterization of neurodevelopmental abnormalities in ipsc-derived striatal cultures from patients with Huntington's disease. *Journal of Huntington's disease*, *8*(3), 257–269.

Mathys, H., Davila-Velderrain, J., Peng, Z., Gao, F., Mohammadi, S., Young, J. Z., ... others (2019). Single-cell transcriptomic analysis of alzheimer's disease. *Nature*, *570*(7761), 332–337.

McColgan, P., Joubert, J., Tabrizi, S. J., & Rees, G. (2020). The Human motor cortex microcircuit: insights for neurodegenerative disease. *Nature Reviews Neuroscience*,

21(8), 401–415.

McColgan, P., & Tabrizi, S. J. (2018). Huntington's disease: a clinical review. *European journal of neurology*, *25*(1), 24–34.

McGirr, S., Venegas, C., & Swaminathan, A. (2020). Alzheimers disease: A brief review. *Journal of Experimental Neurology*, *1*(3), 89–98.

Mead, R. J., Shan, N., Reiser, H. J., Marshall, F., & Shaw, P. J. (2023). Amyotrophic lateral sclerosis: A neurodegenerative disorder poised for successful therapeutic translation. *Nature Reviews Drug Discovery*, *22*(3), 185–212.

Medina, A., Mahjoub, Y., Shaver, L., & Pringsheim, T. (2022). Prevalence and incidence of Huntington's disease: An updated systematic review and meta-analysis. *Movement Disorders*, *37*(12), 2327–2335.

Mees, I., Li, S., Tran, H., Ang, C.-S., Williamson, N. A., Hannan, A. J., & Renoir, T. (2022). Phosphoproteomic dysregulation in Huntington's disease mice is rescued by environmental enrichment. *Brain Communications*, *4*(6), fcac305.

Menalled, L., El-Khodor, B. F., Patry, M., Suárez-Fariñas, M., Orenstein, S. J., Zahasky, B., ... others (2009). Systematic behavioral evaluation of Huntington's disease transgenic and knock-in mouse models. *Neurobiology of disease*, *35*(3), 319–336.

Mende-Mueller, L. M., Toneff, T., Hwang, S.-R., Chesselet, M.-F., & Hook, V. Y. (2001). Tissue-specific proteolysis of Huntingtin (htt) in Human brain: evidence of enhanced levels of n-and c-terminal htt fragments in Huntington's disease striatum. *Journal of Neuroscience*, *21*(6), 1830–1837.

Miller, J., Arrasate, M., Shaby, B. A., Mitra, S., Masliah, E., & Finkbeiner, S. (2010). Quantitative relationships between Huntingtin levels, polyglutamine length, inclusion body formation, and neuronal death provide novel insight into Huntington's disease molecular pathogenesis. *Journal of Neuroscience*, *30*(31), 10541–10550.

Miller, J. P., Holcomb, J., Al-Ramahi, I., De Haro, M., Gafni, J., Zhang, N., ... others (2010). Matrix metalloproteinases are modifiers of Huntingtin proteolysis and toxicity in Huntington's disease. *Neuron*, *67*(2), 199–212.

Moberg, S., & Takahashi, N. (2022). Neocortical layer 5 subclasses: From cellular properties to roles in behavior. *Frontiers in Synaptic Neuroscience*, *14*, 1006773.

Montoya, A., Price, B. H., Menear, M., & Lepage, M. (2006). Brain imaging and cognitive dysfunctions in Huntington's disease. *Journal of Psychiatry and Neuroscience*, *31*(1), 21–29.

Morabito, S., Miyoshi, E., Michael, N., Shahin, S., Martini, A. C., Head, E., ... Swarup, V. (2021). Single-nucleus chromatin accessibility and transcriptomic characterization of alzheimer's disease. *Nature genetics*, *53*(8), 1143–1155.

Morris, L.-A., O'Callaghan, C., & Le Heron, C. (2022). Disordered decision making: a cognitive framework for apathy and impulsivity in Huntington's disease. *Movement Disorders*, *37*(6), 1149–1163.

Morton, A., Nicholson, L., & Faull, R. (1993). Compartmental loss of nadph diaphorase in the neuropil of the Human striatum in Huntington's disease. *Neuroscience*, *53*(1), 159–168.

Morton, A., Skillings, E., Wood, N., & Zheng, Z. (2019). Antagonistic pleiotropy in mice carrying a cag repeat expansion in the range causing Huntington's disease. *Scientific Reports*, *9*(1), 37.

Mouro Pinto, R., Arning, L., Giordano, J. V., Razghandi, P., Andrew, M. A., Gillis, T., ... others (2020). Patterns of cag repeat instability in the central nervous system and periphery in Huntington's disease and in spinocerebellar ataxia type 1. *Human molecular genetics*, *29*(15), 2551–2567.

Moya, M. V., Kim, R. D., Rao, M. N., Cotto, B. A., Pickett, S. B., Sferrazza, C. E., ... Schmidt, E. F. (2022). Unique molecular features and cellular responses differentiate two populations of motor cortical layer 5b neurons in a preclinical model of als. *Cell reports*, *38*(12).

Myers, R., MacDonald, M., Koroshetz, W., Duyao, M., Ambrose, C., Taylor, S., ... others (1993). De novo expansion of a (cag) n repeat in sporadic Huntington's disease. *Nature genetics*, *5*(2), 168–173.

Myers, R., Vonsattel, J., Paskevich, P., Kiely, D., Stevens, T., Cupples, L., ... Bird, E. (1991). Decreased neuronal and increased oligodendroglial densities in Huntington's disease caudate nucleus. *Journal of Neuropathology & Experimental Neurology*, *50*(6), 729–742.

Nalavade, R., Griesche, N., Ryan, D., Hildebrand, S., & Krauss, S. (2013). Mechanisms of rna-induced toxicity in cag repeat disorders. *Cell death & disease*, *4*(8), e752–e752.

Nana, A. L., Kim, E. H., Thu, D. C., Oorschot, D. E., Tippett, L. J., Hogg, V. M., ... Faull, R. L. (2014). Widespread heterogeneous neuronal loss across the cerebral cortex in Huntington's disease. *Journal of Huntington's disease*, *3*(1), 45–64.

Nasir, J., Floresco, S. B., O'Kusky, J. R., Diewert, V. M., Richman, J. M., Zeisler, J., ... Hayden, M. R. (1995). Targeted disruption of the Huntington's disease gene results in embryonic lethality and behavioral and morphological changes in heterozygotes. *Cell*, *81*(5), 811–823.

Novoselova, T. V., Margulis, B. A., Novoselov, S. S., Sapozhnikov, A. M., Van Der Spuy, J., Cheetham, M. E., & Guzhova, I. V. (2005). Treatment with extracellular hsp70/hsc70 protein can reduce polyglutamine toxicity and aggregation. *Journal of neurochemistry*, *94*(3), 597–606.

Ochaba, J., Lukacsovich, T., Csikos, G., Zheng, S., Margulis, J., Salazar, L., ... others (2014). Potential function for the Huntingtin protein as a scaffold for selective autophagy. *Proceedings of the National Academy of Sciences*, *111*(47), 16889–16894.

Offen, D., Sherki, Y., Melamed, E., Fridkin, M., Brenneman, D. E., & Gozes, I. (2000). Vasoactive intestinal peptide (vip) prevents neurotoxicity in neuronal cultures: relevance to neuroprotection in parkinson's disease. *Brain research*, *854*(1-2), 257–262.

Ordway, J. M., Tallaksen-Greene, S., Gutekunst, C.-A., Bernstein, E. M., Cearley, J. A., Wiener, H. W., ... others (1997). Ectopically expressed cag repeats cause intranuclear inclusions and a progressive late onset neurological phenotype in the mouse. *Cell*, *91*(6), 753–763.

Osorio, D., & Cai, J. J. (2021). Systematic determination of the mitochondrial proportion in Human and mice tissues for single-cell rna-sequencing data quality control. *Bioinformatics*, *37*(7), 963–967.

Park, J., Phillips, J. W., Guo, J.-Z., Martin, K. A., Hantman, A. W., & Dudman, J. T. (2022). Motor cortical output for skilled forelimb movement is selectively distributed across projection neuron classes. *Science advances*, *8*(10), eabj5167.

Peinado, J. R., Chaplot, K., Jarvela, T. S., Barbieri, E. M., Shorter, J., & Lindberg, I. (2022). Sequestration of TDP-43216-414 aggregates by cytoplasmic expression of the proSAAS chaperone. *ACS chemical neuroscience*, *13*(11), 1651–1665.

Peng, Q., Wu, B., Jiang, M., Jin, J., Hou, Z., Zheng, J., ... Duan, W. (2016). Characterization of behavioral, neuropathological, brain metabolic and key molecular changes in zQ175 knock-in mouse model of Huntington's disease. *PloS one*, *11*(2), e0148839.

Pineda, S. S., Lee, H., Ulloa-Navas, M. J., Linville, R. M., Garcia, F. J., Galani, K., ... others (2024). Single-cell dissection of the Human motor and prefrontal cortices in ALS and FTLD. *Cell*, *187*(8), 1971–1989.

Pressl, C., Mätlik, K., Kus, L., Darnell, P., Luo, J.-D., Paul, M. R., ... others (2024). Selective vulnerability of layer 5a corticostriatal neurons in Huntington's disease. *Neuron*.

Ravikumar, B., Vacher, C., Berger, Z., Davies, J. E., Luo, S., Oroz, L. G., ... others (2004). Inhibition of mtor induces autophagy and reduces toxicity of polyglutamine expansions in fly and mouse models of Huntington disease. *Nature genetics*, *36*(6), 585–595.

Read, A., & Schröder, M. (2021). The unfolded protein response: an overview. *Biology*, *10*(5), 384.

Rebec, G. V. (2018). Corticostriatal network dysfunction in Huntington's disease: Deficits in neural processing, glutamate transport, and ascorbate release. *CNS neuroscience & therapeutics*, *24*(4), 281–291.

Reilmann, R., Bohlen, S., Kirsten, F., Ringelstein, E. B., & Lange, H. W. (2011). Assessment of involuntary choreatic movements in Huntington's disease—toward objective and quantitative measures. *Movement disorders*, *26*(12), 2267–2273.

Reiner, A., Hart, N. M., Lei, W., & Deng, Y. (2010). Corticostriatal projection neurons–dichotomous types and dichotomous functions. *Frontiers in neuroanatomy*, *4*, 142.

Reiner, A., Shelby, E., Wang, H., DeMarch, Z., Deng, Y., Guley, N. H., ... others (2013). Striatal parvalbuminergic neurons are lost in Huntington's disease: implications for dystonia. *Movement Disorders*, *28*(12), 1691–1699.

Rosas, H., Liu, A., Hersch, S., Glessner, M., Ferrante, R., Salat, D., ... Fischl, B. (2002).

Regional and progressive thinning of the cortical ribbon in Huntington's disease. *Neurology*, *58*(5), 695–701.

Ross, C. A., Aylward, E. H., Wild, E. J., Langbehn, D. R., Long, J. D., Warner, J. H., ... others (2014). Huntington disease: natural history, biomarkers and prospects for therapeutics. *Nature Reviews Neurology*, *10*(4), 204–216.

Rui, Y.-N., Xu, Z., Patel, B., Chen, Z., Chen, D., Tito, A., ... others (2015). Huntingtin functions as a scaffold for selective macroautophagy. *Nature cell biology*, *17*(3), 262–275.

Sánchez, A. M. E., Mejía-Toiber, J., & Massieu, L. (2008). Excitotoxic neuronal death and the pathogenesis of Huntington's disease. *Archives of medical research*, *39*(3), 265–276.

Sano, R., & Reed, J. C. (2013). Er stress-induced cell death mechanisms. *Biochimica et Biophysica Acta (BBA)-Molecular Cell Research*, *1833*(12), 3460–3470.

Sapp, E., Schwarz, C., Chase, K., Bhide, P., Young, A., Penney, J., ... DiFiglia, M. (1997). Huntingtin localization in brains of normal and Huntington's disease patients. *Annals of Neurology: Official Journal of the American Neurological Association and the Child Neurology Society*, *42*(4), 604–612.

Sathasivam, K., Hobbs, C., Mangiarini, L., Mahal, A., Turmaine, M., Doherty, P., ... Bates, G. P. (1999). Transgenic models of Huntington'sdisease. *Philosophical Transactions of the Royal Society of London. Series B: Biological Sciences*, *354*(1386), 963–969.

Saudou, F., & Humbert, S. (2016). The biology of Huntingtin. *Neuron*, *89*(5), 910–926.

Saunders, A., Macosko, E. Z., Wysoker, A., Goldman, M., Krienen, F. M., de Rivera, H., ... others (2018). Molecular diversity and specializations among the cells of the adult mouse brain. *Cell*, *174*(4), 1015–1030.

Schilling, G., Savonenko, A. V., Klevytska, A., Morton, J. L., Tucker, S. M., Poirier, M., ... others (2004). Nuclear-targeting of mutant Huntingtin fragments produces Huntington's disease-like phenotypes in transgenic mice. *Human molecular genetics*, *13*(15), 1599–1610.

Schulte, J., & Littleton, J. T. (2011). The biological function of the Huntingtin protein and its relevance to Huntington's disease pathology. *Current trends in neurology*, *5*, 65.

Schwarz, D. S., & Blower, M. D. (2016). The endoplasmic reticulum: structure, function and response to cellular signaling. *Cellular and molecular life sciences*, *73*, 79–94.

Semaka, A., Creighton, S., Warby, S., & Hayden, M. (2006). Predictive testing for Huntington disease: interpretation and significance of intermediate alleles. *Clinical genetics*, *70*(4), 283–294.

Shakya, M., Yildirim, T., & Lindberg, I. (2020). Increased expression and retention of the secretory chaperone proSAAS following cell stress. *Cell Stress and Chaperones*, *25*, 929–941.

Shetty, A. K., & Bates, A. (2016). Potential of gaba-ergic cell therapy for schizophrenia, neuropathic pain, and alzheimer's and parkinson's diseases. *Brain research*, *1638*, 74–87.

Sieradzan, K., Mechan, A., Jones, L., Wanker, E., Nukina, N., & Mann, D. M. A. (1999). Huntington's disease intranuclear inclusions contain truncated, ubiquitinated Huntingtin protein. *Experimental neurology*, *156*(1), 92–99.

Solberg, O. K., Filkuková, P., Frich, J. C., & Feragen, K. J. B. (2018). Age at death and causes of death in patients with Huntington disease in norway in 1986–2015. *Journal of Huntington's disease*, *7*(1), 77–86.

Song, C., Perides, G., & Liu, Y. F. (2002). Expression of full-length polyglutamine-expanded Huntingtin disrupts growth factor receptor signaling in rat pheochromocytoma (pc12) cells. *Journal of Biological Chemistry*, *277*(8), 6703–6707.

Song, M., Xiong, J.-x., Wang, Y.-y., Tang, J., Zhang, B., & Bai, Y. (2012). Vip enhances phagocytosis of fibrillar beta-amyloid by microglia and attenuates amyloid deposition in the brain of app/ps1 mice. *PLoS One*, *7*(2), e29790.

Soto, C. (2003). Unfolding the role of protein misfolding in neurodegenerative diseases. *Nature Reviews Neuroscience*, *4*(1), 49–60.

Soto, C., & Pritzkow, S. (2018). Protein misfolding, aggregation, and conformational strains in neurodegenerative diseases. *Nature neuroscience*, *21*(10), 1332–1340.

Spillantini, M. G., Schmidt, M. L., Lee, V. M.-Y., Trojanowski, J. Q., Jakes, R., & Goedert, M. (1997). α-synuclein in lewy bodies. *Nature*, *388*(6645), 839–840.

Squitieri, F., Cannella, M., & Simonelli, M. (2002). Cag mutation effect on rate of

progression in Huntington's disease. *Neurological Sciences*, *23*, s107–s108.

Stack, E. C., Kubilus, J. K., Smith, K., Cormier, K., Del Signore, S. J., Guelin, E., ... Ferrante, R. J. (2005). Chronology of behavioral symptoms and neuropathological sequela in r6/2 Huntington's disease transgenic mice. *Journal of Comparative Neurology*, *490*(4), 354–370.

Steffan, J. S., Kazantsev, A., Spasic-Boskovic, O., Greenwald, M., Zhu, Y.-Z., Gohler, H., ... Thompson, L. M. (2000). The Huntington's disease protein interacts with p53 and creb-binding protein and represses transcription. *Proceedings of the National Academy of Sciences*, *97*(12), 6763–6768.

Street, K., Risso, D., Fletcher, R. B., Das, D., Ngai, J., Yosef, N., ... Dudoit, S. (2018). Slingshot: cell lineage and pseudotime inference for single-cell transcriptomics. *BMC genomics*, *19*, 1–16.

Strehlow, V., Heyne, H. O., Vlaskamp, D. R., Marwick, K. F., Rudolf, G., De Bellescize, J., ... others (2019). Grin2a-related disorders: genotype and functional consequence predict phenotype. *Brain*, *142*(1), 80–92.

Strong, T. V., Tagle, D. A., Valdes, J. M., Elmer, L. W., Boehm, K., Swaroop, M., ... Albin, R. L. (1993). Widespread expression of the Human and rat Huntington's disease gene in brain and nonneural tissues. *Nature genetics*, *5*(3), 259–265.

Surmeier, D. J., Obeso, J. A., & Halliday, G. M. (2017). Selective neuronal vulnerability in parkinson disease. *Nature Reviews Neuroscience*, *18*(2), 101–113.

Tabrizi, S. J., Langbehn, D. R., Leavitt, B. R., Roos, R. A., Durr, A., Craufurd, D., ... others (2009). Biological and clinical manifestations of Huntington's disease in the longitudinal TRACK-HD study: cross-sectional analysis of baseline data. *The Lancet Neurology*, *8*(9), 791–801.

Takahashi, T., Kikuchi, S., Katada, S., Nagai, Y., Nishizawa, M., & Onodera, O. (2008). Soluble polyglutamine oligomers formed prior to inclusion body formation are cytotoxic. *Human molecular genetics*, *17*(3), 345–356.

Takano, H., & Gusella, J. F. (2002). The predominantly heat-like motif structure of Huntingtin and its association and coincident nuclear entry with dorsal, an nf-kb/rel/dorsal family transcription factor. *BMC neuroscience*, *3*, 1–13.

Takao, K., Kobayashi, K., Hagihara, H., Ohira, K., Shoji, H., Hattori, S., ... others (2013). Deficiency of schnurri-2, an mhc enhancer binding protein, induces mild chronic inflammation in the brain and confers molecular, neuronal, and behavioral phenotypes related to schizophrenia. *Neuropsychopharmacology*, *38*(8), 1409–1425.

Telenius, H., Kremer, B., Goldberg, Y. P., Theilmann, J., Andrew, S. E., Zeisler, J., ... others (1994). Somatic and gonadal mosaicism of the Huntington disease gene cag repeat in brain and sperm. *Nature genetics*, *6*(4), 409–414.

Thompson, P., Berardelli, A., Rothwell, J., Day, B., Dick, J., Benecke, R., & Marsden, C. (1988). The coexistence of bradykinesia and chorea in Huntington's disease and its implications for theories of basal ganglia control of movement. *Brain*, *111*(2), 223–244.

Thu, D. C., Oorschot, D. E., Tippett, L. J., Nana, A. L., Hogg, V. M., Synek, B. J., ... Faull, R. L. (2010). Cell loss in the motor and cingulate cortex correlates with symptomatology in Huntington's disease. *Brain*, *133*(4), 1094–1110.

Travaglini, L., Nardella, M., Bellacchio, E., D'Amico, A., Capuano, A., Frusciante, R., ... others (2017). Missense mutations of CACNA1A are a frequent cause of autosomal dominant nonprogressive congenital ataxia. *European Journal of Paediatric Neurology*, *21*(3), 450–456.

Trettel, F., Rigamonti, D., Hilditch-Maguire, P., Wheeler, V. C., Sharp, A. H., Persichetti, F., ... MacDonald, M. E. (2000). Dominant phenotypes produced by the hd mutation in st hdh q111 striatal cells. *Human molecular genetics*, *9*(19), 2799–2809.

Turmaine, M., Raza, A., Mahal, A., Mangiarini, L., Bates, G. P., & Davies, S. W. (2000). Nonapoptotic neurodegeneration in a transgenic mouse model of Huntington's disease. *Proceedings of the National Academy of Sciences*, *97*(14), 8093–8097.

Uemura, A., Oku, M., Mori, K., & Yoshida, H. (2009). Unconventional splicing of xbp1 mrna occurs in the cytoplasm during the mammalian unfolded protein response. *Journal of cell science*, *122*(16), 2877–2886.

Van Raamsdonk, J. M., Pearson, J., Rogers, D. A., Bissada, N., Vogl, A. W., Hayden, M. R., & Leavitt, B. R. (2005). Loss of wild-type Huntingtin influences motor dysfunction and survival in the yac128 mouse model of Huntington disease. *Human*

molecular genetics, *14*(10), 1379–1392.

Victorson, D., Carlozzi, N. E., Frank, S., Beaumont, J. L., Cheng, W., Gorin, B., … others (2014). Identifying motor, emotional–behavioral, and cognitive deficits that comprise the triad of HD symptoms from patient, caregiver, and provider perspectives. *Tremor and Other Hyperkinetic Movements*, *4*.

Vidal, R., Caballero, B., Couve, A., & Hetz, C. (2011). Converging pathways in the occurrence of endoplasmic reticulum (ER) stress in Huntington's disease. *Current molecular medicine*, *11*(1), 1–12.

Voelkl, K., Gutiérrez-Ángel, S., Keeling, S., Koyuncu, S., da Silva Padilha, M., Feigenbutz, D., … Dudanova, I. (2023). Neuroprotective effects of hepatoma-derived growth factor in models of huntington's disease. *Life science alliance*, *6*(11).

Voelkl, K., Schulz-Trieglaff, E. K., Klein, R., & Dudanova, I. (2022). Distinct histological alterations of cortical interneuron types in mouse models of Huntington's disease. *Frontiers in Neuroscience*, *16*, 1022251.

Vonsattel, J. P. G., & DiFiglia, M. (1998). Huntington disease. *Journal of neuropathology and experimental neurology*, *57*(5), 369.

Wang, F., Bonam, S. R., Schall, N., Kuhn, L., Hammann, P., Chaloin, O., … Muller, S. (2018). Blocking nuclear export of HSPA8 after heat shock stress severely alters cell survival. *Scientific reports*, *8*(1), 16820.

Wang, Z.-T., Zhang, C., Wang, Y.-J., Dong, Q., Tan, L., & Yu, J.-T. (2020). Selective neuronal vulnerability in alzheimer's disease. *Ageing Research Reviews*, *62*, 101114.

Warby, S. C., Montpetit, A., Hayden, A. R., Carroll, J. B., Butland, S. L., Visscher, H., … Hayden, M. R. (2009). Cag expansion in the Huntington disease gene is associated with a specific and targetable predisposing haplogroup. *The American Journal of Human Genetics*, *84*(3), 351–366.

Webb, S., & Haniffa, M. (2023). Large-scale single-cell rna sequencing atlases of Human immune cells across lifespan: Possibilities and challenges. *European Journal of Immunology*, 2250222.

Wertz, M. H., Mitchem, M. R., Pineda, S. S., Hachigian, L. J., Lee, H., Lau, V., … others (2020). Genome-wide in vivo cns screening identifies genes that modify cns neuronal

survival and mhtt toxicity. *Neuron*, *106*(1), 76–89.

Wetzel, H. H., Gehl, C. R., Dellefave-Castillo, L., Schiffman, J. F., Shannon, K. M., Paulsen, J. S., ... others (2011). Suicidal ideation in Huntington disease: the role of comorbidity. *Psychiatry research*, *188*(3), 372–376.

Wheeler, V. C., Persichetti, F., McNeil, S. M., Mysore, J. S., Mysore, S. S., MacDonald, M. E., ... others (2007). Factors associated with hd cag repeat instability in Huntington disease. *Journal of medical genetics*, *44*(11), 695–701.

Wong, Y. C., & Holzbaur, E. L. (2014). The regulation of autophagosome dynamics by Huntingtin and hap1 is disrupted by expression of mutant Huntingtin, leading to defective cargo degradation. *Journal of Neuroscience*, *34*(4), 1293–1305.

Wu, T., Hu, E., Xu, S., Chen, M., Guo, P., Dai, Z., ... others (2021). clusterprofiler 4.0: A universal enrichment tool for interpreting omics data. *The innovation*, *2*(3).

Wu, X., & Rapoport, T. A. (2018). Mechanistic insights into er-associated protein degradation. *Current opinion in cell biology*, *53*, 22–28.

Yang, M., Luo, S., Wang, X., Li, C., Yang, J., Zhu, X., ... Sun, L. (2021). Er-phagy: a new regulator of er homeostasis. *Frontiers in Cell and Developmental Biology*, *9*, 684526.

Yao, Z., Liu, H., Xie, F., Fischer, S., Adkins, R. S., Aldridge, A. I., ... others (2021). A transcriptomic and epigenomic cell atlas of the mouse primary motor cortex. *Nature*, *598*(7879), 103–110.

Yao, Z., van Velthoven, C. T., Kunst, M., Zhang, M., McMillen, D., Lee, C., ... others (2023). A high-resolution transcriptomic and spatial atlas of cell types in the whole mouse brain. *Nature*, *624*(7991), 317–332.

Yao, Z., van Velthoven, C. T., Nguyen, T. N., Goldy, J., Sedeno-Cortes, A. E., Baftizadeh, F., ... others (2021). A taxonomy of transcriptomic cell types across the isocortex and hippocampal formation. *Cell*, *184*(12), 3222–3241.

Zhang, H., Zhang, C., Vincent, J., Zala, D., Benstaali, C., Sainlos, M., ... others (2018). Modulation of ampa receptor surface diffusion restores hippocampal plasticity and memory in Huntington's disease models. *Nature communications*, *9*(1), 4272.

Zhou, L., Su, S., Yu, J., Wan, S., Xu, X., Li, X., ... others (2022). Schnurri-2 promotes

the expression of excitatory glutamate receptors and contributes to neuropathic pain. *Neuroscience*, *488*, 20–31.

Zuccato, C., & Cattaneo, E. (2007). Role of brain-derived neurotrophic factor in Huntington's disease. *Progress in neurobiology*, *81*(5-6), 294–330.

Zuccato, C., Ciammola, A., Rigamonti, D., Leavitt, B. R., Goffredo, D., Conti, L., ... others (2001). Loss of Huntingtin-mediated bdnf gene transcription in Huntington's disease. *Science*, *293*(5529), 493–498.

Zuccato, C., Tartari, M., Crotti, A., Goffredo, D., Valenza, M., Conti, L., ... others (2003). Huntingtin interacts with rest/nrsf to modulate the transcription of nrse-controlled neuronal genes. *Nature genetics*, *35*(1), 76–83.

Zuleta, A., Vidal, R. L., Armentano, D., Parsons, G., & Hetz, C. (2012). AAV-mediated delivery of the transcription factor XBP1s into the striatum reduces mutant Huntingtin aggregation in a mouse model of Huntington's disease. *Biochemical and biophysical research communications*, *420*(3), 558–563.

5 Acknowledgments

First, I would like to thank Rüdiger Klein for giving me the great opportunity to work on this project in his lab. I also would like to thank him for his insightful contributions to the project, support of the project and for the nice work environment in his lab.

A special thanks goes to Irina Dudanova for supporting me on my PhD journey. Her scientific guidance was crucial for the success of this project. She helped me to grow on this project, supported me with valuable input but also let me develop my own ideas.

Many thanks to my TAC members Conny Kopp-Scheinpflug and Özgün Gökce. Your input was critical, especially in the beginning, to get the project running.

I am also grateful for the assistance of Kerstin Voelkl, which was essential for completing the snRNAseq experiment. Thank you for your support.

I am also grateful for my HiWis Magdalena Böhm and Wing Han Liu for doing all the genotypings needed for this project.

Thanks to Miguel Padilha, Sonja Blumenstock, Irene Riera-Tur, Christian Peters, Songwei He, Ylenia Mastrodicasa, and all other members of the Klein and Dudanova labs for their help in the lab, creating a nice lab atmosphere, and vivid discussions during coffee breaks.

Thanks to my Munich friends for making the time in the city wonderful, and to my friends from Heidelberg for always making my visits home a fun experience.

And finally, lots of thanks to my girlfriend and my family for always encouraging me and being a great support throughout the years.

6 List of publications

Kerstin Voelkl, Sara Gutiérrez-Ángel, Sophie Keeling, Seda Koyuncu, Miguel da Silva Padilha, **Dennis Feigenbutz**, Thomas Arzberger, David Vilchez, Rüdiger Klein, Irina Dudanova (2023) Neuroprotective effects of hepatoma-derived growth factor in models of Huntington's disease, Life science alliance, 6(11).

Irene Riera-Tur, Tillman Schäfer, Daniel Hornburg, Archana Mishra, Miguel da Silva Padilha, Lorena Fernández-Mosquera, **Dennis Feigenbutz**, Patrick Auer, Matthias Mann, Wolfgang Baumeister, Rüdiger Klein, Felix Meissner, Nuno Raimundo, Rubén Fernández-Busnadiego, Irina Dudanova (2022) Amyloid-like aggregating proteins cause lysosomal defects in neurons via gain-of-function toxicity, Life science alliance 5.3 (2022).

Anne Hahn, Johanna J. Salomon, Dominik Leitz, **Dennis Feigenbutz**, Lisa Korsch, Ina Lisewski, Katrin Schrimpf, Pamela Millar-Büchner, Marcus A. Mall, Stephan Frings & Frank Möhrlen (2018) Expression and function of Anoctamin 1/TMEM16A calcium-activated chloride channels in airways of in vivo mouse models for cystic fibrosis research, Pflügers Archiv-European Journal of Physiology, 470, 1335-1348.

Dennis Feigenbutz

Curriculum Vitae

Education

Since Sep 2019 **Ph.D. student in the Molecular Neurodegeneration research group of Prof. Dr. Irina Dudanova in the Department of Prof. Dr. Rüdiger Klein,** Max Planck Institute for biological Intelligence, Martinsried
Project: Transcriptomic analysis of Huntington's disease mice with single-cell resolution

Since Sep 2019 **Member of the IMPRS-BI graduate school,** Munich

2016– 2019 **Masters studies in Molecular Biosciences,** University of Heidelberg
Major in Neurosciences, Grade: 1.2

2013–2016 **Bachelor studies in Molecular Biosciences,** University of Heidelberg, Grade: 2.1

Research and practical experience

July 2018– March 2019 **Master Thesis at the University of Oxford,** Molecular Neurodegeneration Research Group of Dr. George Tofaris, Nuffield Department of Clinical Neurosciences
Thesis Title: Identifying novel modifiers of endogenous α-Synuclein and α-Synuclein aggregation
Grade: 1.0, Self-funded with the Erasmus+ Internship scholarship

Oct 2017– March 2018 **Internship in Project Managment,** Roche Diagnostics, Mannheim,

Oct 2016 – Aug 2017 **Student Research Assistant,** Research group of Prof. Dr. Frings, Institute of molecular Physiology Heidelberg

March 2016– Aug 2016 **Bachelor Thesis,** Research group of Prof. Dr. Frings, Institute of molecular Physiology, Heidelberg
Thesis Title: Expression analysis of proteins in the upper airways, Grade: 1.0

Fellowships

2022 **Add-On Fellowship for Interdisciplinary Life Sciences of the Joachim Herz Foundation**
Awarded with the Add-On Fellowship for Interdisciplinary Life Sciences for my Ph.D. project which combines techniques from neuroscience and bioinformatics

...